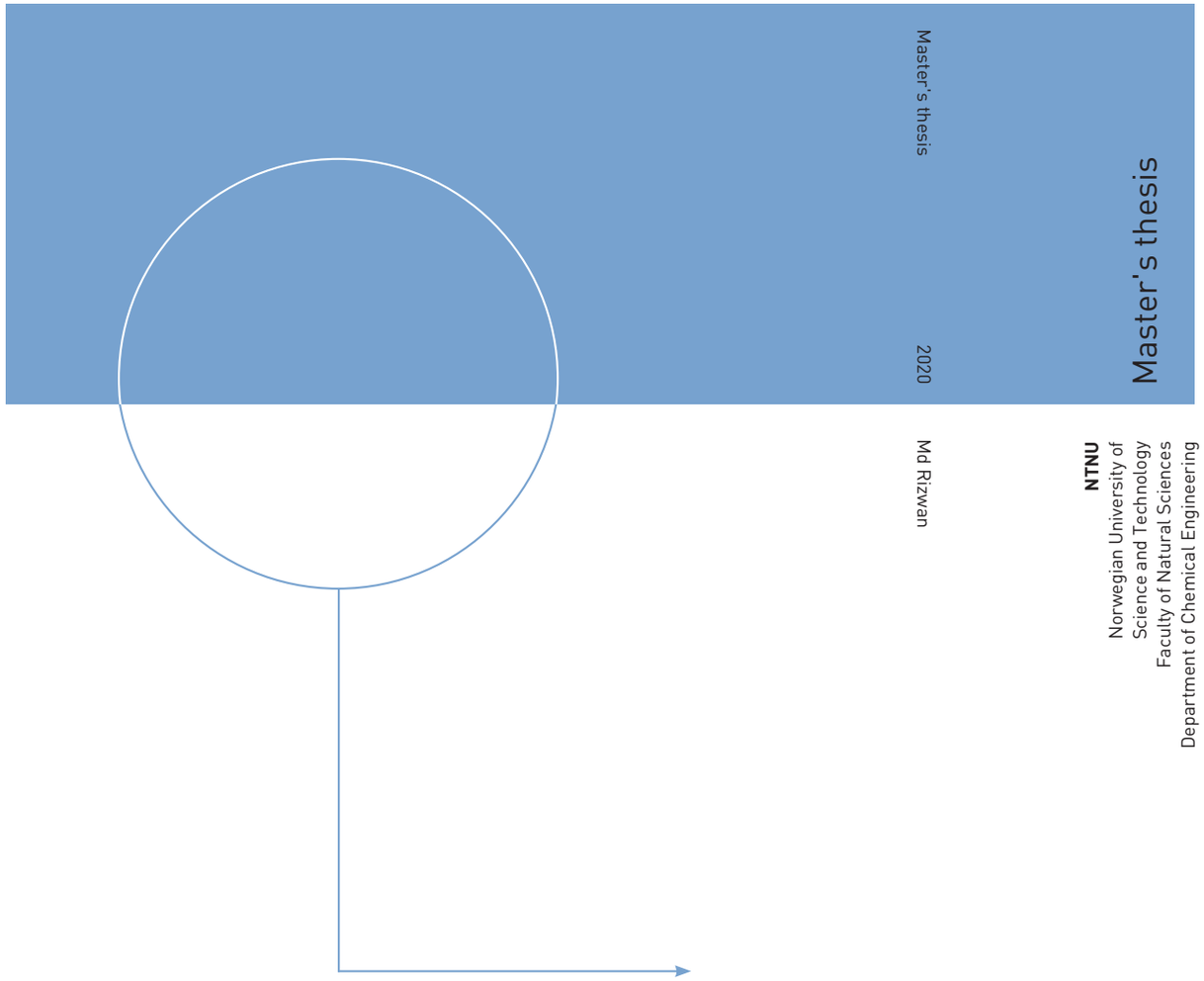

Md Rizwan

Plantwide control of alkaline water electrolyzer plant for hydrogen production

July 2020

NTNU
Norwegian University of
Science and Technology

NTNU
Norwegian University of
Science and Technology

NTNU
Norwegian University of
Science and Technology

Plantwide control of alkaline water electrolyzer plant for hydrogen production

Md Rizwan

MSc in Chemical Engineering
Submission date: July 2020
Supervisor: Johannes Jäschke, IKP
Co-supervisor: Vidar Alstad, Yara International ASA

Norwegian University of Science and Technology
Department of Chemical Engineering

Dedicated to my beloved parents
I feel privileged to be born to the family committed to providing me with the education and support throughout all these years.

Summary

In the efforts to mitigate greenhouse gas emissions, the development of technologies that reduce dependence on fossil fuel-based energy sources is indispensable. At present, hydrogen-based technologies involving the development of the large-scale water electrolysis plant offers one of the most promising solutions for the future energy economy. This project aims to develop a plantwide control structure for a state of the art alkaline water electrolyzer plant. This thesis work is part of a collaboration project between NTNU Norway and Yara International ASA. First, based on the specifications from the supplier [27], a simplified flowsheet for the state of the art electrolyzer plant is introduced. This flowsheet consists of four sub-processes, i.e. electrolyzer assembly, lye circulation system, compressor, and the gas storage system. The design parameters for the flowsheet like lye (i.e. 30% aq. KOH) flowrate into the electrolyzer, coolant flow rate and volume of the buffer tank are estimated. The developed mathematical model of the plant uses empirical correlations given by Ulleberg [45] to define the involved overvoltages in the electrolyzers.

Depending on the features of the sub-processes in the flowsheet, there are in total 12 different flowsheet designs possible. All these flowsheet designs are systematically studied, and the best design is selected. Studying all the flowsheet designs enabled us to decide on the design basis of the cooler in the lye circulation loop, the variability of the inlet lye flowrate, and whether or not the balance of plant systems should be shared. The selected flowsheet design provides the best trade-off between operational benefits and capital investment.

Lastly, the control structure design is suggested for the selected flowsheet design. The integration of the electrolyzer with renewable energy sources like electricity from wind or solar farms give rise to disturbances in the input power. Operating regions and the active constraints are affected by the changes in the total input power and reconfiguration of the control loops is required to achieve steady-state optimal performance. The typical model-based optimization techniques like model predictive control (MPC), can provide easy handling of changing constraints with no need for reconfiguration and can achieve a smooth transition between the active constraint regions. However, such approaches require identification of the actual plant model using process data. This model requires significant development time, cost and regular maintenance to match the actual plant behaviour. Therefore, this work suggests the design of the supervisory control layer using classical advanced control structures like selectors, split range control. The proposed control structure suggests switching logics to switch between the active constraint regions. Thus, this project demonstrates the use of PI(D) based control structures to achieve optimal operation for a state of the art electrolyzer plant.

Preface

This thesis concludes two-year International master's degree program in Chemical Engineering at Norwegian University of Science and Technology (NTNU) Norway. The work presented in this thesis was conducted during Spring 2020 as a collaboration project between Yara International ASA and NTNU Norway.

Firstly, I would like to thank NTNU and Yara International ASA for offering me the opportunity to work on this project. I would particularly like to express deep and sincere gratitude to my co-supervisor Vidar Alstad for the guidance and valuable inputs throughout this project. I am profoundly indebted to him for sharing his knowledge and experience on process control with me. Further, I would like to thank my supervisor Johannes Jäschke for providing priceless insights and constructive feedback on the work during the project meetings. His support and encouragement were pivotal for finishing this thesis.

I would also like to thank my fellow students in the study hall for creating a pleasant working environment. Numerous get together with Jithin, Sandeep and Simen during the challenging times this year has been indispensable in keeping me motivated and driven to work through the end. Finally my constant Ibrija, thank you for proofreading this thesis and also making my life a lot easier with your caring support and lovely smile.

Declaration of Compliance

I, Md Rizwan, hereby declare that this is an independent work according to the exam regulations of the Norwegian University of Science and Technology (NTNU).
Signature:

Place and Date: Trondheim - Gløshaugen, July 2020

Table of Contents

List of Figures

Nomenclature

Acronyms

AEL	alkaline water electrolysis
PEMEL	proton exchange membrane electrolysis
SOEL	solid oxide electrolysis
AC	alternating current
DC	direct current
PHOEBUS	PHOtovoltaik-Elektrolyse-Brennstoffzelle Und Systemtecknik
BoP	balance of plant
MV	manipulated variable
CV	controlled variable
DV	disturbance variable
ACS	advanced control structures
RTO	real time optimization
SOC	self optimizing control
TPM	throughput manipulator
MPC	model predictive control
DOF	degree of freedom
SISO	single input single output
MIMO	multiple input multiple output
VPC	valve position control
SRC	split range control
RGA	relative gain array
SIMC	simple internal model control
DAE	differential algebraic equations
BoL	beginning of life
OS	oversized
EoL	end of life
HX	heat exchanger

Symbol	***Definition***	***Unit***
A	area	m^2
I	current	A
emf	electromotive force	V
U	cell voltage	V
ΔG	change in gibbs energy	J/mol
ΔH	change in enthalpy	J/mol
ΔS	change in entropy	J/mol
r_1	parameter related ohmic resistance of the electrolyzer	Ωm^2
r_2	parameter related ohmic resistance of the electrolyzer	$\Omega m^2/°C$
s	coefficient for overvoltage on electrodes	V
t_1	coefficient for overvoltage on electrodes	m^2/A
t_2	coefficient for overvoltage on electrodes	$m^2°C/A$
t_3	coefficient for overvoltage on electrodes	$m^2°C^2/A$
f_1	parameter related to Faraday efficiency	mA^2/cm^4
f_2	parameter related to Faraday efficiency	
η_F	Faraday efficiency	
F	Faraday constant	
η_e	energy efficiency	
$\dot{n}$	molar flow rate	mol/s
n_c	number of cells in series per stack	
C_t	overall thermal capacity of the electrolyzer	J/K
$\dot{Q}$	heat transfer rate	W
A_s	surface area for radiation and convection	m^2
h_c	convective heat transfer coefficient	W/m^2K
ϵ	emissivity	
T	temperature	K or ° C
k	polytropic exponent	
w	polytropic work	J/mol
α	compressor efficiency	
γ	adiabatic exponent	
E_p	polytropic efficiency	
k_{vlv}	valve constant	
z	valve displacement	
σ	Stefan-Boltzmann constant	W/m^2K^4
R	universal gas constant	$J/molK$

Chapter 1

Introduction

This chapter presents the background for this thesis. First, the motivation behind this project is discussed and then the scope of the work is presented. After that, the main outline of this thesis is explained.

1.1 Motivation

Fritz Haber received 1918 Nobel Prize in Chemistry for the invention of the Haber-Bosch process [28]. Haber discovered how the ammonia, a highly usable form of nitrogen could be synthesized from hydrogen and atmospheric nitrogen. It will not be an overstatement that this invention paved a way to meet the global demand for food. The production of agricultural fertilizers on an industrial scale using ammonia made it possible to grow more food from less land. Thus ammonia has an enormous impact on our society as it enabled to feed billions of people which would not have been possible without the invention of Haber-Bosch process [8] (see Figure 1.1).

Today, fertilizer production consumes about 90% of the total ammonia produced worldwide [47]. The Haber-Bosch process used in fertilizer industry requires hydrogen and nitrogen in the ratio 3:1 at a temperature around 450 °C and 100+ bar pressure.

$$\mathrm{N_2} + 3\,\mathrm{H_2} \longrightarrow 2\,\mathrm{NH_3} \tag{1.1}$$

In the conventional process, the nitrogen is extracted from the air and hydrogen is obtained from steam-methane reforming of the natural gas. This method for hydrogen production using the carbon-based sources contributes to around 1.5% of global greenhouse gas emissions to meet the current demand for agricultural fertilizers [11]. The fertilizer industry is cognizant of its responsibility to feed the plant responsibly and hence is working forward to develop carbon-free technology for hydrogen production.

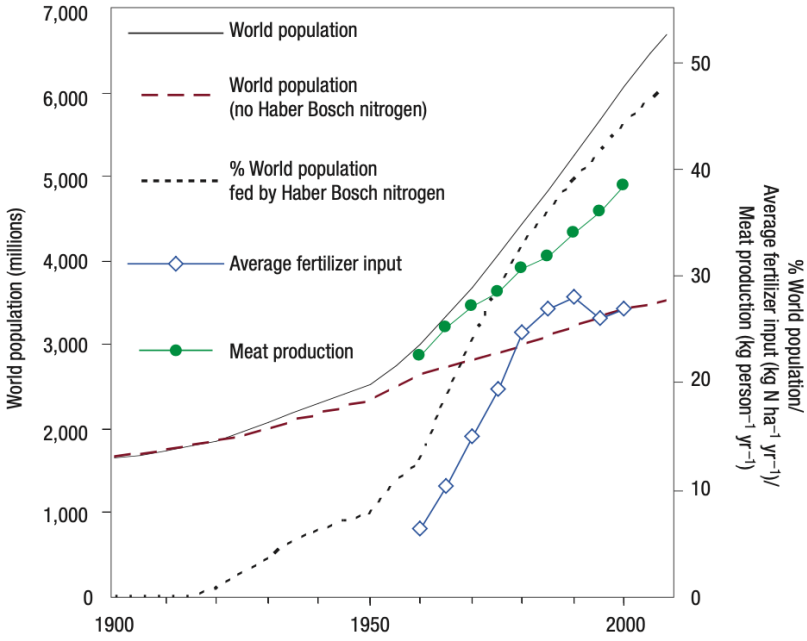

Figure 1.1: Trends in world population and use of nitrogen throughout the twentieth century [8].

1.1.1 Green fertilizer production

Green fertilizer production refers to sustainable fertilizer production without utilizing fossil fuel-based energy sources. Ammonia is the primary building block for the production of all agricultural fertilizers. Thus, to decarbonize current fertilizer production, we should produce ammonia using hydrogen from carbon-free sources such as water electrolysis. Three major water electrolysis technologies that are available today are alkaline water electrolysis (AEL), proton exchange membrane electrolysis (PEMEL) and solid oxide electrolysis (SOEL). Out of these, AEL is the most mature technology and has been around for over a century [7]. Therefore, AEL is the most attractive technology for producing carbon-free hydrogen and hence is selected for this study.

1.2 Scope

In the future, to achieve sustainable development goals for climate action fertilizer industry need to develop and implement technologies that help to reduce the overall greenhouse gas emissions. Hence, for shifting towards green fertilizer production, it is vital to develop water electrolysis technology that can replace steam methane reforming for hydrogen. Earlier work on this topic during the specialization project in Autumn 2019 presented a pilot plant scale model of the electrolyzer plant [33]. This thesis presents a mathematical

model for a state of the art alkaline water electrolyzer plant. The model is implemented in MATLAB using CasADi symbolic framework[3]. The performance of different plant flowsheet configurations depending on the design consideration is studied. After that, the most promising flowsheet design is selected for plantwide control structure design using classical advanced control structures. The insights from this study can be directly used for the installation of a megawatt-scale electrolyzer plant for hydrogen production. Therefore this thesis aims to design a state of the art electrolyzer plant model and then systematically design control structure for the complete electrolyzer plant using simple feedback controllers.

1.3 Outline

This section discusses the organization of the thesis. This thesis consists of six chapter and appendices A-C, including this chapter.

- Chapter 2 contains the technical background related to the plantwide control and supervisory control layer design using classical advanced control structures. Also, a section on the introduction to these classical advanced control structures (i.e. selectors, split range control) is added to give the reader an overview of the control structures and blocks that are used in this thesis.
- Chapter 3 presents an introduction to the alkaline water electrolysis and discusses the mathematical model of the state of the art alkaline water electrolyzer plant in detail. This mathematical description is a continuation of the work from the specialization project [33]. However, to make the model more realistic, the thermal model for the electrolyzers is updated, and the models for the components in the lye circulation loop (i.e. heat exchanger and buffer tank) are added.
- Chapter 4 deals with the design consideration for the flowsheet of the state of the art alkaline water electrolyzer plant. Different flowsheet configurations are possible based on the design of the auxiliary systems, the design basis for the heat exchanger sizing and the variability of the inlet lye flowrate. This work identifies 12 different flowsheet configurations and compares their performances for overall hydrogen production. This chapter concludes by suggesting the flowsheet design, for which we have designed the control structure in Chapter 5.
- Chapter 5 follows the theories introduced in Chapter 2 for plantwide control of the electrolyzer plant. The supervisory control layer structure using classical advanced control structures is suggested.
- Chapter 6 summarizes overall conclusions and evaluates the objectives set out for this work. This chapter also suggests directions for further work on this topic.
- Appendix A includes the parameter values for performance curves of all the electrolyzer
- In Appendix B a table on the performance of different electrolyzer flowsheets as a function of input power is included.

- Appendix C includes source code developed in this project.

Chapter 2

Preliminaries

This chapter introduces to the theoretical background of the work performed in the project. We start by introducing the reader to the systematic procedure for plantwide control. This work proposes the design of supervisory control layer using decentralized control. While using decentralized control, the reconfiguration of control loops is needed to switch between active constraint regions. In this study, we propose to do this switching by using classical advanced control structures (ACS). Hence, this chapter provides necessary details on these classical advanced control structures and also outlines the systematic design procedure for constraint switching using ACS.

2.1 Introduction to plantwide control

Plantwide control refers to the central control philosophy of the overall plant, which deals with the structural decisions of the control system [37]. In short, it is a control structure design for complete chemical plants. Hence, here we emphasize decisions like which variables to control, how to pair input and output variables to form the control loops. A chemical plant can utilize any combination from the thousands of measurements to meet the objectives concerning the stability and economics of the operation. Typically, these goals and objectives are in different time scales ranging from long term planning and scheduling to fast corrective actions for stable operation. Hence, the control system for the operation of any process is divided into several layers. Figure 2.1 shows the typical control hierarchy in a chemical plant. The controlled variables (CVs) link the layers in this decomposition, and upper layers compute the value of the CV setpoints for the layer below. There is a time scale separation between these layers, and therefore it can be assumed that the lower layer immediately implements the setpoints given by the upper layers [37].

Plantwide control considers the three lowest layers in the typical control hierarchy diagram (see Figure 2.1). The local optimization layer recalculates optimum operating conditions for all disturbances by solving a steady-state real-time optimization (RTO) problem and is also termed as RTO layer. The timescale for the decisions in the RTO layer is of hours

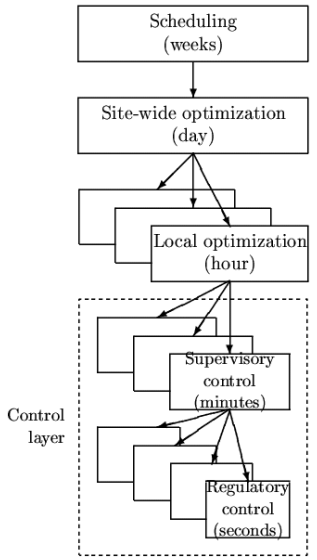

Figure 2.1: Typical control hierarchy in process control [37]

[35]. The typical objective in the RTO layer is to maximize the revenue and minimize the operation costs, thereby optimizing the economics of the process. This layer provides setpoints (c_s) for the controlled variables (c) in the control layer below. The tasks in plantwide control or control structure design involve following decision [37]:

- Selection of controlled variables and their setpoints.
- Selection of manipulated variables.
- Selection of measurements.
- Selection of control configuration.
- Selection of controller type (e.g. PID, decoupler, model predictive control, etc.)

This work designs a plantwide control for a state of the art alkaline water electrolyzer plant. Hence the most important question addressed in this work as very aptly stated by Larsson et al. [18] is:

- *Which 'boxes' should we have and what information should be sent between them?*.

2.2 Procedure for plantwide control

Plantwide control is synonymous to control structure design. It aims to achieve short term stability and long term economic profitability by suggesting links between the variables to be measured and inputs available for manipulation [38]. It is impossible to give a set recipe that can serve as an elixir to design the control structure for all the chemical plants.

However, Skogestad [41] outlines the following procedure to design a control structure systematically:

i. Top-down analysis The top-down analysis is mainly concerned with plant economics. Steady-state behaviour primarily determines the economics of the operations, and therefore, steady-state models are sufficient for the top-down part.

- Step 1: Define operational objective (cost) and the set of constraints that need to be satisfied.
- Step 2: Identify degrees of freedom and optimize operation for disturbances.
- Step 3: Select the primary control variable for implementing the optimal operation. Identify active constraints and control them tightly. Apply the principles of self-optimizing control for unconstrained degrees of freedom.
- Step 4: Select the location of throughput manipulator (TPM). The choice of TPM is important as it determines the structure of the remaining inventory control system.

ii. Bottom-up design The main purpose of bottom-up design is to stabilize the plant.

- Step 5: Identify secondary control variables for regulatory (stabilizing) control layer.
- Step 6: Design the supervisory control layer (using decentralized or multivariable control).
- Step 7: Implement an RTO layer if needed.
- Step 7: Perform nonlinear dynamic simulation for validation.

In this work, we will go through both top-down and bottom-up design procedure to find the control structure for a state of the art electrolyzer plant. We have given special focus to step 6, i.e. the design of the supervisory control layer using the decentralized single-loop control to achieve optimal operation.

The supervisory control layer is responsible for keeping the operation in the right *active constraint region*. Active constraint region is a region in the disturbance space defined by which constraints are active within it [12]. The above procedure for plantwide control applies to a region with a given active constraint set. However, in cases when active constraint set varies depending on the operating point (disturbances) then the supervisory layer is responsible for identifying an optimizing control strategy to move the plant to the new optimal operating point.

Sometimes multivariable controller like Model predictive control (MPC) is used to design the supervisory layer. MPC is a unified, systematic procedure to control multivariable processes, and it requires a dynamic model of the process [24]. The requirement of an accurate model is one of the prohibiting reasons for MPC as it may not be possible or might be too costly to generate and maintain a process model. Another alternate can be to design supervisory control layer using *classical advance control structures* with PID controllers and simple blocks. This decentralized control approach is one of the most common

approaches in the industry. This work suggests the use of classical advanced control structures for the design of supervisory control layer for the electrolyzer plant and handle the changes in the active constraint set using simple logics such as selectors.

Why not a big multivariable control: One might comment on avoiding the most of the steps in the design procedure above by designing a single optimizing controller that stabilizes the process and simultaneously coordinates all the manipulated variables ideally based on dynamic on-line optimization. This approach is nearly impossible even with tomorrows computing power because of fundamental reasons related to the cost of modelling and tuning such a controller. The efforts invested in designing such a controller will be significantly higher than the hierarchical structure used effectively to control most of the chemical plants [39].

2.2.1 Definition of operational objectives and constraints

A clear definition of steady-state economics is instrumental in identifying the control variables. Larsson and Skogestad [18] suggest that the design of the control system should start with the optimization. The objective for optimization, in most cases, is to minimize the production cost and maximizing revenue. However, there are many other possibilities of combining the objective into a scalar cost function J, which we want to minimize. Typically, we achieve the objectives concerning safety by defining them as constraints to the optimization problem.

2.2.2 Selection of manipulated variables and degree of freedom analysis

To select the manipulated variables, Skogestad [41] suggests that we start by the degree of freedom analysis. The number of *control or dynamic degrees of freedom*, N_m (m denotes manipulated) is equal to the number of the independent variables that can be manipulated by external means. This information is usually known from the process insight and consists of the adjustable valves plus other electrical or mechanical variables that can be adjusted. Next, N_{opt} i.e. *optimization degrees of freedom* is identified. These are the degrees of freedom that affect the operational cost, J defined in the previous step. In most cases the cost depends only on the steady-state i.e. N_{opt} is equal to the *steady state degrees of freedom* N_{ss}. However, in order to obtain N_{ss} we need to subtract N_{0m} and N_{0y} from N_m. The definition of N_{0m} and N_{0y} is as below:

- N_{0m}: These are manipulated variables with no steady-state effect. By this, it means that they do not have any effect on the cost and are typically used to get improved dynamic response, e.g. an extra bypass on the heat exchanger.
- N_{0y}: These are output variables that do not have any impact on the steady-state cost, but we need control on them. Typically, these are liquid levels in the buffer tanks.

Thus, the steady-state degrees of freedom are:

$$N_{ss} = N_m - (N_{0m} + N_{0y}) \tag{2.1}$$

Usually, the optimum is subjected to multiple constraints, and many of these are active (i.e. are at the limiting value) at the optimum. The remaining degrees of freedom that are left to optimize the process is known as unconstrained degrees of freedom and are N_{opt}-N_{active}. This count of unconstrained DOF is an important number for the design of the supervisory control layer. These free variables are the manipulated variables that are available to be paired with the selected controlled variables in order to achieve an optimal steady state.

2.2.3 What should we control?

It is of utmost importance to identify and control the right variables. The right variables help in achieving near-optimal operation in the presence of the uncertainties. We can broadly classify control variables as primary and secondary control variables. Primary control variables are the variables that are directly related to ensuring *optimal economic operation*. Skogestad [41] suggests following guidelines for the selection of primary controlled variables:

- Control active constraints
- For unconstrained manipulated variables select the control variables so that keeping them at a constant setpoint will allow the process to operate close to its optimum despite the disturbances and implementation errors. We also refer to these selected variables as self-optimizing control variables, and their identification is less intuitive. Skogestad in the article on self-optimizing control [37], describes the systematic procedure for selection of these control variables.

We term the control variables needed to ensure *satisfactory regulatory control* as secondary control variables (CVs). Correct placement of regulatory control structure for secondary CVs ensures that the plant does not drift too much from the desired steady-state operation point. This regulatory control layer enables the above supervisory layer (see Figure 2.1) to control the plant at a slower time scale. The control objectives, as suggested by Skogestad [41] while selecting secondary control variables for the regulatory layer are:

- Local disturbance rejection: The selection of variables should be such that with secondary variables controlled, the effect of the disturbances on the primary variables should be small. This reduces non-linearity and will allow the basic control layer to operate for a wide range of primary control objectives.
- Stabilization: The regulatory layer should also be able to minimize state drifts. In regulatory control layer, we tightly control the variable that would otherwise drift away due to large disturbance sensitivity. However, controlling these local measurements does not consume any degrees of freedom since the setpoints for the controlled variables will replace the manipulated variables as degrees of freedom.

2.3 Classical advanced control structures

The purpose of this section is to give an introduction of classical advanced control structures. This project aims to achieve the optimal operation of state of the art alkaline water electrolyzer plant using decentralized control. Because of the disturbances, there are

changes in the active constraints. Thus disturbances can invoke reconfiguration of control loops to switch process operation from one active region to another. We propose to do this by using some of the classical advanced control structures such as selectors and split range control. The switching between the regions is required to achieve optimal operation of the electrolyzer plant. For a more detailed description and additional examples on implementation of these advanced control structures, we refer the reader to standard process control books like [43] and [44]. In this discussion on advanced control elements, we are representing controlled variables (CV) by y, manipulated variable (MV) by u and disturbance (DV) is denoted by d.

2.3.1 Cascade control

Cascade control is shown in Figure 2.2. Cascade control is used when there is 1 input (u), 1 main output y_1 and an extra measurement y_2. Typically, the master controller (C_1) in an outer loop is slower and thus the control of primary output y_1 is improved by involving a slave controller C_2. The slave control utilises the extra available measurement y_2. The setpoint for the slave controller (y_2^{sp}) is provided by the master controller. Thus the inner loop rejects rejects disturbances (d_2) on a faster time scale which improves the dynamic response.

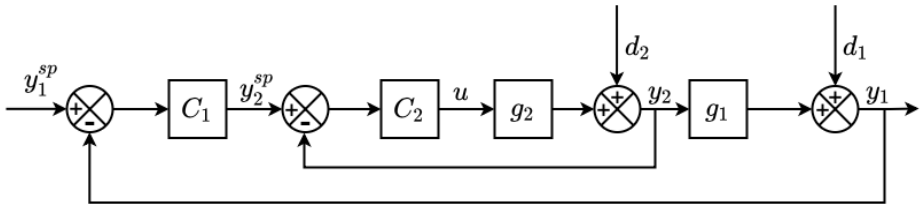

Figure 2.2: Conventional cascade control structure

2.3.2 Feedforward control

Figure 2.3 shows the schematic representation of feedforward control. In feedforward control, the disturbance (i.e., d) and its effect on the output (g_d) is well-known. Feedforward scheme utilizes the measured disturbance d_m to adjust the input u in order to keep the output y constant when there are disturbances.

Feedforward is particularly useful when feedback control is not effective because measurement of y is lacking or delayed. Feedforward is effective when process delay (in g) is larger than measurement disturbance delay (in g_{dm}). Feedforward is usually used in combination with feedback in an additive manner. An alternate implementation of feedforward control is ratio control and curious readers are referred to standard textbooks like [43] for detailed description and more examples on feedforward control.

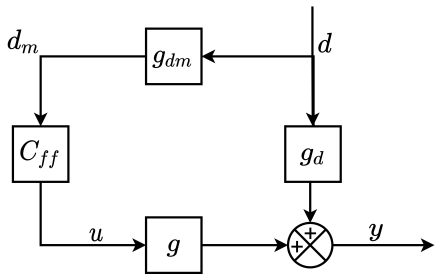

Figure 2.3: Feedforward control structure

2.3.3 Decoupling

Decoupling is used for multivariable control with multiple inputs and multiple outputs, MIMO systems (typically with two inputs and two outputs) to reduce interactions and prepare these systems for single-loop control. Decouplers are designed as feedforward control by considering that for a 2×2 system, u_2 is a disturbance on y_1 and u_1 is a disturbance on y_2.

One way decoupling is the most common scheme and it decouples only one of the interaction. For two way decoupling the "inverse" scheme of Shinskey [36] is recommended (see Figure 2.4) as it keeps the gain g_{11} from u_1 to y_1 unchanged when the decoupling element is added. The decoupled process with this inverse scheme is represented as:

$$G_{\text{decoupled}} = \begin{bmatrix} g_{11} & 0 \\ 0 & g_{22} \end{bmatrix}$$

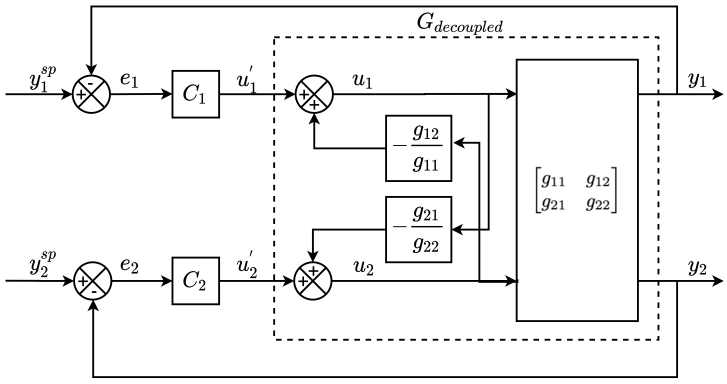

Figure 2.4: Implementation of two way decoupling using inverse Shinskey [36] scheme

2.3.4 Selectors

Selectors are one of the most common elements in the classical advance control structures. There are three major types of selectors, min-, max- and mid-selector. As the name suggests, the output of a min selector is a signal with the minimum value. Similarly, the output from the max selector is signal with the maximum value. Mid selector gives an output signal with the value in the middle. Usually, the combination of min and max selectors gives this mean value.

Min-Max selector

Min-max selectors are used when there is only one input available to control multiple outputs (see Figure 2.5). In practice, this is the case when depending on the operating point (disturbances), the active constraint set may change. In such situations, to maintain the optimal operation, it is required to control all active constraints in respective regions tightly by switching between the controlled variables (CV). Each output y_i has a separate controller and, we use a minimum or maximum selector to select the input value u among the controller outputs (u_i). The following theorem by Krishnamoorthy [16] summarizes the systematic design of selectors for CV-CV switching. This theorem outline the conditions for the possibility of CV-CV switching and the type of selector block required to perform the switch.

Theorem 1 *(CV-CV switching using selectors) Consider a process with one MV and*

- *at most one CV equality that can be given up (setpoint control), denoted by* y_0
- *any number of CV inequality constraints that may be optimally active, denoted by* y_i, $i = 1, ...n$

For each output y_i *design a SISO controller which computes* u_i*, and let the actual input u used to control the system be determined by a min- or max- selector*

$$u = \max_{i \in [1,n]}(u_i) \text{ or } u = \min_{i \in [1,n]}(u_i)$$

Further let a logic variable y_i^{lim} *be defined for each CV inequality constraint (i = 1,2,...,n)*

$$y_i^{\lim} = 1 \text{ for a max - constraint}$$
$$y_i^{\lim} = -1 \text{ for a min - constraint}$$

Then the CV-CV switching is feasible only if

$$sgn(G_i)sgn(y_i^{\lim}) = sgn(G_j)sgn(y_j^{\lim}) \; \forall i, j \in 1, 2, ..., n$$

where G_i *is the steady state process gain for the* i^{th} *CV. Furthermore, if the* $sgn(G_i)y_i^{lim} = 1$*, use a minimum block and if* $sgn(G_i)y_i^{lim} = -1$ *use a maximum selector block.*

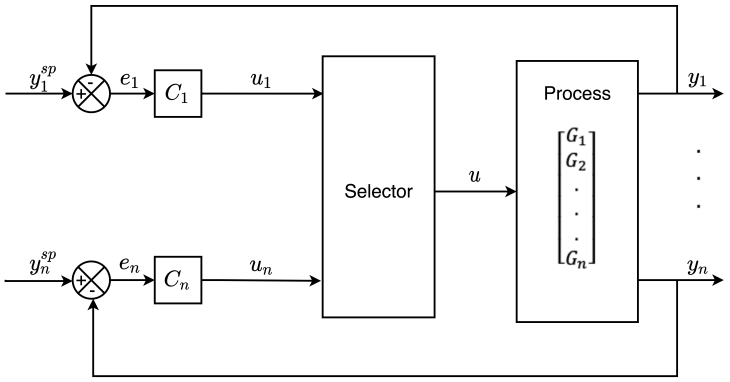

Figure 2.5: Schematic of a min-max selector block for a process with n CVs and 1 MV

Mid-selector

The mid selector is shown in Figure 2.6. In this case there is one input (u), one output (y) and y has both upper and lower bounds $y^{\min}$ and $y^{\max}$. Also, we have a desired setpoint for input i.e. u^{sp}. There are two different controllers on the same output y but with different setpoints $y^{\min}$ and $y^{\max}$. These controllers calculate two separate values of the input say $u^{min'}$ and $u^{max'}$. The mid selector chooses u = *mid*($u^{min'}$,u^{sp},$u^{max'}$) which drives the output y away from y^{min} or y^{max} when the disturbances are such that controller outputs $u^{min'}$ or $u^{max'}$ reach u^{sp}.

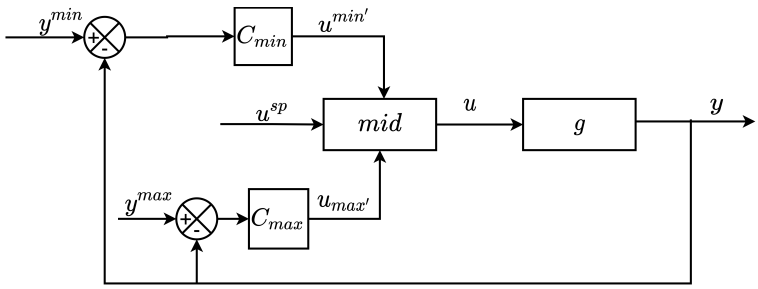

Figure 2.6: Schematic of a mid selector block for a process

2.3.5 Input sequencing

Input sequencing is used when inputs (MVs) available for manipulation are more than the outputs (CVs). There are three alternatives which are commonly used:

- Split range control (standard approach)

- Valve position control (VPC)/ Input resetting control/ mid-ranging control
- Two setpoint controllers

In alternatives 1 and 3 only one input is used at a time whereas in alternative 2 (VPC), we use two inputs when the primary input is close to saturation.

Split range control

Split range control (see Figure 2.7) is used in situations when we need several inputs to cover the whole range as the primary input may saturate. When the internal control signal

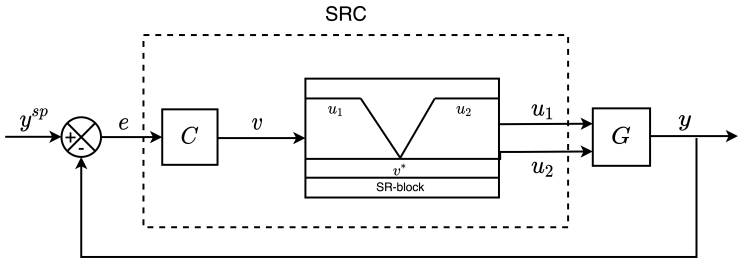

Figure 2.7: Schematic of a split range control

v is below the split valve v^*, u_1 is used to control y, while u_2 is fixed at the limiting value. When v is above v^*, u_2 is used to control y, while u_1 is fixed.

MV to CV constraint switching

MV to CV constraint switching will be required when we are controlling an important CV (y_1 in Figure 2.8) with a MV (u_1) that can saturate. To address this Reyes Lúa et al. [31], suggests following strategy.

When u_1 reaches its saturation value then the control on y_1 is lost if the pairing of $u_1 - y_1$ is continued. Therefore, we need to find another MV (i.e. u_2) which can take over control of important CV (i.e. y_1) from u_1. This MV-MV switching can be performed by any standard input sequencing strategy like SRC. However, it is extremely likely that u_2 is already paired to a less important CV (y_2). Therefore, a selector is used in combination to SRC to perform CV-CV switching (see Figure 2.8). Hence, we terminate the control over less important CV (y_2) to ensure control on the more important CV (y_1) using a MV (u_2) that can never saturate.

Valve position control

Valve position control (VPC) is also called input resetting [43] or midranging control [1]. VPC can be used in three following cases.
Dynamic case with one output and two inputs: This implementation uses valve position control for improving dynamic performance while controlling y when the dynamic

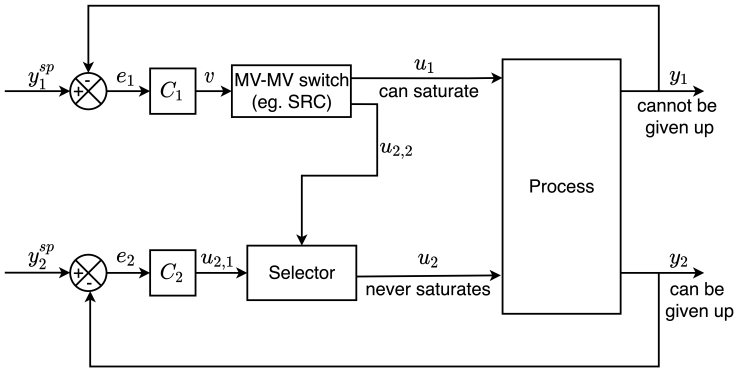

Figure 2.8: Schematic of a MV-CV switching done by combining split range control and a selector

response of the primary input u_1 is too slow (see Figure 2.9). In this case both the inputs u_1 and u_2 are always used. The primary input u_1 can also be used alone to control y, but utilising u_2 improves the dynamic performance. Hence in this case, the input u_2 is used to control y, whereas the primary input u_1 controls u_2 back to its desired steady state value.

Steady state case with one output and two inputs: In this case VPC is used for extend-

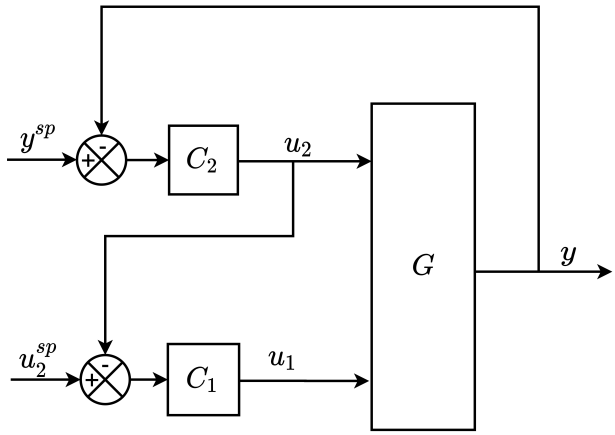

Figure 2.9: Schematic of a valve position control: dynamic case with one output and two inputs

ing steady state range for controlling y when primary input u_1 saturates. Here, u_2 controls u_1 only when it reaches saturation, so most of the time u_2 is not used (see Figure 2.10). This is different than dynamic case where u_2 is actually used to control y, whereas in steady state case u_2 is only active when u_1 reaches saturation or a limit.

Dynamic case with one output and one input: In this case there is one input and one

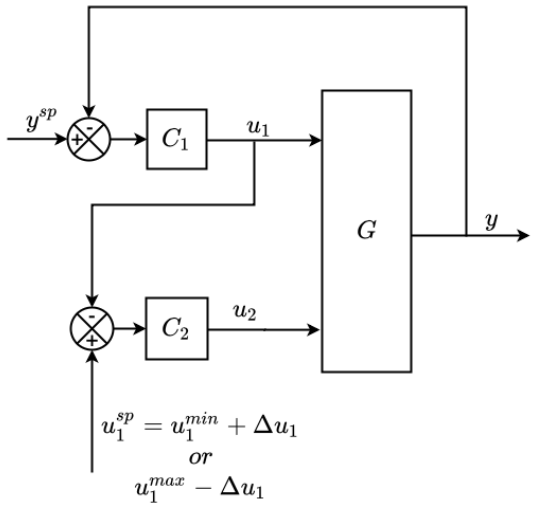

Figure 2.10: Schematic of a valve position control: steady state case with one output and two inputs

output but with two controllers C_y and C_u (see Figure 2.11). This is used for floating control of y. The input u is used to control y (with the controller C_y) while the outer master controller C_u is used to keep u away from its constraint by manipulating setpoint y^{sp} for the controller C_y. Here, it is required that y is controlled at all the times but the setpoint y^{sp} is not important.

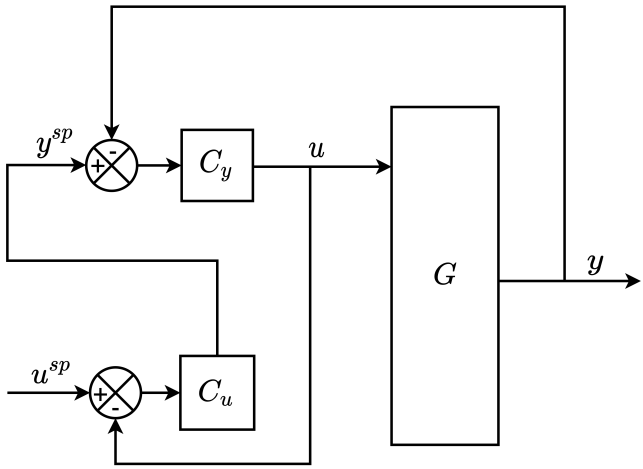

Figure 2.11: Schematic of a valve position control: dynamic case with one output and one input

Two setpoint controllers

This is an alternative to the the split range control. In this case, separate controllers are used for each inputs (MVs) with two different setpoints $y^{sp,1}$ and $y^{sp,2} = y^{sp,1} + \Delta\, y^{sp}$ (see Figure 2.12). The $\Delta\, y^{sp}$ is selected such that only one input is active at a time while other inputs are at their limits.

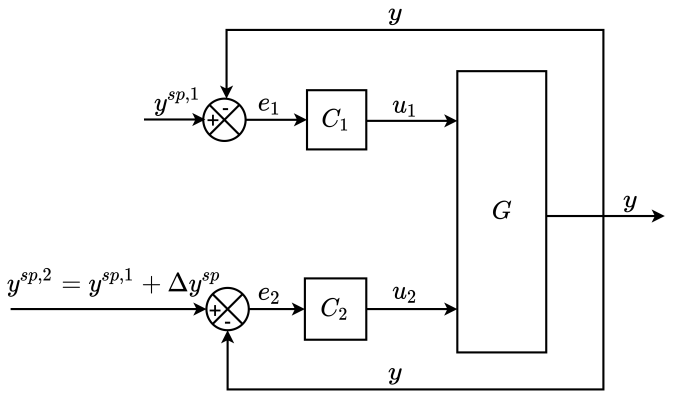

Figure 2.12: Schematic of a two setpoint controllers: an alternative to split range control

2.3.6 Anti-windup

When the controller with integral action is not selected, then the inactive controller's output keeps integrating. For correct implementation, we need to stop the integral action when the controller is no longer active. Anti-windup is used to correctly initialize the states of the controller when the controller is activated again. There are many ways to do this. However, Figure 2.13 shows the most common approach to implement an anti-windup using back-calculation. Here, the difference between the actuator and the controller output ($u^{'}$) is fed to the integral action with a gain of $k_t = 1/\tau_T$. This approach allows the controller output to track the actuator with a time constant of τ_T. Thus, the time constant τ_T decides how fast the controller is driven to the actual actuator position.

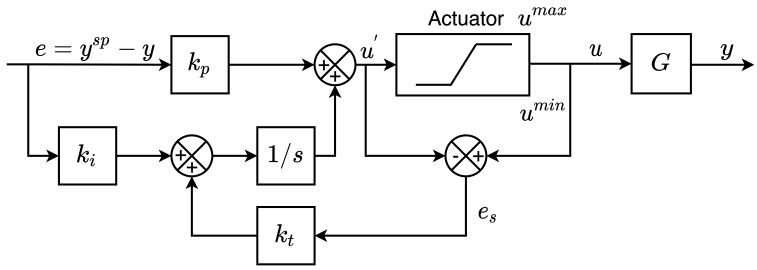

Figure 2.13: Schematic of a controller with anti-windup. Back-calculation is used for input tracking.

2.4 Design of supervisory control layer

The supervisory or advanced control layer has the following major tasks:

- Keep the primary control variables at constant setpoints to ensure optimal economic operation.
- Supervise the performance of the lower regulatory layer. The supervisory layer is responsible for avoiding saturation of MVs used for regulatory control, thus extending the operating range of the regulatory layer.
- Perform switching of the controlled variables and control policies to ensure optimal plant operations when the process encounters disturbances.

There are following two main alternatives for designing the supervisory layer:

- Multivariable control
- Decentralized control

Traditionally, in practice because of its simple and straightforward implementation, decentralized control is used. However, in recent decades multivariable control like MPC is also becoming more widespread. However, there is always a trade-off between the improved performance and efforts needed for the development and implementation of the multivariable control in the supervisory control layer.

2.4.1 Multivariable control

Multivariable control involves unified, systematic procedures like MPC to control multiple-input multiple-output (MIMO) interacting processes with operation spanning across different active constraint regions. A multivariable controller can explicitly handle constraints and thus eliminate the need for complicated logic to switch between the active constraint regions. However, multivariable constrained control needs an updated dynamic plant model and may be less transparent. Also, it is more sensitive to the changes and uncertainty in the plant operation and hence has reliability issues like fear of everything going down at the same time. [41].

Model predictive control

Model predictive control (MPC) is the most widely used multivariable, model-based control approach due to its ability to handle constraints in the manipulated and controlled variables. Figure 2.14 illustrates the principle of model predictive control. Mayne [23] describes model predictive control as a form of control which solves an open-loop optimal control problem at each sampling instant to obtain the current control action. MPC uses the current state of the plant ($x_t^{'}$) as the initial state. The solution of the optimization yields an optimal control sequence and the first control move ($u_t^{'}$) in this sequence is applied to the plant. The Algorithm 1 of state feedback MPC is:

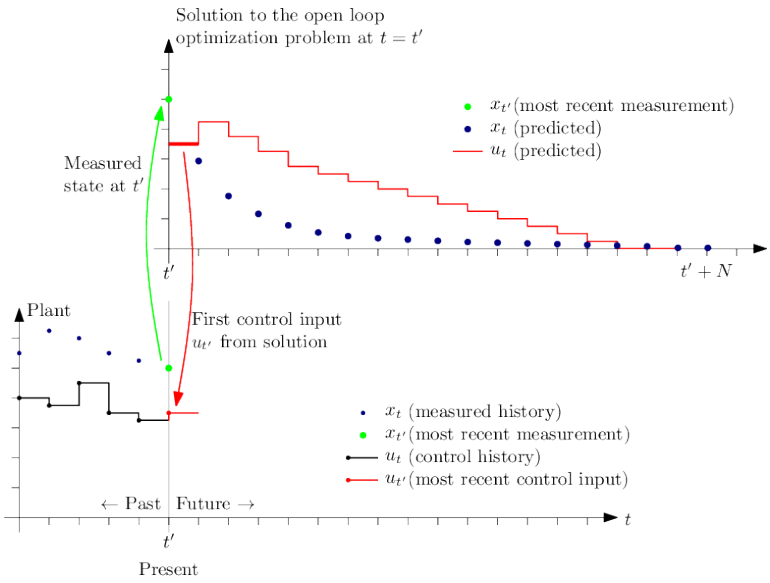

Figure 2.14: Illustration of MPC principle [9]

Algorithm 1: State feedback MPC procedure [9]

for t = 0,1,2,...**do**;
Get the current state $x_t^{'}$;
Solve the dynamic optimization problem on the prediction horizon from t to t+N with $x_t^{'}$ as the initial condition.;
Apply the first control move $u_t^{'}$ from the solution above.;
end for

2.4.2 Decentralized control

The decentralized control is the simplest approach to control MIMO plants. It is the most used approach in the industry for the design of supervisory control layer. Advantages with decentralized control are [41]:

- online tuning is possible
- no or minimal model requirements
- easy to fix and maintain

However, as there are no free lunches, the challenges with the decentralized control structure design approach are:

- need to determine the pairing of input and output variables
- may under-perform severely for the interacting processes

- complicated logics are needed for reconfiguration of control loops when the active constraints move

In this work, we will attempt to follow the decentralized control approach for the design of the supervisory control layer using classical advanced control structures. This design approach is straightforward but requires process insight and engineering intuition of the seasoned process control engineers. Also, the decentralized control design approach has a significant advantage as it addresses the challenges related to the human aspect, since this is most tried and tested approach in practice [34].

Input output pairing For decentralized single-loop control of multivariable processes, variables pairing is such that the interactions are minimum. We can utilize systematic approaches like the relative gain array (RGA) to decide the pairing of the variables. RGA provides two important information [6]:

- A measure of process interactions
- A recommendation on the choice of pairing for input and output

For a multivariable process with n inputs and n outputs, RGA matrix is defined as

$$\text{RGA}(\mathbf{G}) \equiv \Lambda = (\mathbf{G}) \otimes (\mathbf{G^{-1}})^T$$

here $\mathbf{G}$ is a $n \times n$ non-singular square matrix that represents steady state gain of the plant from inputs to the output, and $\otimes$ denotes Schur product (element by element multiplication). RGA has several interesting properties for steady-state processes like the sum of all the elements in each row or column is 1. The relative gains are dimensionless and hence remain unaffected by choice of the units or scaling of variables. Based on RGA analysis following recommendation are proposed for input-output pairing[43]:

- Choosing the variable pairings corresponding to RGA elements close to 1 minimizes the interaction between the loops
- Avoid pairing on the negative steady-state relative gain, as this will lead to instability if one of the loops become inactive

In addition to the RGA analysis following general guidelines are useful in deciding the input-output pairing while designing the supervisory control layer:

- Pair-close rule: In order to avoid large time delays and sluggish control, we should pair control variables (CV) to the manipulated variable (MV) located closer to it [43]
- Important CVs (usually the regulatory layer CV) should not be paired with the inputs (MVs) that may optimally saturate [26]
- Inputs (MVs) that may optimally saturate must be paired with the CVs that may be given up

Also, to note here that it is possible to achieve the same optimum using different pairings and the above rules are guidelines that can help reduce the number of logic blocks required to make the switch between the active constraint regions.

Controller Tuning For decentralized single loop control, the design of each controller is important to achieve overall good performance. Hence, this section provides an introduction on the controller tuning. The proportional-integral-derivative (PID) controller equation in time domain is:

$$u(t) = u_0 + K_{\mathrm{C}} \left(e(t) + \frac{1}{\tau_{\mathrm{I}}} \int_0^t e(\tau) d\tau + \tau_{\mathrm{D}} \frac{d}{dt} e(t) \right) \tag{2.2}$$

here u_0 is the bias term, $e(t)$ is the error term at time t which measure deviation of the controlled variables from the desired setpoints. K_C is controller gain, τ_I is the integral time and τ_D is the derivative time.

Although K_C, τ_I and τ_D are only three parameters that we need to determine for the controller tuning; however, without a systematic procedure, it is tough to tune a controller correctly. There are several model-based PID tuning methods available in literature [32],[49],[40]. In this work, we have used simple internal model control (SIMC) method proposed by Skogestad [40] for all controller tunings. SIMC tuning rule results in simple PI/PID settings that work well for a wide range of processes and provides satisfactory performance both for setpoint tracking and disturbance rejection.

For controller tuning using SIMC rule, the dynamic effect of change in input (u) on output (y) is modelled as a first order or second order plus time delay process. In transfer function form, first order+ delay model for PI- control is

$$g_1(s) = \frac{k}{(\tau_1 s + 1)} e^{-\theta s}$$

where, k is the process gain, τ_1 is the dominant lag time constant and θ is the effective time delay in the response. Similarly, the second order plus time delay model for PID-control is,

$$g_2(s) = \frac{k}{(\tau_1 s + 1)(\tau_2 s + 1)} e^{-\theta s}$$

here, τ_2 is the second order lag time constant. These process parameters can be obtained from step tests or by approximating the complicated process models using Skogestad half rule [40]. SIMC tuning rules based on the model formulation for a first order process results in a PI controller with settings

$$K_{\mathrm{C}} = \frac{1}{k} \frac{\tau_1}{(\tau_{\mathrm{C}} + \theta)}$$

$$\tau_I = \min \{ \tau_1, 4 (\tau_C + \theta) \}$$

Similarly for a second order process, tuning parameters for a cascade (series) form of the PID controller using SIMC rule are:

$$K_{\mathrm{C}} = \frac{1}{k} \frac{\tau_1}{(\tau_{\mathrm{C}} + \theta)}$$

$$\tau_I = \min\left\{\tau_1, 4\left(\tau_C + \theta\right)\right\}$$

$$\tau_{\mathrm{D}} = \tau_2$$

Thus, using SIMC rule we have only one tuning parameter τ_C i.e. close loop time constant. Skogestad [40] suggests value of τ_C = θ, i.e. effective time delay for a good trade-off between robustness and speed of the response. For τ_C less than θ the controller has fast speed of response and good disturbance rejections but may result in oscillations; while τ_C greater than θ favors stability, robustness and small input variations.

2.4.3 Digital implementation of PID controller

The PID controller in the continuous-time domain is given by Equation 2.2. However, in a digital implementation of the control strategy, the controller inputs and outputs are discrete-time signals rather than continuous signals. There are two alternative forms of the digital PID control equation, the position form and velocity form. In this work, the digital implementation of the PID controller uses velocity form. This section describes the velocity form of the PID controller. Curious readers are referred to standard texts like [35] for detailed discussions on digital PID control.

The purpose of PID control law in Equation 2.2 is to reduce the error $e(t)$ between the measured controlled variable $y_m(t)$ and the setpoint $y_{sp}(t)$, given as

$$e(t) = y_{sp}(t) - y_m(t)$$

The discrete time representation of PID controller in Equation 2.2 at time instant k according to [35] is:

$$u_k = u_{k-1} + K_C\left[(e_k - e_{k-1}) + \frac{\Delta t}{\tau_I}e_k + \frac{\tau_D}{\Delta t}\left(e_k - 2e_{k-1} + e_{k-2}\right)\right] \tag{2.3}$$

Here, Δt is the sampling period i.e. the time between successive measurements of the controlled variable.

2.5 The problem of handling changes in active constraint set

In many process operations, the active constraint set changes as a function of disturbances. The disturbances might change some of the active constraints such that if they were active earlier, they might not be active anymore or other inactive ones earlier might become active now. Thus, when using decentralized single-loop control, this will invoke reconfiguration of control loops to ensure tight control of all the active constraints. Also, changes in the active constraint set might require efforts to identify new self-optimizing variables in the new active region. This is illustrated in the Figure 2.15. Grey shaded region represents the infeasible region. For disturbance d_1 the optimum occurs when constraint g (shown in red line) is active while for disturbance d_2, the constraint g is no longer active. Such process

behaviour, in practice, will require the reconfiguration of control loops since now for disturbance d_2 this problem transforms into an unconstrained optimization problem and we will need to find a self-optimizing variable to achieve optimal plant performance.

Handling the changing set of active constraints is indeed a difficult problem. Several approaches are suggested in the literature for the design of supervisory control layer when active constraint region changes during operation. One such approach by Manum [22] extends the nullspace method by Alstad et al. [2] for determining self-optimizing control variable to cover changes in the active set. This method uses a parametric program to find the active regions and value of controlled variables in each region is used to decide when to switch between regions. Since the number of active regions grows exponentially with the increasing number of constraints; therefore, the size of the problem limits the application of this method by Manum [22]. A survey paper on self-optimizing control by Johannes [13] summarizes all the previous work in this area. It concludes that handling the changing set of active constraints is still one of the difficult issues when using self-optimizing control and remains one of the open issues for further research.

In this work, we have decomposed the disturbance space into different active set regions by solving a numerical optimization problem offline. After that, we have suggested a basic control structure for the nominal operating region. With the disturbances, the active constraint set will change, and therefore we have used selectors logics to switch between the active regions. More on this is covered in Chapter 5.

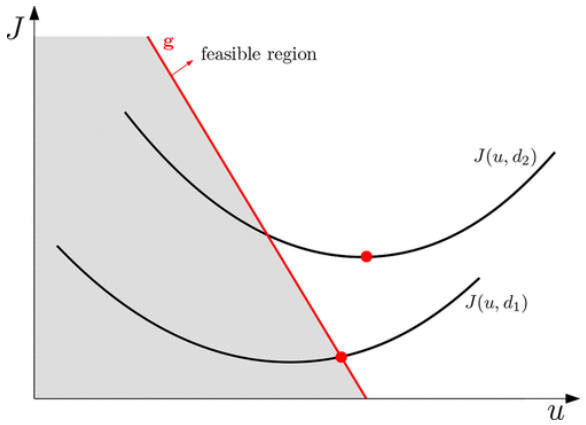

Figure 2.15: Illustration of the problem with changing active constraint set. For d_1 disturbance optimum happens at the constraint whereas for d_2 the optimum is unconstrained [16]

2.6 Design procedure for constraint switching using classical advanced control structures

Reyes Lúa [20] proposed a systematic procedure for constraint switching using advanced control structure. This approach for the design of the supervisory control layer has the following main steps:

- *Step A1: Define all the inputs (MVs) and control objectives (CVs) and distinguish between the CV and MV constraints.*
  The control objectives for the supervisory layer are primary controlled variables identified from Step 3 of the top-down analysis. The supervisory control layer aims to implement this in practice. For a known process, we can define these objectives from the process knowledge and engineering intuition. However, it is also possible to find the control objectives for the supervisory layer by solving an offline steady state optimization problem.

- *Step A2: Define a priority list for the constraints to identify constraints that we can give up to guarantee feasible operation.*
  When the disturbance occurs, the process might move to a different active constraint region, and there are two types of constraints:

  – MV constraint: When a manipulating variable reaches its limiting value than it is no longer possible to utilize it to adjust the control variables. Thus, it means saturated MV is not available for control and the control of the variable paired this MV is lost.

  – CV constraint: When a CV constraint becomes active, then controlling that CV to its limiting value is optimal. This approach is tricky because if a CV that was inactive earlier becomes active now (or vice versa) because of disturbances, then it requires reconfiguration of control loops to maintain optimum operations.

  Thus the following priority list is proposed by Reyes Lúa et al.[21] to guarantee feasible operation:

  – Physical MV inequality constraints: These are physical process limits that we cannot violate at any cost. These include examples like maximum or minimum opening of the valves, maximum pump speed.

  – Critical CV inequality constraints: These constraints are critical, but it might be possible to give them up for a short duration. Typical examples are maximum temperature or maximum pressure.

  – Non-physical MVs and less critical CVs (both equality and inequality constraints): It is possible to give up these constraints. These can be CV setpoints (equality constraints). Non-physical MVs are the input constraints that are not limited by physical limits. Minimum liquid flow in the distillation column to ensure proper wetting can be an example of such non-physical constraint.

  - Desired throughput: When we reach a bottleneck, we can give up the constraint on the desired throughput.
  - Self-optimizing variables: Self-optimizing variables relate to the economics of the operations, and these constraints are most comfortable to give up.

  Usually, when it is not feasible to satisfy all the constraints using the available MVs, then the constraints at the end of the priority list are given up first.

- *Step A3: Identify relevant active constraint switching schemes.*
  Once all the constraints are identified and prioritized from Step A1 and Step A2, we decide the required switches between the active regions. The switching is required when disturbance moves the operating point to a different active constraint region and the priority list from Step A2 helps in identifying the likely switches.

- *Step A4: Propose a control structure for the nominal operating point.*
  Once we finish Step A1-A3 next, we move on to design the control structure for the base case operating point. This base case is the nominal operating point where almost all the constraints in the priority list can be satisfied. In this step, the control structure design follows all the standard guidelines of plantwide control like pair-close rule [43] and input saturation rule [26] to achieve an excellent dynamic response. Input saturation rule recommends that we pair an MV that can saturate to the CV that we can give up.

- *Step A5: Design control structures to handle the constraint switches identified in Step A3.*
  After deciding the control structure for the nominal operating point, we move on to design the control structure for other active constraint regions. There are following ways to decide the switching logic between the active regions:

  - Selector performs CV-CV switching. The systematic procedure proposed by Krishnamoorthy [16] can be used for this task.
  - MV-CV switching is required only when the input saturation rule [26] is not followed. The MV that is likely to saturate should be paired to a less critical CV.
  - MV-MV switching can be done using split range control, valve position control or controllers with different setpoint values [20].

  It is crucial to use anti-windup in all the cases when any available controller is deactivated to ensure that the controller that is not selected does not wind up. Thus for CV-CV switching, anti-windup is used so that the deselected controllers do not wind up. Similarly, in MV-CV switching if we use SRC and selector in combination, then anti-windup is required for the controller that does not manipulate the input from SRC (i.e. controller C_2 in Figure 2.8).

Chapter 3

Basic theory and plant model development

This chapter introduces the reader to the basics of alkaline water electrolysis. Secondly, it explains the mathematical model of the state of the art alkaline water electrolyzer plant. The developed mathematical model presents underlying sub-processes of the physical system (i.e. electrolyzer assembly, lye circulation system, compressor and the gas storage) in detail.

3.1 Technology: Alkaline water electrolysis

Electrolysis is the decomposition of water into hydrogen and oxygen by passing a direct electric current between two electrodes separated by an aqueous electrolyte with good ionic conductivity.

In an alkaline water electrolyzer cell (shown in Figure 3.1), the electrolyte is usually aqueous potassium hydroxide (KOH). The cation i.e. potassium ion K^+ and anion i.e. hydroxide ion OH^- take care of the ionic transport. The anodic and cathodic reactions taking place are:

$$\begin{aligned} &\text{Anode: } 2\mathrm{OH}^-(aq) \rightarrow \frac{1}{2}\mathrm{O}_2(g) + \mathrm{H}_2\mathrm{O}(l) + 2e^- \\ &\text{Cathode: } 2\mathrm{H}_2\mathrm{O}(l) + 2e^- \rightarrow \mathrm{H}_2(\mathrm{g}) + 2\mathrm{OH}^-(aq) \end{aligned} \tag{3.1}$$

For this study, we have considered atmospheric alkaline water electrolyzers. These electrolyzers have operating temperature varying from 70-100 °C and operating pressure between 1 and 30 bars [45]. The electrodes are immersed in an alkaline aqueous solution with weight concentration (20-30 wt.%). Therefore, the electrodes must be corrosion resistant, should have good electrical conductivity and catalytic properties. These properties allows for a better electrochemical transfer.

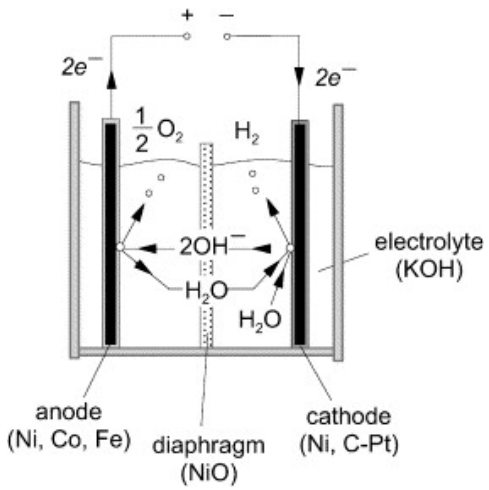

Figure 3.1: Schematic of the alkaline electrolyzer cell [45]

Physically an electrolyzer consists of several cells. There are two electrolyzer stack configurations based on how these cells are connected namely, monopolar and bipolar cell configuration.

In the monopolar configuration, the electrolyzer stack consists of several cells connected in parallel, electrically and geometrically (see Figure 3.2). Hence, the voltage between individual pair of cells is directly equal to the total cell voltage, and the sum of cell current is equal to the total current. In this configuration, the diaphragm separates the anodic and cathodic sections, with an electrode in each section. Therefore, the same electrochemical reaction (reduction/oxidation) occurs on both sides of each electrode.

In bipolar design (see Figure 3.3), individual cells of electrolyzer stack are connected in series. Hence, the total current is directly equal to the current passing through each individual cell and the sum of voltages between individual pairs is equal to the total cell voltage. Bipolar plate separate individual cells in this configuration. This bipolar plate acts as anode for one cell and as cathode for the other cell. Therefore, two different electrochemical reaction occurs on both sides of each bipolar plate.

Most commercial alkaline electrolyzers today are bipolar as they are more compact, gives shorter current paths in electrical wires and electrodes and has better electrolyzer efficiency. However, there are also some disadvantages with the bipolar designs like, parasitic currents which are generated in the cell because of the movement of the ions in the migration electric field and can cause corrosion problems.

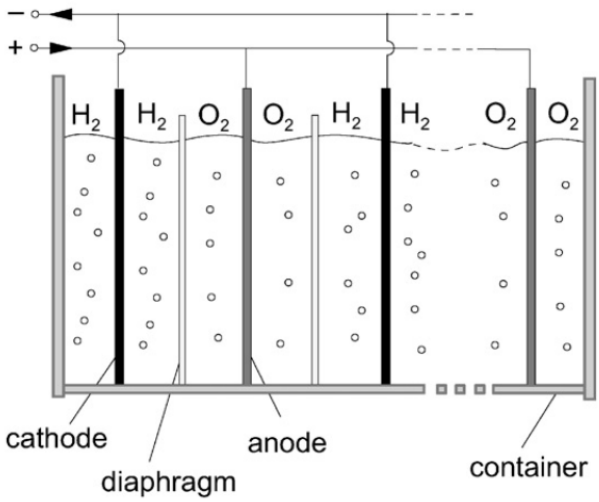

Figure 3.2: Principle of monopolar electrolyzer design [45]

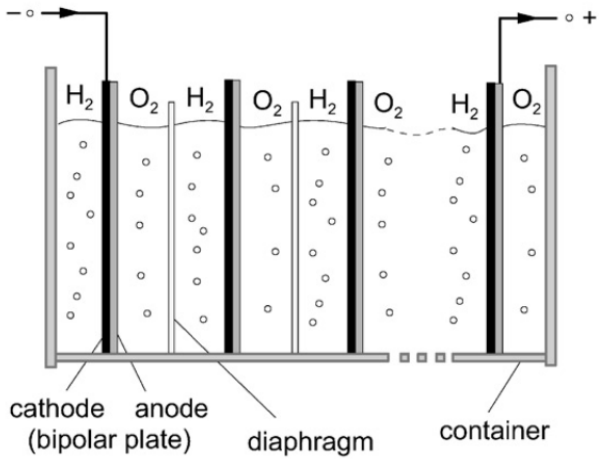

Figure 3.3: Principle of bipolar electrolyzer design [45]

3.2 Mathematical model of electrolyzer plant

This section describes the mathematical equations and assumptions used for modelling of the state of the art alkaline water electrolyzer plant. Firstly, the simplified plant flowsheet is introduced, followed by a detailed description of each of the sub-processes in the flowsheet. The mathematical description of the electrolyzer plant is very similar to the plant

model developed during specialization project [33], and some parts of the plant model are repeated here for the sake of continuity. However, as concluded in the previous study [33], to make the electrolyzer plant model more realistic, detailed modelling of the components in the lye circulation system (i.e. buffer tank and heat exchanger) is added in this work.

Also to be noted, similar to the work during the specialization project [33], here also we have discussed the standalone operation of alkaline electrolyzers, and we disregard any coupling to the power source. This simplification allows us to use input power as a disturbance variable. This is in contrast to a more realistic scenario wherein we might include power system modelling, then the electrolyzer voltage is a disturbance variable. CasADi [3] framework is used for the symbolic modeling in MATLAB. Numerical integrator IDAS is used to perform the simulation of Differential-Algebraic Equations (DAE) system, and the optimization problem is solved using IPOPT solver. Both of these solvers are available in the open-source software SUNDIALS suite [10]. All simulations use a fixed time interval of one second. The MATLAB source code is included in Appendix C.

3.2.1 Plant flowsheet

Figure 3.4 shows a simplified flowsheet for the state of the art alkaline water electrolyzer plant. The flowsheet consists of following basic sections:

- Electric power supply: Renewable sources like wind or solar farms supplies the power required for the electrolysis. The power from renewable sources is available as alternating current. However, the electrolysis process requires direct current (DC); therefore, it is necessary to convert the alternating current (AC) from these power sources to direct electric supply. A rectifier performs this AC to DC conversion. In a practical scenario, multiple electrolyzers share a common transformer to lower the supply voltage to operating voltage (i.e. V_{el}) before rectifier converts the supplied alternating current to direct electric current. Hence, all the electrolyzers with shared transformer operate across a common voltage. A large scale electrolyzer plant will have around 100-150 electrolyzers. Thus flowsheet design with multiple electrolyzers sharing a common transformer is economically more attractive. In contrast, having a separate transformer for each electrolyzer will be an investment intensive decision.

- Electrolyzers: Water is split to hydrogen and oxygen using DC power supply and lye feed (i.e. 30% aq. KOH) as inputs. All the electrolyzers are assumed to have the same number of cells. On commissioning, all the electrolyzers are new and have identical performance characteristics. This is referred to as *State 1* in this study. However, as the plant gets old, electrolyzers are expected to have different degradation profiles and thus will have different performance characteristics. In the study, we refer to this as *State 2*.

- Gas separators and lye circulation system: The gas separators separate produced gas-liquid mixture from anodic (O_2 and lye) and cathodic (H_2 and lye) chambers of the electrolyzers. The liquid lye recovered from gas separators is mixed with

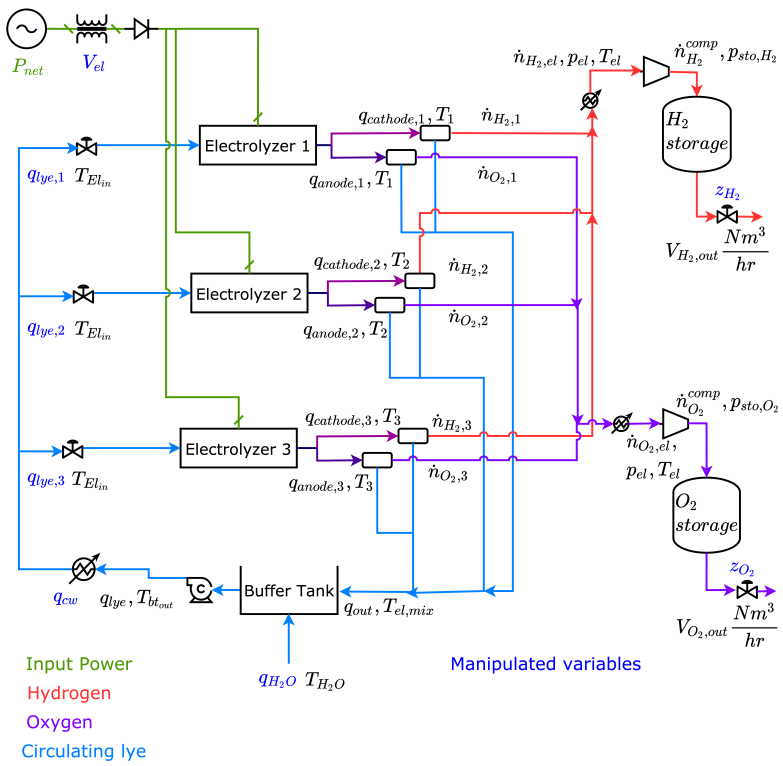

Figure 3.4: Simplified state of the art electrolyzer plant flowsheet

additional water in the buffer tank to maintain electrolyte concentration and then chilled using heat exchangers before it is recycled back and fed to the electrolyzers.

- Gas purification and storage: The hydrogen and oxygen obtained from the gas separators are dried to remove residual traces of electrolyte. Once purified, the gases are then compressed and stored in respective pressurized vessels.

The auxiliary systems, i.e. transformer, rectifier and cooler in the lye circulation system are the supporting components that are needed to produce hydrogen. In this work, have referred to them as the balance of plant (BoP) systems. These systems influence the operational performance of the flowsheet and have a significant contribution to the capital investment required for setting up a state of the art alkaline water electrolyzer plant. The disturbances are mainly because of the intermittencies in the supplied input power (i.e. P_{net}). Following degrees of freedom are available to control the electrolyzer plant (shown with blue colour in Figure 3.4):

- Voltage, V_{el} across electrolyzer. The electrolyzers sharing a common transformer have the same voltage across all the electrolyzers. However, if the plant has a separate transformer for each of the electrolyzer, then electrolyzers can have different operating voltage V_{el}

- Splitted inlet lye flowrate $q_{lye,1}$, $q_{lye,2}$ and $q_{lye,3}$ to the electrolyzers
- q_{cw}, i.e. cooling water flowrate through the heat exchanger in lye circulation loop
- Valve opening of the outlet flow valves for the hydrogen and oxygen storage tanks, z_{H_2} and z_{O_2}
- Makeup water flowrate, q_{H_2O}. Electrolysis process consumes water; therefore, additional water is added to the lye in the buffer tank to maintain the concentration of the electrolyte solution

It is important to note that in this study, lye flowrates $q_{lye,1}$, $q_{lye,2}$ and $q_{lye,3}$ are manipulated individually. Thus they are independent of each other. This simplification means that changing any one of them will change the total lye flowrate across the electrolyzer assembly. Also, in order to maintain the flexibility of the developed model, the 4 sub-processes, i.e. electrolyzer, compressor, lye circulation system and gas storage, are modelled independently. Following sections will describe the model equations and assumptions considered for modelling each of these sub processes.

3.2.2 Electrolyzer modeling

The electrolyzer is modelled as a separate process unit including interconnected thermodynamic, electrochemical and thermal effects. These effects are described in the following sections using the mathematical model described by Ulleberg [45].

Thermodynamic model

Thermodynamics provides a framework for describing reaction equilibrium and thermal effects in electrochemical reactors. It also provides a basis for defining the driving forces for transport phenomena in electrolytes and led to the description of the properties of electrolyte solutions. The Ulleberg's model assumes maximum electrolyzer temperature of 100 °C. In alkaline electrolysis, the total reaction for water splitting is:

$$H_2O\ (\mathrm{l}) + \text{electrical energy} \longrightarrow H_2\ (\mathrm{g}) + \frac{1}{2}\,O_2 \tag{3.2}$$

The thermodynamic model for the above reaction is based on following assumptions,[45]:

- Hydrogen and oxygen are ideal gases
- Water is an incompressible fluid
- The gas and liquid phases are separate

Based on these assumptions, the total change in enthalpy ΔH for splitting water is the enthalpy difference between the products and reactants. This is also true for the change in entropy ΔS.
The change in Gibbs energy ΔG, is expressed by

$$\Delta G = \Delta H - \mathrm{T}\Delta S \tag{3.3}$$

At standard conditions (25°C and 1 bar) the change in Gibbs energy is positive since the splitting of water is non-spontaneous. The standard Gibbs energy for water splitting is $\Delta G°$= 237 kJ/mol. For an electrochemical process operating at constant pressure and temperature, the maximum possible useful work (i.e. the reversible work) is equal to the change in Gibbs energy ΔG. Faraday's law is used to relate the electrical energy (emf) needed to split water, and the chemical conversion rate in molar quantities. The emf for a reversible electrochemical process, or the reversible cell voltage, is expressed by

$$U_{rev} = \frac{\Delta G}{\mathrm{zF}} \tag{3.4}$$

The total amount of energy needed in water electrolysis is equivalent to the change in enthalpy ΔH. The change in Gibbs energy ΔG, includes thermal irreversibilities TΔS, which is equal to heat demand for a reversible process. The standard enthalpy for water splitting is, $\Delta H°$= 286 kJ/mol.

The cell voltage at which the supplied energy participates both in ΔG and TΔS, and there is no heat generation or heat absorption from outside of the system is referred to as thermoneutral cell voltage. The total energy demand ΔH is related to the thermoneutral cell voltage by the expression

$$U_{tn} = \frac{\Delta H}{\mathrm{zF}} \tag{3.5}$$

At standard conditions U_{rev} = 1.229 V and U_{tn} = 1.482, but these will change with temperature and pressure. In the applicable temperature range, U_{rev} decreases slightly with increasing temperature, while U_{tn} remains almost constant. Increasing pressure increases U_{rev} slightly, while U_{tn} remains constant.

Electrochemical model

When direct current is supplied to the electrolysis cell to produce hydrogen, the cell voltage is always higher than reversible cell voltage (U_{rev}) because of irreversibilities. These irreversibilities are mainly overvoltages and parasitic currents that leads to energy losses in the cell and limit the cell efficiency. The overvoltage is composed of ohmic, activation and concentration voltages, i.e.

$$\mathrm{U} = U_{rev} + U_{ohm} + U_{act} + U_{con} \tag{3.6}$$

U_{ohm} is the overvoltage caused because of ohmic losses in the cell elements (electrodes, current collectors, interconnections, etc.). This U_{ohm} is proportional to the electric current that flows through the cell and imparts linear nature of the U-I characteristics curve as shown in the figure Figure 3.5.

U_{act} is the activation overvoltage and is due to electrode kinetics. The charge transfer between the chemical species and the electrodes needs energy. This energy barrier that the charge has to overcome to go from the reactants to the electrodes and vice versa highly depends on the catalytic properties of the electrode materials. It causes an overvoltage across the electrodes, U_{act}. The anodic half-reaction produces a much higher activation

overvoltage than the cathodic half-reaction. U_{act} is highly nonlinear and behaves with a logarithmic tendency for the electric current flowing through the cell [46].

U_{con} is known as concentration voltage; this is because of mass transport processes (convection and diffusion). Transport limitations reduce reactant concentration while creating a higher concentration of products at the interface between the electrode and the electrolyte. However, for alkaline electrolysis, this U_{con} is significantly smaller than U_{ohm} and U_{act} and is, therefore, not considered in this study.

The electrode kinetics is modeled using empirical voltage-current (U-I) relationships as given by Ulleberg [45]

$$\mathrm{U} = U_{rev} + \frac{r_1 + r_2\mathrm{T}}{\mathrm{A}}\,\mathrm{I} + s\ log_{10}\left(\frac{t_1 + \frac{t_2}{\mathrm{T}} + \frac{t_3}{T^2}}{\mathrm{A}}\,\mathrm{I} + 1\right) \tag{3.7}$$

Here, r_1 and r_2 are ohmic resistance parameters, s, t_1, t_2 and t_3 are overvoltage coefficients and A is the electrode area.

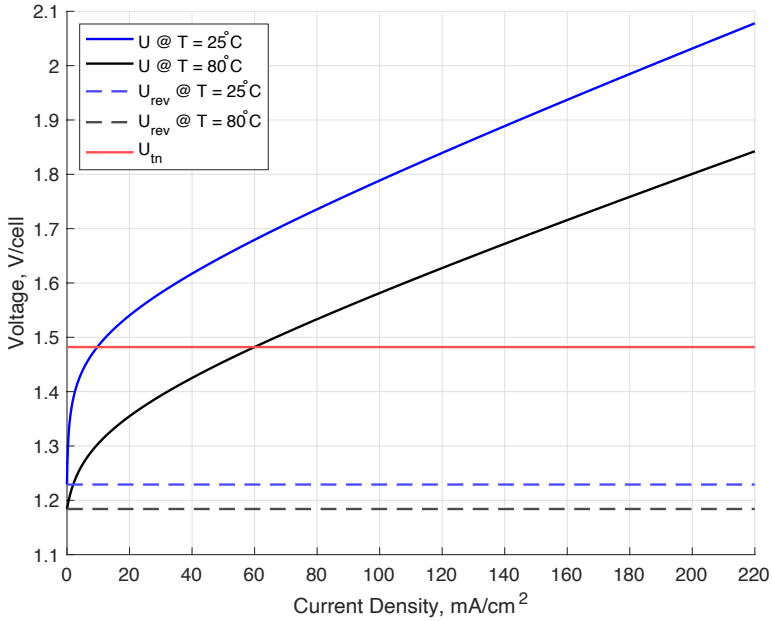

Figure 3.5: U-I curve for a typical electrolyzer

Performance characteristic curve (see Figure 3.5) characterizes the performance of an electrolyzer by plotting the cell voltage against the current density. The electrochemical performance is highly dependent on the process temperature. Figure 3.5 shows U-I characteristic curves of an alkaline electrolyzer for operation temperature of 25 °C and 80 °C. These U-I curves typically use current density to make it possible to compare cells with different parameter values. Increase in temperature for a given current reduces reversible cell voltage,

ohmic and activation overvoltages which also reduces the cell voltage. However, increasing current at a given temperature increases cell voltage and the related overvoltages (see Figure 3.5).

At lower current densities, a logarithmic relationship is observed, which suggests that activation phenomena are predominant while at the higher current density ohmic losses are considerable. The cell voltage and consequently cell power consumption is lower at higher temperatures for any current density.

The U-I curves in Figure 3.5 shows that when the cell voltage is lower than U_{rev}, the cell current is zero, and the electrolysis reaction cannot take place. At lower current densities when cell voltage lies between U_{rev} and U_{tn}, external heating is needed for electrolysis to happen. However, when the cell voltage is higher than U_{tn}, the supplied power is always higher than the minimum power required for the electrolysis process to occur. Hence, the electrolysis process will occur spontaneously. The water electrolysis at these values of cell voltage is exothermic and generates heat which is proportional to (U_k - U_{tn}) where U_k is the operating cell voltage.

Faraday efficiency is defined as the ratio between the actual and theoretical maximum amount of hydrogen produced in an electrolyzer. Faraday efficiency is caused by the parasitic current losses and the contamination of electrolyte because of dissolution of H_2 in O_2. The fraction of parasitic currents to total current increases with decreasing current densities. Also, an increase in temperature will reduce resistance that increases parasitic current and lowers Faraday efficiency. An empirical relation given by [45] accurately depicts this phenomena for a given temperature as:

$$\eta_F = \frac{(\frac{\mathrm{I}}{\mathrm{A}})^2}{f_1 + (\frac{\mathrm{I}}{\mathrm{A}})^2} f_2 \tag{3.8}$$

Here, f_1 and f_2 are parameters related to Faraday efficiency. A is the electrode area and I is the current through the cell. According, to Faraday's law hydrogen production rate in an electrolyzer cell is proportional to transfer rate of electrons at the electrodes, which in turn is equivalent to the electrical current in the external circuit. Hence, hydrogen production rate in an electrolyzer which consists of several cells connected in series, is given as

$$\dot{n}_{H_2} = \eta_F \frac{n_C \mathrm{I}}{\mathrm{zF}} \tag{3.9}$$

Here, z is the number of electrons transferred per reaction and F is the Faraday constant. For water splitting reaction z = 2 and Faraday constant has a value of 96485. The water consumed during the electrolysis process and be calculated from stoichiometry using Equation 3.9 and Equation 3.2 i.e.

$$\dot{n}_{H_2O} = \dot{n}_{H_2} = 2\,\dot{n}_{O_2} \tag{3.10}$$

Another important parameter for electrolyzer is electrical efficiency η_e. Electrical efficiency is defined as the ratio of thermoneutral voltage (U_{tn}) to the cell voltage (U),

$$\eta_e = \frac{U_{tn}}{\mathrm{U}} \tag{3.11}$$

It represents the ratio between energy contained in the hydrogen produced to the energy needed to electrolyze the water consumed during the process. For a given temperature, increasing current density increases cell voltage that in turn reduces electrical efficiency. However, at given current density, increasing temperature reduces cell voltage which increases electrical efficiency.

Thermal model

Thermal balance for an electrolyzer is written per stack basis using lumped thermal capacitance model. The schematic of electrolyzer is shown in Figure 3.6. The energy balance

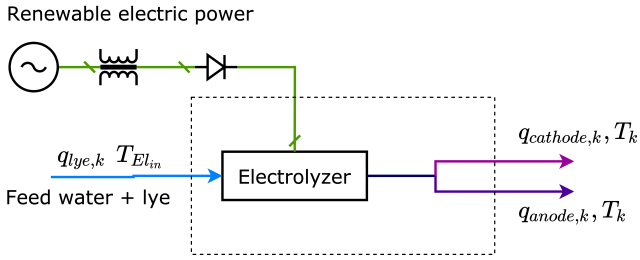

Figure 3.6: Schematic diagram of an electrolyzer

over the control volume, shown with dashed lines in Figure 3.6 is

$$\dot{Q}_{acc} = \dot{Q}_{in} - \dot{Q}_{out} + \dot{Q}_{gen} - \dot{Q}_{loss} \tag{3.12}$$

$\dot{Q}_{acc}$ is the energy accumulated in the electrolyzer, $\dot{Q}_{in}$ is thermal energy of the incoming lye feed, $\dot{Q}_{out}$ is the thermal energy of outlet streams leaving anodic and cathodic sections of the electrolyzer. $\dot{Q}_{gen}$ is the internal heat generated in the electrolyzer when it is operated at voltages above thermoneutral voltage. This is given by the second term on the right hand side of Equation 3.14. $\dot{Q}_{loss}$ is the total heat loss to the ambient by convection and radiation. The heat loss model assumes that heat loss from electrolyzer to the surroundings is taking place by both convection and radiation [25], i.e.:

$$\frac{\dot{Q}_{loss}}{A_s} = \frac{\dot{Q}_{conv}}{A_s} + \frac{\dot{Q}_{rad}}{A_s} = h_c \left(T_k - T_a\right) + \sigma\epsilon \left(T_k^4 - T_a^4\right) \tag{3.13}$$

$\dot{Q}_{conv}$ and $\dot{Q}_{rad}$ are the heat loss to surrounding by convection and radiation respectively. A_s is the active area for radiation and convection, h_c is the convective heat transfer coefficient, $5.5[W/m^2, K]$ [15], σ is the Stefan-Boltzmann constant, $5.67 \times 10^{-8}[W/m^2K^4]$ and ϵ is the emissivity constant. Emissivity ϵ is assumed to be 0.8 and the area of radiating surface A_s is taken to be 0.1 $m^2/kA, cell$ of nominal current [19]. For the state of the art electrolyzer considered in this study, the electrolyzer stack has 230 cells (see Table 4.1) and nominal current of 5.72 kA. Thus, the active surface area for radiation and convection is calculated to be 131.56 m^2.

The thermal balance for the electrolyzer is written as:

$$C_t \frac{dT}{dt} = q_{lye,k} C_{p,lye} \left(T_{El_{ln}} - T_k\right) + n_c \left(U - U_{tn}\right) I_k - A_s \left[h_c \left(T_k - T_a\right) + \sigma\epsilon \left(T_k^4 - T_a^4\right)\right] \tag{3.14}$$

Here, C_t is the overall thermal capacity of the electrolyzer. This study assumes that the thermal capacity of the electrolyzer scales linearly with the power. This simplification allows us to determine C_t for the state of the art electrolyzer. The reported thermal capacity of the PHOEBUS electrolyzer (26 kW, 7 bar) in Jülich [45] is used as basis for the calculation. For the state of the art electrolyzer in this study, the nominal power consumption by electrolyzer is 2.135 MW (see Table 4.1). Thus, overall thermal capacity (C_t) of the state of the art electrolyzer was calculated to be 49,421.3 kJ/K. The ambient temperature (T_a) is 20°C for all the calculations. T_k is the electrolyzer temperature, and U is the cell voltage. Perfect level control for the electrolyte inside the anodic and cathodic chambers is assumed. There is no mass accumulation inside the electrolyzer, and the heat capacity of inlet and outlet lye streams is assumed to be equal.

3.2.3 Lye circulation system

The gas separators separate the gas lye mixture generated from electrolyzers. The separation process is assumed to be ideal, and all the losses are assumed to be negligible to keep the model simple. The enthalpy of gas streams produced (H_2 and O_2) is assumed to be equal to the enthalpy of water consumed during the electrolysis process. In order to maintain the concentration of lye in the electrolyzer system, the liquid streams from the gas separators are collected in the buffer tank, and additional water is added. The heat capacity of 30% KOH electrolyte is taken as 3.1 $J/g°C$ [29].

Calculation of the mixed lye stream temperature from the gas separator
The control volumes considered for modelling of the lye circulation system are marked in Figure 3.7. The temperature of the lye after mixing electrolyte streams from all the electrolyzers is given by

$$T_{el,mix} = \frac{\Sigma(q_{lye,k}.T_k.C_{p,lye}) - \Sigma(q_{H_2O_{loss,k}}.T_k.C_{p,w}) + \Sigma(q_{H_2O_{loss,k}}).(C_{p,w} - C_{p,lye}).T_{ref}}{\Sigma q_{lye,k}.C_{p,lye} - \Sigma q_{H_2O_{loss,k}}.C_{p,lye}} \tag{3.15}$$

where $q_{H_2O_{loss,k}}$ is the rate of the water consumed during electrolysis, this is calculated using Equation 3.10. T_k and $q_{lye,k}$ are the temperature and inlet lye flow rate of the k^{th} electrolyzer. $C_{p,w}$ and $C_{p,lye}$ are the heat capacities of water and the lye solution respectively. T_{ref} is the reference temperature for the enthalpy calculation which is chosen as 25°C.

Mass and energy balances for the buffer tank
The mixed lye stream from the gas separators is collected in the buffer tank. The schematic of the buffer tank is shown in Figure 3.8. To keep the model simple, the temperature of the additional water (i.e.T_{H_2O}) added to the buffer tank is assumed to be equal to the temperature of the liquid in the buffer tank, $T_{bt,out}$.
The **mass balance** for the buffer tank is written as:

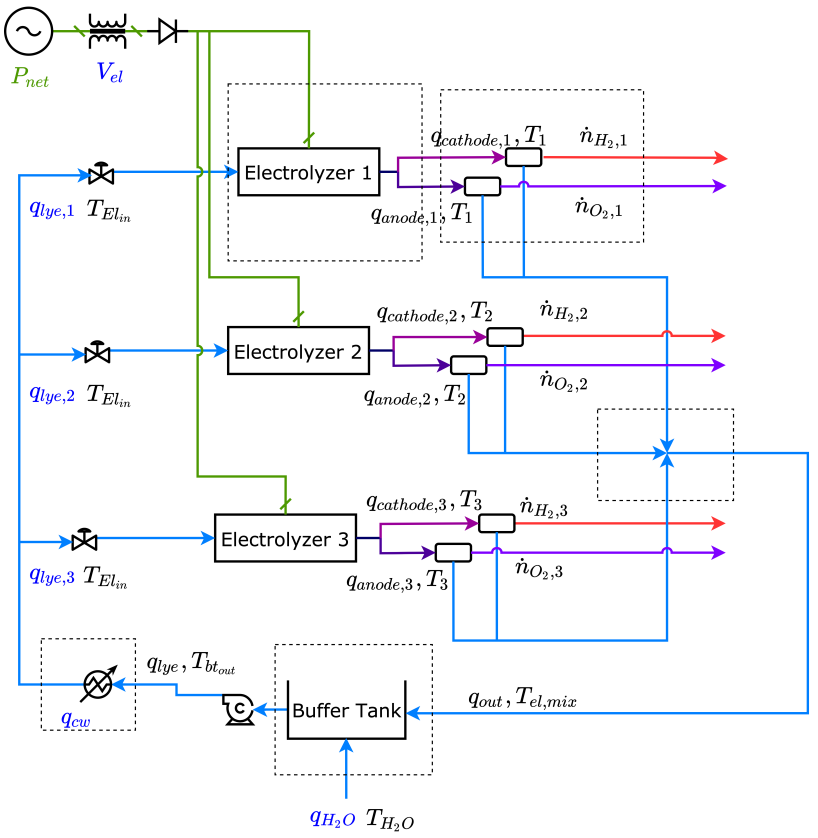

Figure 3.7: Schematic diagram of the lye circulation system. The control volume are marked with a dashed line.

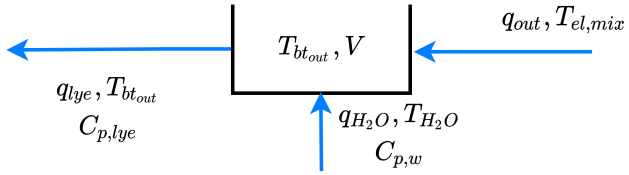

Figure 3.8: Schematic diagram of a buffer tank

$$\rho_{lye} A_{bt} \frac{dh_{bt}}{dt} = q_{out} + q_{H_2O} - q_{lye} \tag{3.16}$$

Where, ρ_{lye} is the density of the lye stream, V is the volume of the buffer tank, A_{bt} is the cross sectional area of the buffer tank, h_{bt} is the height of the liquid in the buffer tank and q_{out}, q_{H_2O} and q_{lye} are the mass flow rates of the respective streams.

The **energy balance** equation for the buffer tank is:

$$\begin{aligned}\frac{d(\rho_{lye}VC_{p,lye}T_{bt_{out}})}{dt} &= q_{out}C_{p,lye}\left(T_{el,mix}-T_{ref}\right)+q_{H_2O}C_{p,w}\left(T_{H_2O}-T_{ref}\right)\\ &\quad -q_{lye}C_{p,lye}\left(T_{bt_{out}}-T_{ref}\right)\end{aligned} \tag{3.17}$$

The right hand side of the equation above can be rewritten as:

$$\begin{aligned}C_{p,lye}T_{bt_{out}}\frac{d\left(\rho_{lye}V\right)}{dt}+\rho_{lye}C_{p,lye}V\frac{d\left(T_{bt_{out}}\right)}{dt} &= q_{out}C_{p,lye}\left(T_{el,mix}-T_{ref}\right)\\ +q_{H_2O}C_{p,w}\left(T_{H_2O}-T_{ref}\right)-q_{lye}C_{p,lye}\left(T_{bt_{out}}-T_{ref}\right)&\end{aligned} \tag{3.18}$$

Simplifying eq.(3.18) using eq. (3.16) we get,

$$\begin{aligned}\rho_{lye}VC_{p,lye}\frac{dT_{bt_{out}}}{dt} &= q_{out}C_{p,lye}\left(T_{el,mix}-T_{bt_{out}}\right)+q_{H_2O}\left(C_{p,w}T_{H_2O}-C_{p,lye}T_{bt_{out}}\right)\\ &\quad -\left(q_{out}C_{p,lye}+q_{H_2O}C_{p,w}-q_{lye}C_{p,lye}\right)T_{ref}\end{aligned} \tag{3.19}$$

Heat exchanger modelling

The heat exchanger in the lye circulation loop is used to cool the lye before it is sent back to the electrolyzers. The schematic diagram of the counter-current flow heat exchanger is given in Figure 3.9.

The equations for energy balances on the hot and cold side of the heat exchanger are [42]:

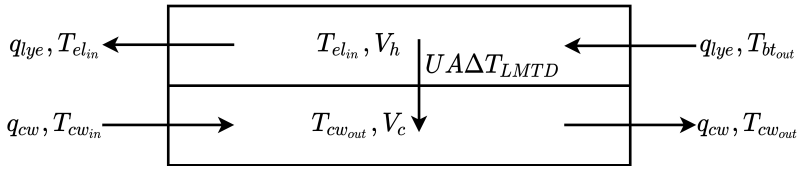

Figure 3.9: Schematic diagram of counter-current flow heat exchanger

$$\left(\rho_{lye}V_hC_{p,lye}\right)\frac{dT_{El_{in}}}{dt} = q_{lye}C_{p,lye}\left(T_{bt_{out}}-T_{El_{in}}\right)-UA\Delta T_{\text{LMTD}} \tag{3.20}$$

$$\left(\rho_{cw}V_cC_{p,cw}\right)\frac{dT_{cw_{out}}}{dt} = q_{cw}C_{p,cw}\left(T_{cw,in}-T_{cw,out}\right)+UA\Delta T_{\text{LMTD}} \tag{3.21}$$

Where, subscript h and c denotes the hot and the cold streams respectively. Further, ρ_{cw} is the density of the cooling water, V_h and V_c are the volumes of the hot and cold side of the heat exchanger respectively, C_p is the heat capacity $[J/g.K]$, q_{cw} is the mass flow rate of cooling water $[g/s]$, U is the heat transfer coefficient, and A is the heat exchanger area. ΔT_{LMTD} is the logarithmic mean temperature difference (LMTD) for counter-current flow and is given by

$$\Delta T_{LMTD} = \frac{\left(T_{bt_{out}}-T_{cw_{out}}\right)-\left(T_{El_{in}}-T_{cw_{in}}\right)}{\ln\left(\frac{T_{bt_{out}}-T_{cw_{out}}}{T_{El_{in}}-T_{cw_{in}}}\right)} \tag{3.22}$$

3.2.4 Compressor

The hydrogen from the atmospheric electrolyzer is at atmospheric pressure and therefore, a compressor is needed to compress hydrogen to high pressure for storage, as shown in Figure 3.4. The compressors available in process industry today can be categorized into two distinct categories: reciprocating and rotary compressors.

The developed electrolyzer plant model, a variable speed centrifugal compressor is considered. For simplicity, the model assumes that is there is perfect control of the compressor power such that all the power required by the compressor to operate is available. Centrifugal compressor is a type of rotary compressor that compresses gas using centrifugal force. In a centrifugal compressor, impeller and the shaft are only moving parts, and it consists of a housing with flow passages for gas. Work is done on the gas by the impeller mounted on a rotating shaft. After this, the gas is discharged at high velocity into a diffuser. In the diffuser, the velocity of the gas is reduced, thus converting its kinetic energy to static pressure.

The calculation of the performance of centrifugal compressors is based on a polytropic compression step. The polytropic process is expressed as

$$PV^x = \text{constant} \tag{3.23}$$

where x denotes the polytropic exponent and P, V represents pressure and volume of the process. This polytropic compression describes the actual process involving both heat transfer and friction happening within the compressor. The relationship between molar flowrate of hydrogen out of the compressor, $\dot{n}_{H2}^{comp}$ and compressor power is [48]

$$\dot{n}_{H2}^{comp} = \frac{\alpha}{w} Power_{comp} \tag{3.24}$$

and

$$w = \frac{xRT_{el}}{x-1}\left[\frac{p_{sto}}{p_{el}}^{\frac{x-1}{x}}\right] \tag{3.25}$$

where w is the polytropic work, α is the compressor efficiency, for this work we have used $\alpha = 0.63$. $Power_{comp}$ is compressor power, T_{el} and p_{el} are inlet gas temperature and pressure to the compressor, p_{sto} is the outlet gas pressure from the compressor and is equal to the hydrogen pressure in the storage tank and R is the gas constant.

As shown in the plant flowsheet, (Figure 3.4) $\dot{n}_{H2}^{comp}$ is assumed to be equal to the total flowrate of hydrogen out from all the electrolyzers, $\dot{n}_{H2}^{el}$. Solving Equation 3.24 and Equation 3.25 for $Power_{comp}$,

$$Power_{comp} = \frac{\dot{n}_{H2}^{comp}}{\alpha}.\frac{xRT_{el}}{x-1}\left[\frac{p_{sto}}{p_{el}}^{\frac{x-1}{x}}\right] \tag{3.26}$$

A centrifugal compressor is a type of rotary compressor and has fixed pressure ratio, therefore $Power_{comp}$ is a dependent variable that is calculated from Equation 3.26. As given

in [5] the polytropic exponent, x is related to adiabatic component γ, through polytropic efficiency E_p as,

$$\frac{x-1}{x} = \frac{\gamma-1}{\gamma} \cdot \frac{1}{E_p} \tag{3.27}$$

The polytropic efficiency of the centrifugal compressor is between 0.7 to 0.75 as mentioned in [5]. For the calculations in this study, it is assumed that E_p = 0.75. The adiabatic exponent γ for hydrogen which is a diatomic molecule is 1.4. For this study, from Equation 3.27 polytropic exponent x = 1.62, which is used for all the simulations.

Similarly, since O_2 is also a diatomic molecule, therefore γ and x for oxygen are same as that for hydrogen. Also, to keep the model simple, we have used Equation 3.26 to calculate power requirements of the oxygen compressor ($\dot{n}_{O_2}^{comp}$ is calculated from stoichiometry).

3.2.5 Gas Storage

Hydrogen Storage

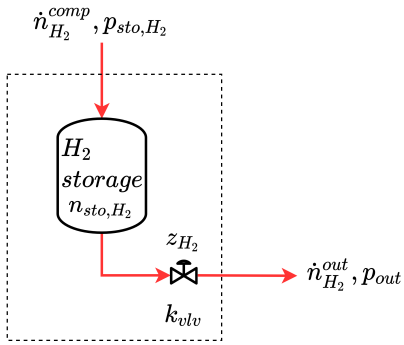

Figure 3.10: Schematic diagram of H_2 gas storage. The control volume is marked with a dashed line

The overall mole balance of a gas storage, as shown in Figure 3.10 can be expressed as

$$\frac{\mathrm{d}n_{sto,H_2}}{\mathrm{dt}} = \dot{n}_{H_2}^{comp} - \dot{n}_{H_2}^{out} \tag{3.28}$$

where n_{sto} is the molar holdup in the storage tank and $\dot{n}_{H_2}^{out}$ is the molar outlet flow. Inserting ideal gas $n = pV/RT$ in Equation 3.28

$$\frac{\mathrm{d}p_{sto,H_2}}{\mathrm{dt}} = \frac{(T_{sto} + 273.15)\mathrm{R}}{V_{sto}}(\dot{n}_{H_2}^{comp} - \dot{n}_{H_2}^{out}) \tag{3.29}$$

where V_{sto} is the storage volume, T_{sto} is the storage temperature in °C and R is the gas constant. The operating pressure storage p_{sto,H_2} is the dynamic state variable.
The outlet molar flow is given by the valve equation

$$\dot{n}_{H_2}^{out} = k_{vlv}\, z \sqrt{p_{sto,H_2} - p_{out}} \tag{3.30}$$

Here k_{vlv} is the valve constant and z is the valve displacement. The storage temperature T_{sto} is assumed to be ideally controlled to 25 °C. The pressure of the electrolyzer is assumed to be constant. The pressure in the vessel increases as it is filled with more gas. However, the pressure of the inlet stream does not change. Note that the pressure of the inlet stream must be higher than the storage pressure in order to get it into the storage.

Oxygen Storage

The oxygen production is calculated directly from the stoichiometry. Stoichiometry of the electrolysis reaction as given by Equation 3.10.
The overall mole balance for oxygen gas storage is given by Equation 3.28, and assuming ideal gas behaviour the equation becomes

$$\frac{\mathrm{d}p_{sto,O_2}}{\mathrm{dt}} = \frac{(T_{sto} + 273.15)\mathrm{R}}{V_{sto}}(\dot{n}_{O_2}^{comp} - \dot{n}_{O_2}^{out}) \tag{3.31}$$

There is no accumulation of gases in the compressor, therefore $\dot{n}_{O_2}^{comp} = \dot{n}_{O_2}^{el}$. Similar to the hydrogen storage, T_{sto} is ideally controlled at 25 °C.
The outlet molar flow is given by the valve equation

$$\dot{n}_{O_2}^{out} = k_{vlv}\, z \sqrt{p_{sto,O_2} - p_{out}} \tag{3.32}$$

Chapter 4

Flowsheet Selection

This chapter investigates different electrolyzer flowsheets designs. The first section discusses the design basis of a state of the art alkaline water electrolyzer plant. This section calculates the flowsheet design parameters like lye flowrate, volume of the gas storage tanks and the buffer tank.

After that in the second section, different flowsheets configurations [1]are introduced. These flowsheets differ based on the design of the BoP systems, the design basis for heat exchanger sizing and can have either fixed or varying inlet lye flow rates. In total, there are 12 different possible flowsheet configurations. The third section presents a steady-state optimization problem for the operation of the electrolyzer plant. In this section, flowsheets are compared based on the results of the steady-state optimization problem.

Finally, the last section concludes the results from the study and recommends a flowsheet design which is practically most attractive. Later on, in the following Chapter 5 the control structure is designed for the selected design.

4.1 Design basis

This study considers a state of the art electrolyzer plant consisting of three alkaline water electrolyzer, lye circulation system, and gas purification and storage systems. The electrolyzer plant has a nominal power consumption of $6.41MW$ ($2.135MW/stack$) when all three electrolyzers are new and are operating at $80°C$. The peak load of the renewable energy system is assumed to be $7MW$. Each electrolyzer stack consists of 230 cells, each with a cell electrode area of $2.6m^2$ connected in series with a common lye inlet and lye/gas outlet system. The design parameters for the state of the art electrolyzer plant are given in Table 4.1, these values are taken from [27] and [30].

[1]The author has used design and configuration interchangeably to refer to the flowsheet of the electrolyzer plant

Table 4.1: Design parameters of the electrolyzer plant

Specification	Value	Unit
Electrolyte	30% aq. KOH	-
Electrode area	2.6	m^2
Number of cells	230	-
Lye circulation rate	6.648	kg/s
Heat capacity of lye	3.101	kJ/kgK
Cooling water flow rate	20.698	kg/s
Heat capacity of water	4.186	kJ/kgK
State 1 production rate	485	Nm^3/hr
Minimum current density	32	mA/cm^2
Maximum current density	198.5	mA/cm^2
Minimum electrolyzer temperature	25	$°C$
Maximum electrolyzer temperature	80	$°C$
State 1 power consumption/ El stack	2.135	MW

At the start of the production, all three electrolyzers are assumed to be new and have identical performance characteristics (see Figure 4.1). The parameter values for the U-I curve of these electrolyzers are given in Appendix A. This state of the electrolyzers plant is referred to as *State 1*. However, during the operation electrolyzers may have different degradation timelines. In that scenario, these electrolyzers will have different performance characteristics. This state is termed as *State 2* of the electrolyzer plant. In this state, the U-I curves (see Figure 4.2) of the electrolyzers will be different. When in state 2, electrolyzer 1 is the new electrolyzer, and electrolyzer 2 and 3 are the degraded electrolyzers. Electrolyzer 1 is the best performing electrolyzer with the highest energy efficiency. In contrast, electrolyzer 3 is a representative of the electrolyzer at the end of the lifetime. Thus, electrolyzer 3 will have the worst performance among all three electrolyzers. The U-I curve parameters for state 2 of the electrolyzer plant are also given in Appendix A.

4.1.1 Calculation of the inlet lye flowrate and volume of gas storage tanks

Inlet lye flowrate to the electrolyzer decides the size of the overall electrolyzer assembly. Additionally, it is an important design parameter to ensure that there is sufficient lye available for the water decomposition reaction. A good estimate of the lye circulation rate can be done by

$$Power.(1 - \eta_e) = q_{lye}.C_{p,lye}.\Delta T \tag{4.1}$$

The above equation assumes that the enthalpy change is because of the change in the electrolyzer temperature, and there is no heat loss to the surroundings. η_e is the electrical efficiency (see Equation 3.11), this is calculated as 0.807 for the state of art electrolyzer

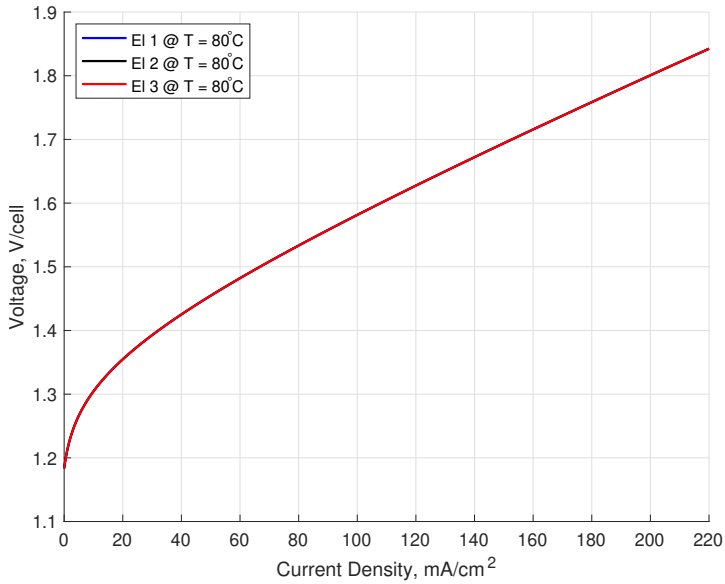

Figure 4.1: Performance characteristics for the new (i.e. *State 1*) electrolyzers

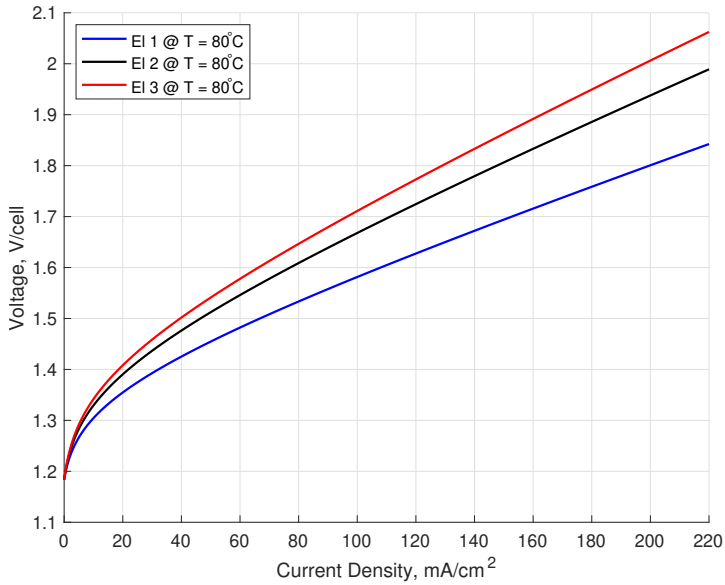

Figure 4.2: Performance characteristics for the degraded (i.e. *State 2*) electrolyzers

based on the supplier's specifications [27]. For practical application, the nominal ΔT of 20 $°C$ is assumed across the electrolyzer for the design. Solving Equation 4.1 the inlet lye circulation rate was calculated as $6.648 kg/s$.

The volume of gas storage tanks is dependent on the maximum design pressure, production rate and the production volume that we desire to store. For the state of the art electrolyzer plant in this study, the gas storage tanks for hydrogen and oxygen are designed to a maximum pressure of 30 bar and can store 6 hr of production volume. Minimum outlet supply pressure is 19 bar for both H_2 and O_2. Hence, given a constant pressure drop of 1 bar across the outlet valve, the minimum storage pressure of 20 bar. For the given specifications the volume of the storage tanks, assuming the ideal gas behaviour is

$$\mathrm{V} = \frac{n_{H2}\mathrm{RT}}{\Delta p} \tag{4.2}$$

where, n_{H_2} are the moles of hydrogen produced in 6 hours during the operation of electrolyzer plant in state 1. Δp is the maximum pressure differential across the outlet valve, i.e. 10 bar. Solving, Equation 4.2 volume of hydrogen tank is calculated to 965 m^3 and from stoichiometry (Equation 3.2) the volume of oxygen storage tank is 482.5 m^3.

4.2 Description of electrolyzer plant flowsheets

The electrolyzer plant flowsheet can have different design specifications. This section outlines all possible flowsheet designs considered in this study. These flowsheet configurations differ based on the following qualities:

- Balance of plant systems: As seen in the previous chapter, the balance of plant (BoP) systems of the electrolyzer plant includes transformer and the heat exchanger in the lye circulation loop. These BoP systems are either shared or installed as separate units for the electrolyzers.
  The flowsheet with **shared BoP systems** is shown in Figure 4.3. In this configuration, the electrolyzers have a shared transformer and lye circulation system. Since all the electrolyzers share a common transformer, the voltage across all the electrolyzers is equal. In such a configuration, according to [33] the best performing electrolyzer dictates the performance of the overall assembly. The lye from the gas separators is collected and recirculated into the electrolyzer stacks after cooling in a big heat exchanger.
  Figure 4.4 shows the flowsheet of an electrolyzer plant with **separate BoP systems**. In this configuration, each electrolyzer has a separate transformer, and a lye circulation system for its operation. The electrolyzers are no longer constrained to operate at the same voltage, and thus higher overall hydrogen production is achievable at the cost of higher initial capital investments. This flowsheet has a higher capital investment cost because of additional investment in auxiliary systems (i.e. the transformer and the heat exchangers in the lye circulation loop).

- Heat exchanger design basis: The heat exchanger is present in the lye circulation loop and is responsible for cooling down the lye before sending it back into the electrolyzer. At the design stage, we have the three specifications for the design of the heat exchanger. First, the temperature difference between hot stream inlet and outlet

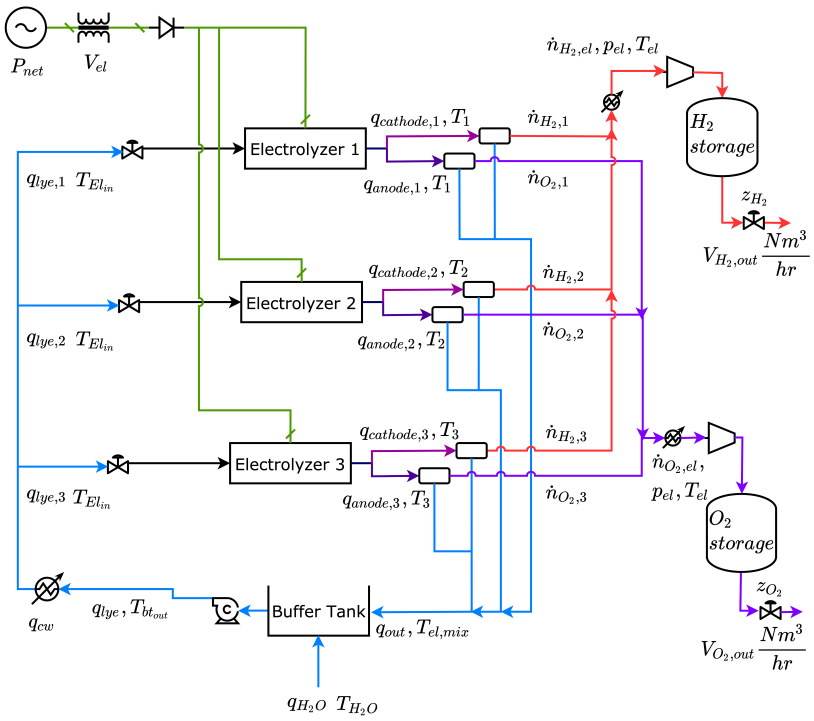

Figure 4.3: Flowsheet 1: Electrolyzer plant flowsheet with shared BoP systems

temperatures is 14 °C. Second, the difference between the cold stream outlet and inlet temperatures is 10 °C. Third, the lye and cooling water flowrate are assumed to be constant (see Table 4.1). With ageing, the electrolyzer energy efficiency reduces, and it will generate more heat. Therefore, the electrolyzer performance will be limited by the maximum operating temperature of the electrolyzer for a given cooling duty of heat exchanger. That is why there is a potential to increase the overall hydrogen production by using larger heat exchangers. The larger heat exchanger will allow to take out more heat from the system as the electrolyzer are aged.
This study includes three different heat exchanger designs. ***HX$_{BoL}$*** is the heat exchanger design based on the cooling demand of the new electrolyzers at the beginning of their lifetime. This heat exchanger design limits the performance of the electrolyzers when the electrolyzers are subsequently degraded, i.e. are in state 2. Second, the oversized heat exchanger design ***HX$_{OS}$*** is the heat exchanger with UA value 75% higher than the HX_{BoL}. The larger heat exchanger size for HX_{OS} allows for higher heat removal in the cooler and thus increases the overall hydrogen production. Lastly, the third heat exchanger ***HX$_{EoL}$*** is designed based on the cooling demand of the degraded electrolyzers at the end of the lifetime. The size of shared heat exchanger (i.e. UA value) for the flowsheet with shared BoP systems and individual heat exchangers (i.e. UA_i) for flowsheet with separate BoP systems is summarized in Table 4.2.

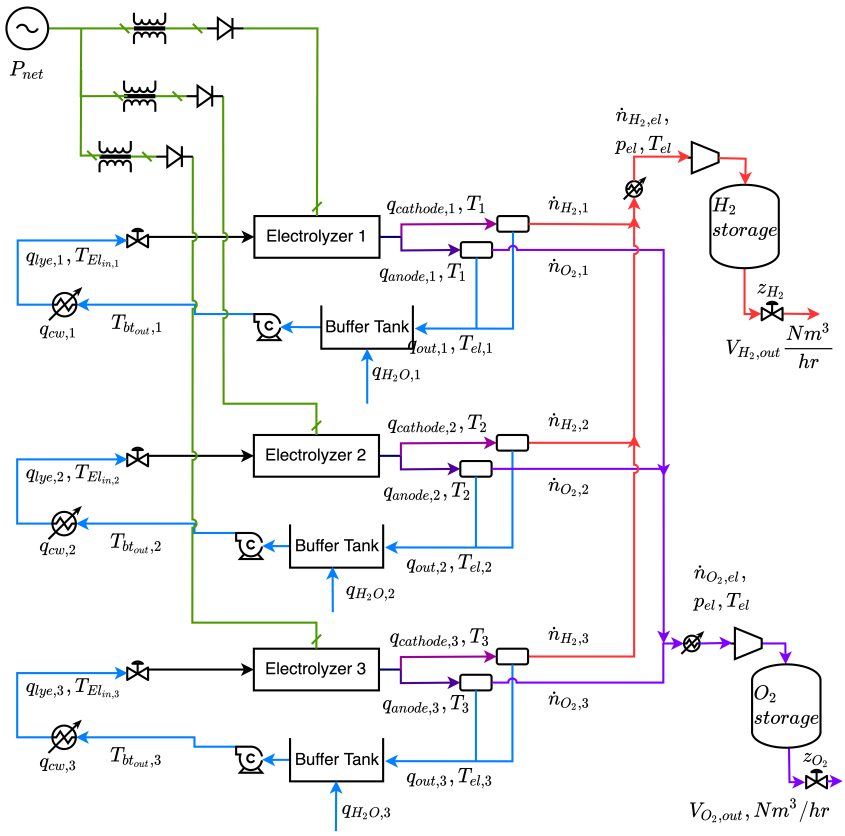

Figure 4.4: Flowsheet 2: Electrolyzer plant flowsheet with separate BoP systems

Table 4.2: Size of the heat exchanger (UA value) for different heat exchanger design basis

Heat exchanger design basis	**Shared HX** UA $[kW/K]$	**Individual HX** UA_i $[kW/K]$ $\forall\ i \in 1,2,3$
New electrolyzers, $\boldsymbol{HX_{BoL}}$	15.21	5.07
Oversized design, $\boldsymbol{HX_{OS}}$	26.61	8.87
Degraded design, $\boldsymbol{HX_{EoL}}$	20.48	6.83

- Variability of inlet lye flowrate: The lye coming into the electrolyzers can be either fixed ($\boldsymbol{q_{lye,\,fix}}$) or can be varying ($\boldsymbol{q_{lye,\,var}}$). Fixing the inlet lye flowrate makes the operation of the electrolyzers more constrained and thus is expected to decrease the overall hydrogen production. This reduction in the performance is because, with the fixed inlet lye flowrate, the degraded electrolyzers have limited flexibility to alter their operating temperatures. However, the electrolyzer plant flowsheets with fixed inlet lye flowrate are attractive because of the possibilities of a simpler control struc-

ture design that might require less equipment and thus lower investments.
This work studies the electrolyzers plant flowsheets with both fixed and variable inlet lye flowrate. The inlet lye flowrate is fixed to the nominal values for the respective flowsheets when all the electrolyzers are new.

Therefore, depending on features of the constituent elements of the flowsheet, there are in total $2 \times 3 \times 2 = 12$ possible flowsheet designs. Each individual electrolyzer flowsheet configuration is represented using $\mathbf{F_{1\text{-}2}}$ $\mathbf{HX_{BoL/OS/EoL}}$ $\mathbf{q_{lye,\ var/fix}}$. Following nomenclature is used to describe the identification elements for flowsheet configuration:

- $\mathbf{F_1}$ represents the flowsheets with *shared BoP systems* whereas the flowsheets with *separate BoP systems* are indicated as $\mathbf{F_2}$.

- $\mathbf{HX_{BoL}}$ represents that the heat exchanger used for the flowsheet is designed based on the cooling requirement of the new electrolyzers. $\mathbf{HX_{OS}}$ denotes the oversized heat exchanger design and $\mathbf{HX_{EoL}}$ indicate that the heat exchanger design is based on the cooling demand of the degraded electrolyzers.

- $\mathbf{q_{lye,\ var}}$ is representative of the flowsheet in which the inlet lye flowrate is varying whereas $\mathbf{q_{lye,\ fix}}$ indicates that the flowsheet has a fixed inlet lye flowrate.

Hence $\mathbf{F_2}$ $\mathbf{HX_{EoL}}$ $\mathbf{q_{lye,fix}}$ represents the electrolyzer flowsheet having separate BoP systems and heat exchanger design based on the cooling demand of the degraded electrolyzer and having a fixed inlet lye flowrate.

4.3 Steady state optimization

This section discusses the steady-state optimization results for the electrolyzer plant. The electrolyzer plant model developed in the previous chapter is used to solve the nonlinear steady-state optimization (steady-state RTO) problem for all the flowsheet configurations outlined before. The objective is to maximize the production of the hydrogen from the plant. The steady-state solution is obtained for different values of the total input power, P_{net}.

The operational objective of the electrolyzer plant to achieve maximum overall hydrogen production from all the three electrolyzers.

4.3.1 Operational constraints

Flowsheet 1: Electrolyzer plant with shared BoP systems

The input constraints for the electrolyzer plant flowsheet with shared BoP (see Figure 4.3) systems are:

$$\begin{aligned} 0.5\frac{kg}{s} \leq q_{lye,k} \leq 10\frac{kg}{s} \\ 10^{-5}\frac{kg}{s} \leq q_{cw} \leq 80\frac{kg}{s} \\ 0 \leq z_{H_2} \leq 1 \\ 0 \leq z_{O_2} \leq 1 \end{aligned} \tag{4.3}$$

Where, $q_{lye,k}$ is the lye flowrate at the inlet of the k_{th} electrolyzer, q_{cw} is the cooling water flow rate in the heat exchanger present in the lye circulation loop and z_{H_2}, z_{O_2} are the outlet valve openings for the hydrogen and oxygen storage tanks. Also, the process constraints are:

$$\begin{aligned} 32\frac{mA}{cm^2} \leq I_{den,k} \leq 198.5\frac{mA}{cm^2} \\ 25°C \leq T_k \leq 80°C \\ T_k - T_{El_{in}} \leq 30°C \end{aligned} \tag{4.4}$$

Here, $I_{den,k}$ is the current density of electrolyzer and should be within these limits because at low current densities, the electrolyzer performance is poor due to the gas permeation through the membrane and leakage current at the stack level [4]. This causes significantly higher specific electricity consumption for lower current density values. On the other hand, the higher current densities causes high temperatures in the electrolyzer which leads to high corrosive effects of the electrolyte [14]. For the similar reasons, there are temperature limits on the electrolyzer temperature, T_k. The inlet lye feed coming in the electrolyzer has to be sufficiently hot so that temperature gradients inside the electrolyzer can be avoided. This is achieved by ensuring that the difference between the inlet lye temperature ($T_{El,in}$) and electrolyzer temperature (T_k) is always less than 30 °C.

Flowsheet 2: Electrolyzer plant with separate BoP systems

Similar to the shared BoP systems flowsheet, the input constraints for the flowsheet 2 (see Figure 4.4) are:

$$\begin{aligned} 0.5\frac{kg}{s} \leq q_{lye,k} \leq 10\frac{kg}{s} \\ 10^{-5}\frac{kg}{s} \leq q_{cw,k} \leq 26.67\frac{kg}{s} \\ 0 \leq z_{H_2} \leq 1 \\ 0 \leq z_{O_2} \leq 1 \end{aligned} \tag{4.5}$$

Also, the process constraints are:

$$\begin{aligned} 32\frac{mA}{cm^2} \leq I_{den,k} \leq 198.5\frac{mA}{cm^2} \\ 25°C \leq T_k \leq 80°C \\ T_k - T_{El_{in,k}} \leq 30°C \end{aligned} \tag{4.6}$$

4.3.2 Steady state result analysis

Turndown ratio: The operational flexibility of the electrolyzer plant is an important characteristics that governs its application in the renewable energy systems. This flexibility can be assessed from the turndown ratio which is defined as the ratio of the minimum hydrogen produced by the electrolyzer plant to the hydrogen produced by the electrolyzer plant with nominal power consumption. Therefore flowsheet 1 and flowsheet 2 are compared for the turn down ratio, as it provides an important metrics to comment on the operational aspects of the electrolyzer flowsheet. Thus lower value of turndown ratio corresponds to higher flexibility and similarly, higher value for turndown ratio translates to less flexible operations.

Table 4.3: Comparison of plant flowsheets with shared and separate BoP systems for nominal H_2 production and turndown ratio

Plant flowsheet	**Nominal H_2 production,** Nm^3/hr	**Turndown ratio**
$F_1HX_{BoL}q_{lye,var}$ *State 1, Flowsheet 1*	1455	16.2%
$F_1HX_{BoL}q_{lye,var}$ *State 2, Flowsheet 1*	1219	22.3%
$F_2HX_{BoL}q_{lye,var}$ *State 1, Flowsheet 2*	1455	16.2%
$F_2HX_{BoL}q_{lye,var}$ *State 2 Flowsheet 2*	1296	19.3%

The flowsheet 1 has a nominal hydrogen production of 1455 Nm^3/hr and 1219 Nm^3/hr while in state 1 (i.e. with new electrolyzers) and state 2 (i.e. with subsequently degraded electrolyzers) respectively (see Table 4.3). However, for flowsheet 2 with the degraded electrolyzers, i.e. in state 2, the hydrogen production rate is 1296 Nm^3/hr. The hydrogen production rate for flowsheet 2 is higher than flowsheet 1 because unlike flowsheet 1 (shared BoP) the electrolyzers in flowsheet 2 (separate BoP) are not constrained by the shared transformer and cooler. Therefore, all the electrolyzers in the flowsheet 2 can operate across different voltage and can maximize their performances.

Moreover, we see that in *State 1* both flowsheets have almost identical performances (see Table 4.3). Thus, if the electrolyzers are new, flowsheet 1 is the preferred plant design because of its lower investment costs due to shared BoP systems.

The initial turndown ratio for flowsheet 1 is 16.2%. However, for the flowsheet 1 in state 2, the turndown ratio is observed to increase to 22.3%. This suggests that with ageing, the operational flexibility of the electrolyzer plant is reduced. The decrease in performance is because the old electrolyzers will have reduced energy efficiency and will generate more heat. However, as there are limits on the operating temperature, the degraded electrolyzers will operate at lower current densities and thus will produce less hydrogen. Similarly, the turndown ratio for the flowsheet 2 at state 1 and state 2 is 16.2% and 19.3% respectively.

Thus, compared to flowsheet 1, flowsheet 2 has higher operational flexibility throughout the lifetime of the electrolyzer plant. Hence, we can conclude that flowsheet 2 having separate transformer and heat exchanger for each electrolyzer has higher operational benefits when compared to flowsheet 1, which has lower capital investment costs.

Also, the flowsheet 1 and flowsheet 2 are compared for different design basis for the heat exchanger (see Figure 4.5). The vertical axis represents % loss in the production, which is incurred with flowsheet 1 compared to flowsheet 2. The non-negative % loss represents that flowsheet 2 has higher hydrogen production rate than flowsheet 1, which is observed for all three heat exchanger designs. As the electrolyzer plant gets old (i.e. state 2 of the flowsheets), the degraded electrolyzers will generate more heat because of reduced energy efficiency. Therefore, the performance of degraded electrolyzers will be limited by the maximum operating temperature of the electrolyzer. The larger heat exchanger size (i.e. HX_{OS}) allows for more cooling in the lye circulation loop. Thus, the degraded electrolyzers in State 2 will operate at the higher current density for the longer part of their lifetime. This increases the overall hydrogen production for flowsheets with larger heat exchanger. Hence, the loss in production for flowsheet 1 w.r.t flowsheet 2 for oversized heat exchanger design (HX_{OS}) is higher compared to the other two designs (i.e. HX_{EoL} and HX_{New}) as seen in Figure 4.5. As a side note, it should also be noted that the loss is 100% for lower input power as this corresponds to the situation when there is no feasible solution for flowsheet 1 while flowsheet 2 is still feasible (see Figure 4.5).

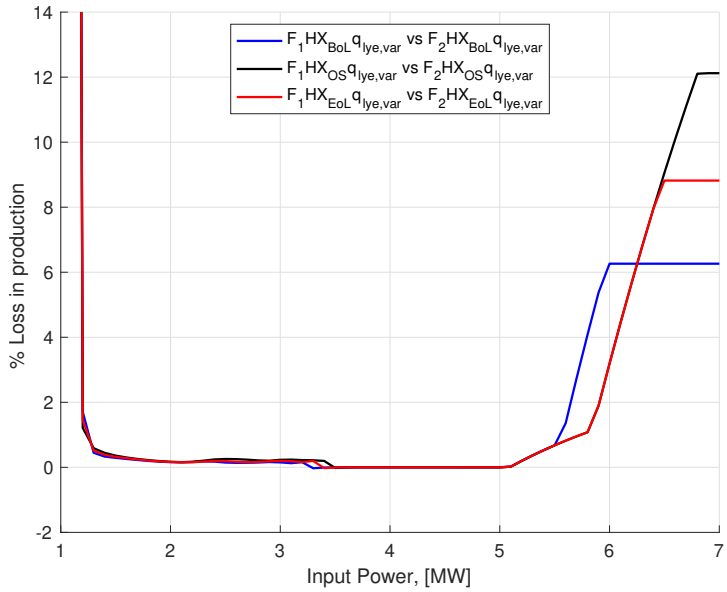

Figure 4.5: Comparison of the loss in production between flowsheet 1 (shared BoP) vs flowsheet 2 (separate BoP)

Fixing the inlet lye flowrate will decrease the hydrogen production of the electrolyzer plant

because of reduced flexibility. Therefore, the flowsheet with separate BoP systems having an oversized heat exchanger and varying inlet lye flowrate (i.e. **F_2 HX_{OS} $q_{lye,var}$**) is the best flowsheet design. This is also corroborated from Appendix B which summarizes the total hydrogen production corresponding to different input power from all the flowsheet design for both state 1 and state 2 of the electrolyzer plant.

It should be noted that flowsheet **F_2 HX_{OS} $q_{lye,var}$** has separate BoP systems, largest heat exchanger (i.e. HX_{OS}) and varying inlet lye flowrate. Therefore it will have the highest investment costs. That is why, before going with this design it is important to compare this design to all the other flowsheet designs.

Comparison of electrolyzer plant designs in *State 2* w.r.t flowsheet F_2 HX_{OS} $q_{lye,var}$
In order to make systematic comparisons w.r.t. F_2 HX_{OS} $q_{lye,var}$, the %loss in performance is defined as:

$$\%\text{Loss}_{\text{f,i,j}} = \frac{\dot{n}_{H_2,el}|_{\text{F}_2\text{HX}_{\text{OS}}\text{q}_{\text{lye,var}}} - \dot{n}_{H_2,el}|_{\text{F}_\text{f}\text{HX}_\text{i}\text{q}_{\text{lye,j}}}}{\dot{n}_{H_2,el}|_{\text{F}_2\text{HX}_{\text{OS}}\text{q}_{\text{lye,var}}}} \times 100 \tag{4.7}$$

The subscript f, i and j represents flowsheet, heat exchanger design basis and variability of inlet lye flowrate respectively.

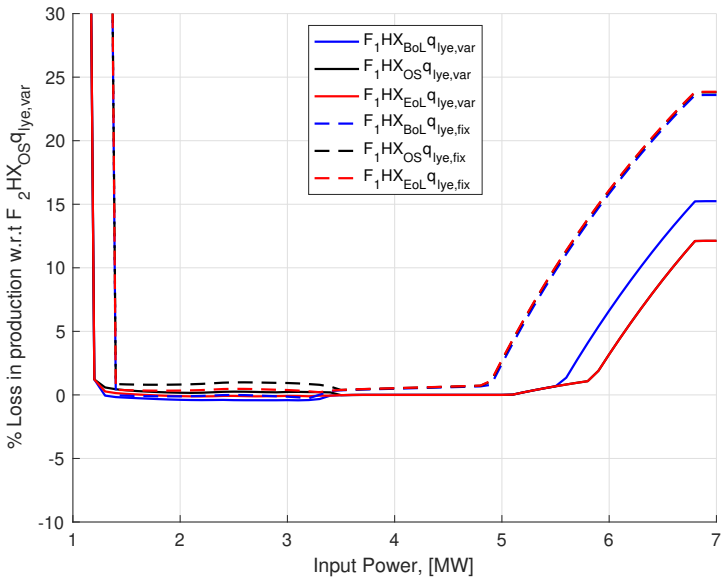

Figure 4.6: *State 2* %loss comparison of all flowsheets with shared BoP systems w.r.t most investment intensive design (i.e. flowsheet F_2 HX_{OS} $q_{lye,var}$)

Figure 4.6 summarizes the %loss in the performance of flowsheet 1 (shared BoP) compared to the flowsheet F_2 HX_{OS} $q_{lye,var}$. The nomenclature decided earlier identifies the flowsheets. For flowsheet 1, the loss is minimum for heat exchanger design, HX_{EoL} and

varying inlet lye flowrate. This is shown in the solid red line in Figure 4.6. Also, it should be noted here that the plot for the flowsheet with oversized heat exchanger design and varying inlet lye flowrate (shown with black solid line in Figure 4.6, F_1 HX_{OS} $q_{lye,var}$) is identical to the red solid line representing flowsheet F_1 HX_{EoL} $q_{lye,var}$. This suggests that there is an upper limit to which the increasing heat exchanger size is going to increase the production for flowsheet 1. The electrolyzers in flowsheet 1 are sharing BoP systems; therefore, they are constrained by the common operating voltage, which is decided by the best performing electrolyzer (i.e. electrolyzer 1 in this case study). That is why larger heat exchanger size, i.e. HX_{OS} does not increase the production of overall hydrogen in the *State 2* of the flowsheet 1 and F_1 HX_{EoL} $q_{lye,var}$ is the best flowsheet design for the flowsheet with shared BoP systems.

The higher losses in the performance for fixed inlet lye flowrate (shown with dashed lines in Figure 4.6) Figure 4.6) reiterates the result established earlier, that fixing the inlet lye flowrate for the flowsheet with shared BoP systems is not a good idea.

The loss in production is highest at maximum input power, i.e. 7 MW, because flowsheet 1 (shared BoP) has lower nominal power consumption than flowsheet 2 (separate BoP). The nominal power for flowsheet 1 corresponds to the input power after which we observe a steep increase in the loss% (like 5.8 MW for the solid red plot in Figure 4.6). This is because of the reason that separate BoP systems enable flowsheet 2 to operate at higher input power, thus allowing it to produce more hydrogen. Thus, flowsheet 2 has higher nominal power than flowsheet 1 (which is 6.8 MW for flowsheet F_2 HX_{OS} $q_{lye,var}$). However, for all the input power values less than the nominal power consumption of flowsheet 1, the loss in the production is almost zero, and both the flowsheet designs have near-identical performances (see Figure 4.6). Therefore, it is concluded that higher capital investments for flowsheet 2 w.r.t flowsheet 1 will pay off only if the electrolyzer plant is expected to operate at input powers higher than the nominal power for flowsheet 1 for most of the time. Similarly, the %loss in the performance of electrolyzer plant with separate BoP systems w.r.t most investment intensive design (i.e. flowsheet F_2 HX_{OS} $q_{lye,var}$) is shown in the Figure 4.7. Contrary to the flowsheet 1, for the flowsheet 2, the electrolyzers have separate BoP systems and thus can reach maximum possible current densities. That is why the heat exchanger size has a direct influence on the H_2 production rate. Thus larger heat exchanger size, i.e. HX_{OS} has the highest hydrogen production rate and thus has least performance loss.

It is interesting to note that in flowsheet 2 with separate BoP systems, the effect of fixing the inlet lye flowrate is insignificant (max. around 2%, see Figure 4.7). This is because, in the flowsheet 2, individual electrolyzers are not restricted to operate at a fixed voltage dictated by the best performing electrolyzer. This enables degraded electrolyzers to achieve the maximum temperature and thereby the loss in the production because of fixed lye flowrate is minimal. Hence it can be concluded that fixing a lye flowrate is near-optimal for the plant flowsheet with separate BoP systems and will simplify the control structure design. However, for plant flowsheet with a shared BoP system, the losses because of fixed lye flowrate are significant at higher input power. Therefore, it will be advisable to operate

the plant at varying lye flowrate if flowsheet 1 is selected.

The %loss in the production are higher for input powers around $7MW$ because of the lower nominal power consumption for rest of the flowsheet 2 designs when compared to most investment intensive design i.e. F_2 HX_{OS} $q_{lye,var}$. Thus, if the electrolyzer plant is expected to receive lower input powers for most of the time then all the flowsheet designs with separate BoP systems are equally good (w.r.t F_2 HX_{OS} $q_{lye,var}$).

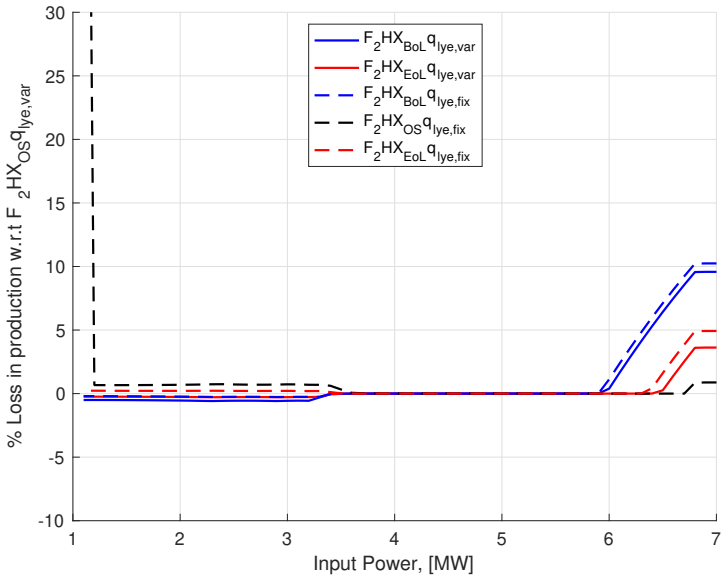

Figure 4.7: *State 2* %loss comparison of all flowsheets having separate BoP systems w.r.t most investment intensive design (i.e. flowsheet S_2 F_2 HX_{OS} $q_{lye,var}$)

Comparison of electrolyzer plant designs in *State 1* w.r.t flowsheet F_2 HX_{OS} $q_{lye,var}$
In the previous section, we established that higher hydrogen production is achieved for the larger size of the cooler in lye circulation loop with varying inlet lye flowrate. Thus, flowsheet design F_2 HX_{OS} $q_{lye,var}$ is expected to have maximum hydrogen production rate in state 1 as well. Also, from the previous discussion, we know that when all the electrolyzers are new, both flowsheet 1 (shared BoP) and flowsheet 2 (separate BoP) have identical performances.

However, it is important to note that at lower input power ($P_{net} \leq 3.9\ MW$) flowsheet F_2 HX_{BoL} $q_{lye,var}$ has maximum hydrogen production rate. This flowsheet has maximum negative loss w.r.t F_2 HX_{OS} $q_{lye,var}$ (see Figure 4.8 and Figure 4.9). This is an artefact of the electrolyzer plant model developed for this study. At lower input power, larger heat exchanger size will have higher cooling and thus will lead to reduced electrolyzer operating temperatures and hence will have lower overall hydrogen production. However this is in contradiction to the practical operation scenario, wherein at lower input power we

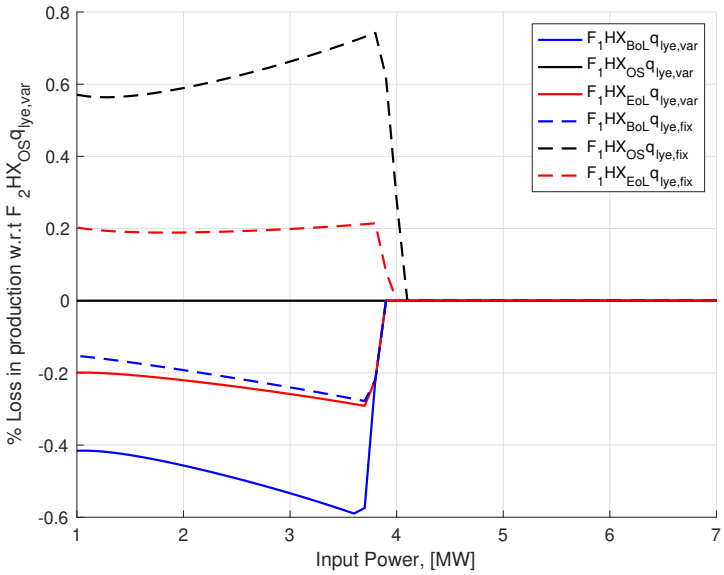

Figure 4.8: *State 1* %loss comparison of all flowsheets having shared BoP systems w.r.t most investment intensive design (i.e. flowsheet F_2 HX_{OS} $q_{lye,var}$)

will shut off the cooling in the lye circulation loop. Thus, with no cooling, all the three heat exchanger designs will have identical performances even at low input power. This is not included in the model because of the associated numerical difficulties with the zero coolant flowrate while solving the flowsheet optimization problem.

Hence, it can be concluded that the decision for optimal flowsheet selection should be taken based on the performances of the flowsheets in state 2. The results from state 1 can be used to comment on the practical limitations of the developed mathematical model at lower input powers.

4.4 Conclusions: Selection of optimal flowsheet design based on steady state optimization results

After the study of all 12 possible configurations for the electrolyzer plant flowsheets, the following conclusions are drawn

- Flowsheet 2 (i.e. separate BoP systems) has a higher hydrogen production rate than flowsheet 1 (shared BoP systems) when operating at input powers higher than nominal power consumption for flowsheet 1. Therefore, additional capital expenditures in flowsheet 2 will be beneficial if the renewable power source is expected to provide input power higher than the nominal power consumption of flowsheet 1 for most of the time.

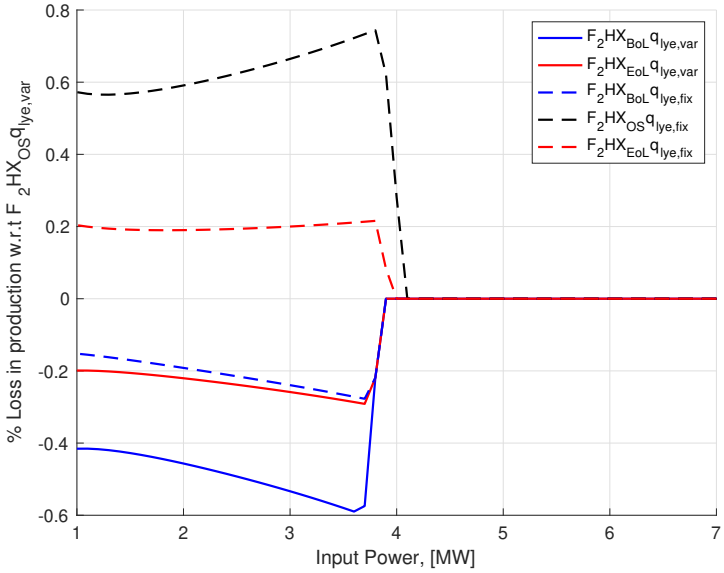

Figure 4.9: *State 1* %loss comparison of all flowsheets having separate BoP systems w.r.t most investment intensive design (i.e. flowsheet F_2 HX_{OS} $q_{lye,var}$)

- For all the input power values lower than the nominal power consumption of flowsheet 1, both the flowsheets have almost identical performance. Therefore if the supplied power from a renewable source is less than the nominal power consumption of the flowsheet 1, then flowsheet 1 is the better design because of the lower capital investment and almost identical performance compared to flowsheet 2.
- Heat exchanger design has a significant impact on the performance of both the flowsheets and a higher hydrogen production rate is achieved with the larger heat exchanger sizes. However, there is an upper limit to which the increasing heat exchanger size is beneficial. For flowsheet 1 (i.e. shared BoP) the best heat exchanger design is decided based on the cooling demand of the electrolyzers at the end of their lifetime (i.e. HX_{EoL}). Contrary to this, for flowsheet 2, the heat exchanger design based on oversized design HX_{OS} is identified as the best design.
- The loss in the performance because of fixed inlet lye flowrate is significant for flowsheet 1 (i.e. shared BoP systems), especially at higher input power. That is why fixing lye flowrate for flowsheet 1 is a bad idea.
- For flowsheet 2 (i.e.separate BoP systems) fixing the lye flowrate has insignificant losses in the performance and has the potential benefits of the simple control structure design. Hence for further analysis on flowsheet 2, inlet lye flowrate can be fixed to a constant value.

Chapter 5

Online process optimization for electrolyzer plant using classical advanced control structures

In this chapter, a control structure for the state of the art electrolyzer plant flowsheet is designed. As mentioned previously in Chapter 4, different flowsheet configurations are possible based on design decisions. Hence, in this chapter control structure is suggested for one selected flowsheet design i.e. flowsheet $\mathbf{F_1\ HX_{EoL}\ q_{lye,var}}$. Furthermore, the electrolyzers in flowsheet $F_1\ HX_{EoL}\ q_{lye,var}$ are considered to be in *State 2*, i.e. they are degraded and have non identical performances.

The supervisory control layer is designed using classical advanced control structures[1]. Operating regions and the active constraints are affected by the changes in the total input power to the electrolyzer plant. Therefore, it is necessary to find a control structure that maintains the steady-state optimal operation in different active constraint regions. In this work, the procedures described in Chapter 2 are applied to define such control structure.

5.1 Introduction

The control layer can be decomposed into supervisory control layer and regulatory control layer. The objective of supervisory control layer is mainly related to the economics of the plant. Thus the supervisory layer control structure deals with the implementation of the near-optimal operation. While regulatory layer ensures the stability and works to keep the process stable at the operating point.

[1]The author has used term classical advanced control structures to refer to selectors, split range control, valve position control, etc. These are discussed in detail in Chapter 2

Figure 5.1 shows a typical hierarchical decomposition in optimization-based control. The optimization layer has the setpoints for the control variables (CV^{sp} or y^{sp}) as degrees of freedom. The control layer aims to keep outputs y at the optimal values (i.e. y^{sp}) computed by the RTO layer. However, the practical implementation of the optimization-based control requires identification of the actual plant model using process data. This model requires significant development time and regular maintenance to match the actual plant behaviour. Therefore, chemical industry is more inclined to use single loop control structures implemented using PID controllers. Also, the human aspects of such simple feedback controllers are higher since it is by far most trusted and used technology in practice [34].

The objective of this chapter is to move the optimization layer into the control layer.

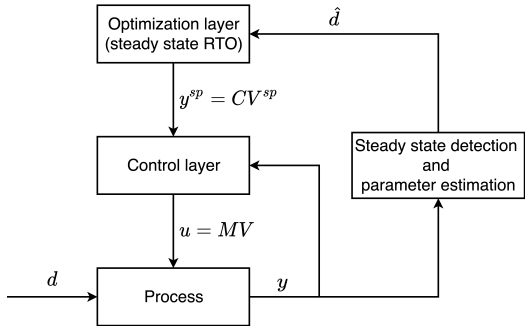

Figure 5.1: Hierarchical decomposition in optimization based control

This work suggests a control structure for the state of the art alkaline water electrolyzer plant using classical advanced control structures. The control elements like selectors and split range control are used to steer the plant to near-optimal performances when disturbances occur. Also, it is essential to be noted here that this work does not aim to convince the reader to choose either one of the PI(D) based control structures or model-based optimization routines (like MPC). Instead, this work should be viewed as an attempt to demonstrate that the systematic procedures given in research literature like [16] and [20] for PI(D) based control can prove useful to achieve optimal operation for a state of the art electrolyzer plant.

5.2 Degree of freedom analysis and design of regulatory layer

For the electrolyzer plant, the operational objective is to achieve maximum hydrogen production ($V_{H_2,out}$, see Figure 5.2), subject to system itself and operational constraints.

$$\min_{u} -V_{H_2,out} \tag{5.1}$$

s.t.

$$\begin{aligned} f(u,x,d) &= 0 \\ g(u,x,d) &\leq 0 \end{aligned} \tag{5.2}$$

Here, $f(x, u, d) = 0$ represents the system equations for the electrolyzer plant model equation which are described in Chapter 3.

x are the algebraic and differential state variables of the electrolyzer plant model.

u are the manipulated variables (MVs),

$$u = [V_{el},\ q_{lye,1},\ q_{lye,2},\ q_{lye,3},\ q_{cw},\ q_{H_2O},\ z_{H_2},\ z_{O_2}]^T$$

d is the disturbance variable i.e. P_{net}, the input power to the electrolyzer plant.

$g(u, x, d) \leq 0$ are the physical and operational constraints for the flowsheet $\mathbf{F_1}$ $\mathbf{HX_{EoL}}$ $\mathbf{q_{lye,var}}$. These constraints are given by Equation 4.3 and Equation 4.4, however they are reformulated as:

$$\begin{aligned}
&\boldsymbol{g_1} : q_{lye,1}^{\min}/q_{lye,1} - 1 \leq 0\\
&\boldsymbol{g_2} : q_{lye,2}^{\min}/q_{lye,2} - 1 \leq 0\\
&\boldsymbol{g_3} : q_{lye,3}^{\min}/q_{lye,3} - 1 \leq 0\\
&\boldsymbol{g_4} : q_{lye,1}/q_{lye,1}^{\max} - 1 \leq 0\\
&\boldsymbol{g_5} : q_{lye,2}/q_{lye,2}^{\max} - 1 \leq 0\\
&\boldsymbol{g_6} : q_{lye,3}/q_{lye,3}^{\max} - 1 \leq 0\\
&\boldsymbol{g_7} : q_{cw}^{\min}/q_{cw} - 1 \leq 0\\
&\boldsymbol{g_8} : q_{cw}/q_{cw}^{\max} - 1 \leq 0\\
&\boldsymbol{g_9} : z_{H_2}^{\min}/z_{H_2} - 1 \leq 0\\
&\boldsymbol{g_{10}} : z_{H_2}/z_{H_2}^{\max} - 1 \leq 0\\
&\boldsymbol{g_{11}} : z_{O_2}^{\min}/z_{0_2} - 1 \leq 0\\
&\boldsymbol{g_{12}} : z_{0_2}/z_{O_2}^{\max} - 1 \leq 0\\
&\boldsymbol{g_{13}} : I_{den,1}^{\min}/I_{den,1} - 1 \leq 0\\
&\boldsymbol{g_{14}} : I_{den,2}^{\min}/I_{den,2} - 1 \leq 0\\
&\boldsymbol{g_{15}} : I_{den,3}^{\min}/I_{den,3} - 1 \leq 0\\
&\boldsymbol{g_{16}} : I_{den,1}/I_{den,1}^{\max} - 1 \leq 0\\
&\boldsymbol{g_{17}} : I_{den,2}/I_{den,2}^{\max} - 1 \leq 0\\
&\boldsymbol{g_{18}} : I_{den,3}/I_{den,3}^{\max} - 1 \leq 0\\
&\boldsymbol{g_{19}} : T_1^{\min}/T_1 - 1 \leq 0\\
&\boldsymbol{g_{20}} : T_2^{\min}/T_2 - 1 \leq 0\\
&\boldsymbol{g_{21}} : T_3^{\min}/T_3 - 1 \leq 0\\
&\boldsymbol{g_{22}} : T_1/T_1^{\max} - 1 \leq 0\\
&\boldsymbol{g_{23}} : T_2/T_2^{\max} - 1 \leq 0\\
&\boldsymbol{g_{24}} : T_3/T_3^{\max} - 1 \leq 0\\
&\boldsymbol{g_{25}} : \Delta T_{El,in}/\Delta T_{El,in}^{\max} - 1 \leq 0\\
&\boldsymbol{g_{26}} : P_{cons}/P_{net} - 1 \leq 0
\end{aligned} \tag{5.3}$$

Here, $\Delta\ T_{El,in}$ = $max(T_k) - T_{El_{in}}$ is the constraint on the temperature difference between the inlet lye stream and the electrolyzer. This temperature difference has to be less

than 30 °C for each electrolyzer. Thus temperature gradients inside all the electrolyzers are avoided by ensuring that the incoming lye is sufficiently hot. P_{cons} is the power consumed by the electrolyzer plant and this has to always less than than the input power P_{net}.

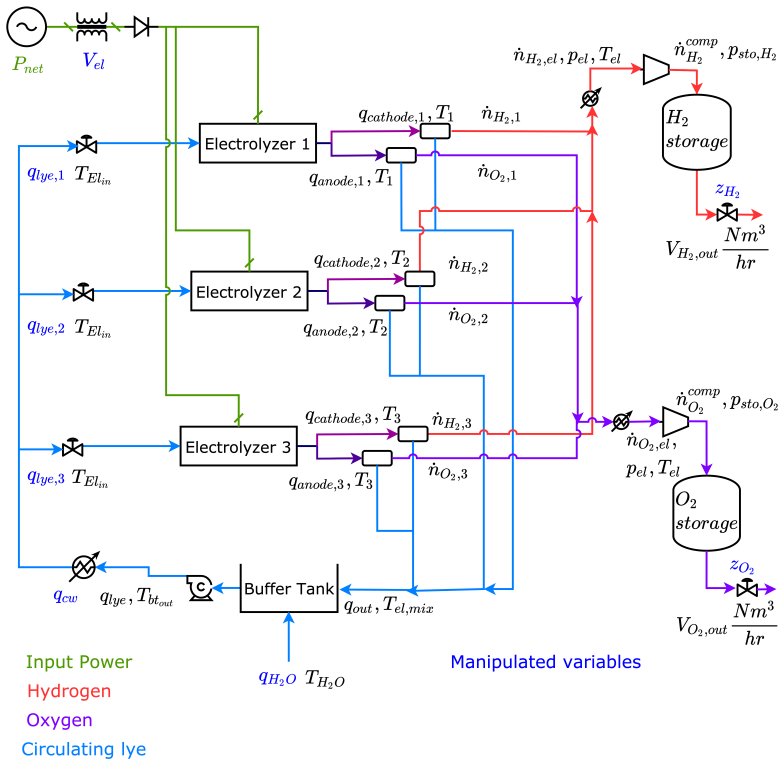

Figure 5.2: Electrolyzer plant flowsheet with shared BoP systems

Now, following the plantwide control design procedure introduced in Chapter 2, degrees of freedom available for optimization, N_{opt} also called as steady state degrees of freedom by [41] are:

$$N_{opt} = N_m - N_0 \tag{5.4}$$

Here, N_m = number of elements in u vector, i.e. 8
N_0 indicates the states with zero steady state effect. This includes liquid level in the buffer tank and the pressure of hydrogen and oxygen gas storage tanks. Controlling these states will consume 3 degrees of freedom. The design of the regulatory control layer and suggested MV-CV pairings and control loops for the states with zero steady state effect is shown in Figure 5.3.

Thus, the steady state degrees of freedom, N_{opt} = 5;

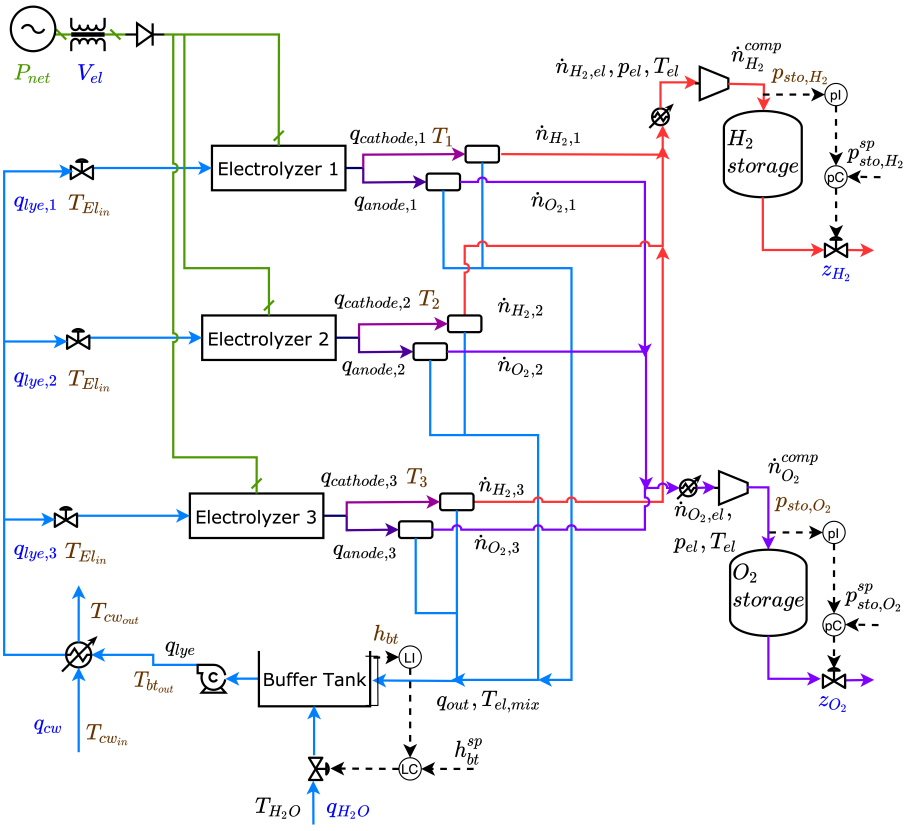

Figure 5.3: Electrolyzer plant flowsheet with control loops for state with zero steady state effects closed

5.3 Design of supervisory control layer using advanced control structures

In this section, we have designed the supervisory layer control structure using advanced control structures. The systematic procedure introduced earlier in Chapter 2, proposed by Reyes Lúa [20] is followed.

5.3.1 Step A1: Control objectives, MVs and CVs for supervisory layer

The electrolyzer plant has five available manipulated variables (N_{opt}). These steady state degrees of freedom are utilized to achieve optimal operation. These manipulated variables (u_1) are:

$$u_1 = [V_{el},\ q_{lye,1},\ q_{lye,2},\ q_{lye,3},\ q_{cw}]^T \tag{5.5}$$

The measurements y available for the design of the control layers are shown in brown in Figure 5.3:

$$y = [T_1,\ T_2,\ T_3,\ T_{bt_{out}},\ T_{El_{in}},\ T_{cw_{in}},\ T_{cw_{out}},\ h_{bt},\ p_{sto,H_2},\ p_{sto,O_2}]^T \tag{5.6}$$

To achieve steady-state optimal operation, we will control all the active constraints and find a self-optimizing variable for unconstrained degrees of freedom if any (this is Step 3 of top-down analysis in plantwide control procedure by Skogestad [41]).

5.3.2 Step A2: Priority list for constraints

The priority list of constraints for the electrolyzer plant is defined as follows. This list is defined using the listing rules introduced in Chapter 2:

- (P1) *Physical MV inequality constraints:* These are physical limits of the inputs that cannot be violated. For the electrolyzer plant these are:

$$\begin{aligned}
\boldsymbol{g_4} &: q_{lye,1}/q_{lye,1}^{\max} - 1 \leq 0 \\
\boldsymbol{g_5} &: q_{lye,2}/q_{lye,2}^{\max} - 1 \leq 0 \\
\boldsymbol{g_6} &: q_{lye,3}/q_{lye,3}^{\max} - 1 \leq 0 \\
\boldsymbol{g_8} &: q_{cw}/q_{cw}^{\max} - 1 \leq 0 \\
\boldsymbol{g_9} &: z_{H_2}^{\min}/z_{H_2} - 1 \leq 0 \\
\boldsymbol{g_{10}} &: z_{H_2}/z_{H_2}^{\max} - 1 \leq 0 \\
\boldsymbol{g_{11}} &: z_{O_2}^{\min}/z_{0_2} - 1 \leq 0 \\
\boldsymbol{g_{12}} &: z_{0_2}/z_{O_2}^{\max} - 1 \leq 0
\end{aligned}$$

- (P2) *Critical CV constraints:* These are important output that can be given up for a short while. For the electrolyzer plant following constraints are identified as (P2) priority constraints:

$$\begin{aligned}
\boldsymbol{g_{13}} &: I_{den,1}^{\min}/I_{den,1} - 1 \leq 0 \\
\boldsymbol{g_{14}} &: I_{den,2}^{\min}/I_{den,2} - 1 \leq 0 \\
\boldsymbol{g_{15}} &: I_{den,3}^{\min}/I_{den,3} - 1 \leq 0 \\
\boldsymbol{g_{16}} &: I_{den,1}/I_{den,1}^{\max} - 1 \leq 0 \\
\boldsymbol{g_{17}} &: I_{den,2}/I_{den,2}^{\max} - 1 \leq 0 \\
\boldsymbol{g_{18}} &: I_{den,3}/I_{den,3}^{\max} - 1 \leq 0 \\
\boldsymbol{g_{19}} &: T_1^{\min}/T_1 - 1 \leq 0 \\
\boldsymbol{g_{20}} &: T_2^{\min}/T_2 - 1 \leq 0 \\
\boldsymbol{g_{21}} &: T_3^{\min}/T_3 - 1 \leq 0 \\
\boldsymbol{g_{22}} &: T_1/T_1^{\max} - 1 \leq 0 \\
\boldsymbol{g_{23}} &: T_2/T_2^{\max} - 1 \leq 0 \\
\boldsymbol{g_{24}} &: T_3/T_3^{\max} - 1 \leq 0 \\
\boldsymbol{g_{25}} &: \Delta T_{El,in}/\Delta T_{El,in}^{\max} - 1 \leq 0
\end{aligned}$$

- (P3) *Non physical MV and less critical CV constraints:* Non physical MV constraints are the input constraints that are not limited by the physical limits. These

are identified as:

$$\begin{aligned}
\boldsymbol{g_1} &: q_{lye,1}^{\min}/q_{lye,1} - 1 \leq 0 \\
\boldsymbol{g_2} &: q_{lye,2}^{\min}/q_{lye,2} - 1 \leq 0 \\
\boldsymbol{g_3} &: q_{lye,3}^{\min}/q_{lye,3} - 1 \leq 0 \\
\boldsymbol{g_7} &: q_{cw}^{\min}/q_{cw} - 1 \leq 0
\end{aligned}$$

- (P4) *Desired throughput:* The power consumed by the electrolyzer plant P_{cons} decides the overall throughput from the electrolyzer plant. Therefore, (P4) constraint is:

$$\boldsymbol{g_{26}} : P_{cons}/P_{net} - 1 \leq 0$$

  Here it is to be noted that $P_{cons} > P_{net}$ is not possible as the maximum power available to the electrolyzer plant is P_{net}. Therefore, giving up desired throughput (i.e. P4) means $P_{cons} < P_{net}$.

- (P5) *Self optimizing variable:* Self optimizing variable, c has the lowest priority that means to maintain feasible operations it is given up before any of P1-P4 constraints.

5.3.3 Step A3: Active constraint switches

As discussed earlier, the primary disturbance for the system is input power P_{net}. The disturbances will change active constraint set, and some of the constraints that were active earlier might no longer be active now, or some other constraints may become active. Therefore, the optimal operation for the new operating point demands the reconfiguring of the control loops. From Chapter 2 we know that when an input (MV) reaches its limiting value, then the control of output variable (CV) paired to it is lost. However, when an output (CV) constraint becomes active, then it should be controlled tightly to its limiting value. Based on this knowledge, we define switching logic for the design of the supervisory control layer using advanced control structures.

For this system, there are 26 constraints and thus has 2^{26} potential active constraint regions. In this work, three ranges of the input power are considered, **High Power Range**, **Medium Power Range** and **Low Power Range**. High power range corresponds to the input power P_{net} values higher than the nominal power consumption for the flowsheet F_1 HX_{EoL} $q_{lye,var}$, which is 5.8 MW (see red solid line in Figure 4.6). Medium power range corresponds to 5.1 $MW \leq P_{net} \leq$ 5.8 MW. Lastly, low power range corresponds to input power between 3.4 $MW \leq P_{net} <$ 5.1 MW. The active constraint regions for output variables (CVs) and input variables (MVs) as a function of disturbance variable (i.e. input power, P_{net}) are shown in the Figure 5.4 and Figure 5.5 respectively. These are identified by solving an offline steady state optimization problem.

In high power region, active constraints are:

$$\begin{aligned}
\boldsymbol{g_4} &: q_{lye,1}/q_{lye,1}^{max} - 1 = 0, \\
\boldsymbol{g_{16}} &: I_{den,1}/I_{den,1}^{max} - 1 = 0, \\
\boldsymbol{g_{23}} &: T_2/T_2^{max} - 1 = 0, \\
\boldsymbol{g_{24}} &: T_3/T_3^{max} - 1 = 0, \\
\boldsymbol{g_{25}} &: \Delta T_{El,in}/T_{El,in}^{max} - 1 = 0
\end{aligned} \tag{5.7}$$

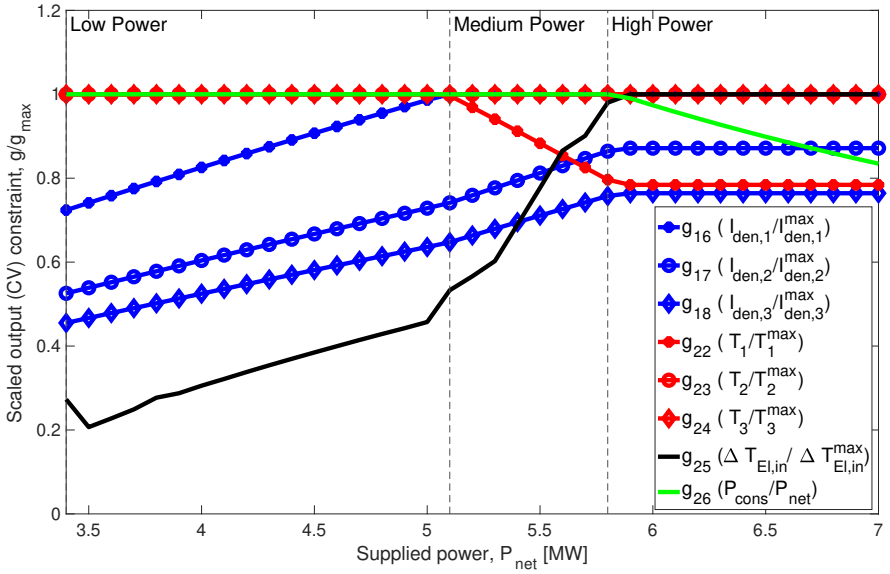

Figure 5.4: Optimal output (CV) constraint values as a function of disturbance. The three operating regions are clearly marked.

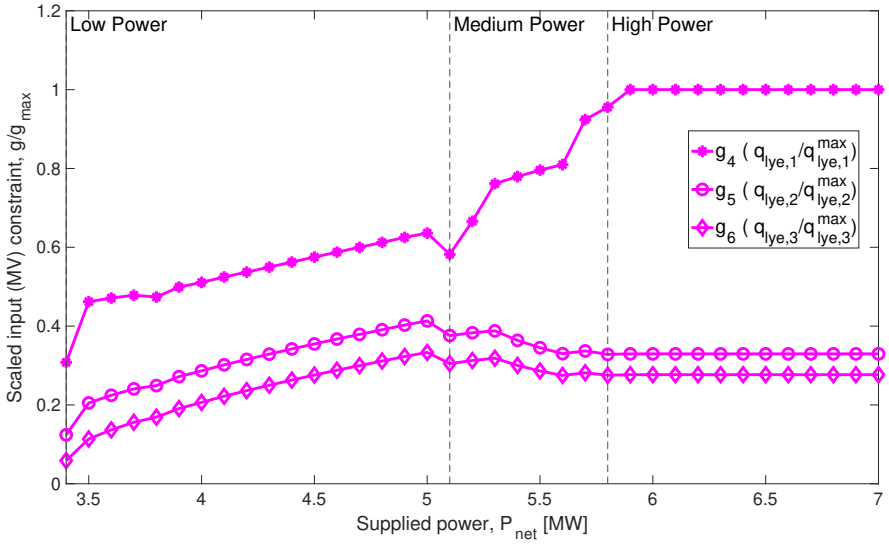

Figure 5.5: Optimal input (MV) constraint values as a function of disturbance. The three operating regions are clearly marked.

In medium power region, active constraints are:

$$\begin{aligned} \boldsymbol{g_{16}} &: I_{den,1}/I_{den,1}^{max} - 1 = 0, \\ \boldsymbol{g_{23}} &: T_2/T_2^{max} - 1 = 0, \\ \boldsymbol{g_{24}} &: T_3/T_3^{max} - 1 = 0, \\ \boldsymbol{g_{26}} &: P_{cons}/P_{net} - 1 = 0 \end{aligned} \tag{5.8}$$

In low power region, active constraints are:

$$\begin{aligned} \boldsymbol{g_{22}} &: T_1/T_1^{max} - 1 = 0, \\ \boldsymbol{g_{23}} &: T_2/T_2^{max} - 1 = 0, \\ \boldsymbol{g_{24}} &: T_3/T_3^{max} - 1 = 0, \\ \boldsymbol{g_{26}} &: P_{cons}/P_{net} - 1 = 0 \end{aligned} \tag{5.9}$$

In practice, base case operation corresponds to medium power range, i.e. when electrolyzer plant is consuming all the supplied input power during optimal operation. In high power range, excess input power is available and therefore, auxiliary systems like heating coils are needed to dump the excess energy. It is crucial to consume available excess input power for power grid balancing. Whereas in low power range, less power is available and the electrolyzer plant can have higher hydrogen production rate if more energy, i.e. electricity is accessible.

5.3.4 Step A4: Control structure for nominal case, i.e. Medium Power Range

The medium power range corresponding to 5.1 $MW \leq P_{net} \leq$ 5.8 MW is the base case, and we can satisfy all the constraints in this region. The objective is now to control all the active constraints tightly and select a self-optimizing variable for the remaining unconstrained degrees of freedom.

Before we dive into the control structure design, it is essential to take a moment and analyze the U-I performance curve carefully. The U-I performance curve for electrolyzers is given in Figure 5.6. Since all the electrolyzers are sharing a single transformer (shared BoP flowsheet), they will operate across the same electrolyzer voltage. Thus, at a given cell voltage if all the electrolyzer stacks have the equal number of cell, then it is possible to achieve optimal performance either by controlling temperature (T_k) or current density ($I_{den,k}$). In short, current density and temperature are dependent on each other for a given cell voltage. Thus, controlling one of them will enable control on the other as well.

Therefore, for the design of the supervisory control layer we propose to pair degrees of freedom as follows:

- $q_{lye,1}$ controls $I_{den,1}$ to $I_{den,1}^{max} = 198.5\ mA/cm^2$, tightly since it is an active constraint.
- $q_{lye,2}$ and $q_{lye,3}$ are paired to T_2 and T_3 respectively. This will allow to maintain the temperatures of degraded electrolyzers to the maximum limiting value, i.e.

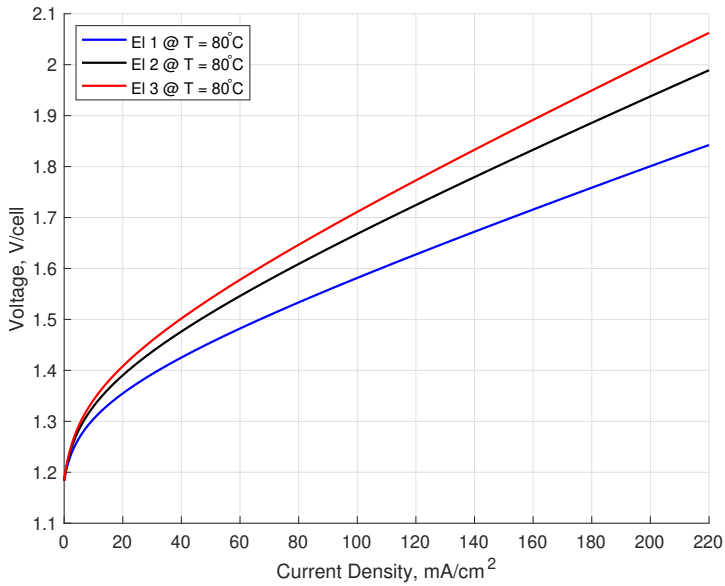

Figure 5.6: Performance characteristics for the degraded (i.e. *State 2*) electrolyzers

$T_2^{max} = T_3^{max} = 80\ °C$. For a given cell voltage the degraded electrolyzers are able to maximize their hydrogen production by operating at the maximum limiting temperatures.

- V_{el} is manipulated to match the power consumption P_{cons} by the electrolyzer assembly to the total input power P_{net}.
- With all the above pairing decided, we are left with one unconstrained degree of freedom i.e. q_{cw}, cooling water flowrate in the heat exchanger in lye circulation loop.
  It is important to note that, the cooler in the lye circulation loop is the unit that can remove the heat from the electrolyzer plant most effectively. Therefore, the search of self optimizing variable c should utilize available measurements (T_k, $T_{bt_{out}}$, $T_{El_{in}}$, $T_{cw_{in}}$, $T_{cw_{out}}$) for temperatures feedback to install a duty controller which will manipulate q_{cw} to ensure optimal operation.
  However, in this work we have not suggested the exact self optimizing variable c, because of the limited availability of time and this can be taken up in further studies. This self optimizing variable can be a linear measurement combination ($c = Hy$) proposed by Alstad and Skogestad [2] or a linear gradient combination ($c = N^T \nabla_u J(u,d)$) proposed by Krishnamoorthy [17]. Curious readers are referred to read the respective listed citations for complete details on these methods. Also, it is important to note here that the selected self optimizing variable is valid only for the particular active region. Therefore, it will be incorrect to track the same self optimizing variable c in all other regions.

The base control structure is shown in Figure 5.7.

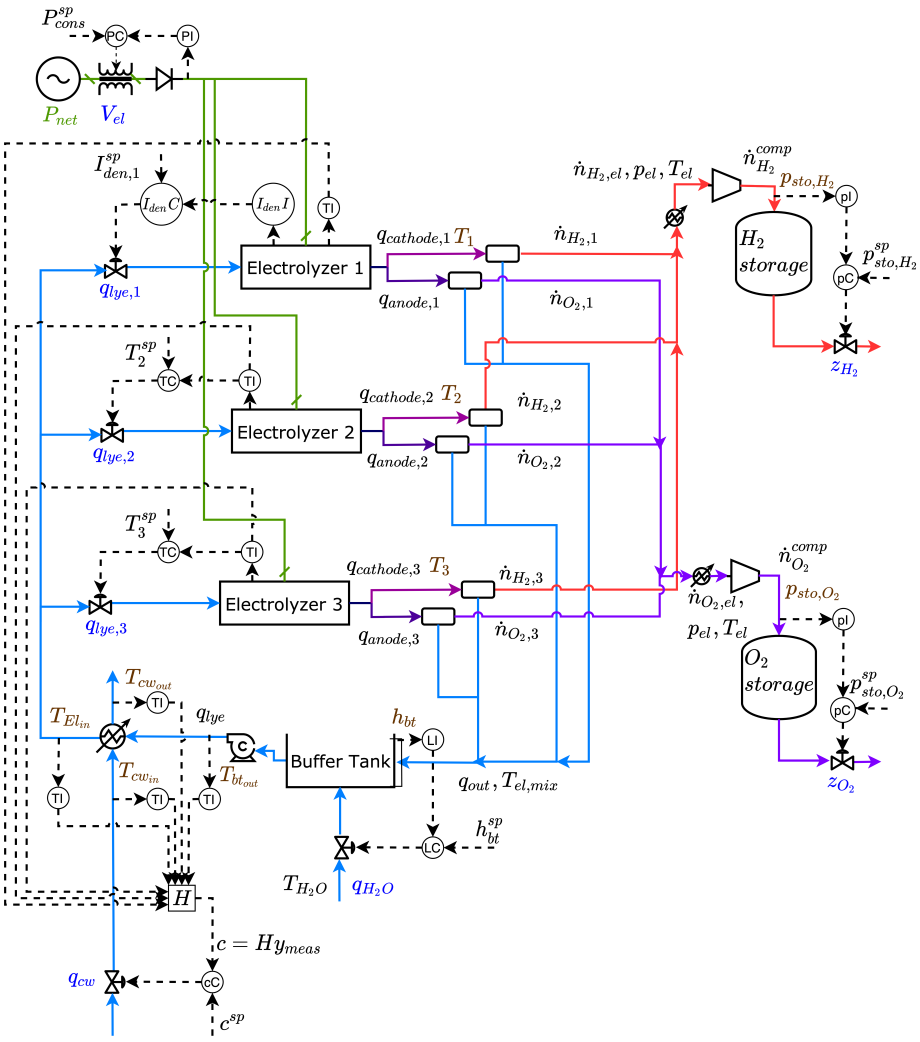

Figure 5.7: Basic control layer for the state of the art electrolyzer plant

5.3.5 Step A5: Control structure for active constraint switching

In this step the supervisory layer control structure using advanced control structures is proposed. The strategies introduced earlier in Section 2.3.4 and Section 2.3.5 are used to switch between the active constraint regions.

Switch from medium power range to low power range:

When the input power is reduced from medium power range to low power range then controlling the active constraints of medium power range i.e. Equation 5.8 is no longer useful

and to achieve steady state optimal performance it is required to control the active constraints in the low power range (see Equation 5.9).

Because of lower input power to the electrolyzers, even the best performing electrolyzer, i.e. Electrolyzer 1 is not able to operate at maximum current density, i.e. $I_{den,1}^{max}$. All the electrolyzers are now required to maintain operations at the maximum allowed temperature in order to produce maximum hydrogen. Thus the CV-CV switching is suggested for $I_{den,1}$ and T_1. Using the systematic design procedure for CV-CV switching proposed by Krishnamoorthy [16], we will use a max selector to execute this switching (see Figure 5.8).

Operation in low power region does not violate any constraints, and we still have one unconstrained steady-state degree of freedom, i.e. q_{cw}. We propose to pair this unconstrained DOF to the self-optimizing variable that will provide the temperature feedback to the duty controller to manipulate q_{cw}, thus ensuring optimal performance. Again, the choice of self optimizing variable c for this region might be different from self optimizing variable in the medium power range. The systematic selection of this variable c for respective regions will be dealt in detail in the future work planned for this project.

Switch from medium power range to high power range:

In the cases when the input power is higher than the nominal power (i.e. 5.8 MW) of the flowsheet, the operation switches to high power range. Equation 5.7 details the active constraints for this operation.

In this operation range, the inlet lye flowrate to electrolyzer 1 reaches its maximum limit. Hence, it is no longer available for manipulation. Also, for operation at higher input power, due to increased inlet lye flowrates, the temperature difference between incoming lye stream and the electrolyzer (i.e. $\Delta T_{El,in}$) must be capped to a maximum value. This limiting value ($\Delta T_{El,in}^{max}$) is selected arbitrarily as 30 $^{\circ}C$ in this study to avoid the temperature gradients inside electrolyzers. To maintain control on $I_{den,1}$, we do an MV-CV switching using split range control (SRC) and a min selector (see Figure 5.8). The SRC allows to utilize electrolyzer voltage (i.e. V_{el}) to control current density of electrolyzer 1 ($I_{den,1}$) to its maximum value (i.e. 198.5 mA/cm^2). Also, since, V_{el} was earlier paired to P_{cons}, thus using it to control $I_{den,1}$ now means that we need to give up control on P_{cons} which is performed by min selector. Stopping the control of P_{cons} does not add to additional losses since from Equation 5.7 we know that P_{cons} is no longer active in high power mode region and hence we decide to give it up to control $I_{den,1}$ which is an active constraint.

Also, in this region, we do not have any unconstrained degrees of freedom and the constraint of $\Delta T_{El,in}$ is active. Thus, we require a selector to do CV-CV switching between self-optimizing variable, c and $\Delta T_{El,in}$. This switching ensures that all the active constraints are tightly controlled to their limiting values using the available degrees of freedom. Figure 5.8 shows the complete control structure for the state of the art electrolyzer plant. This control structure handles all three operating regions.

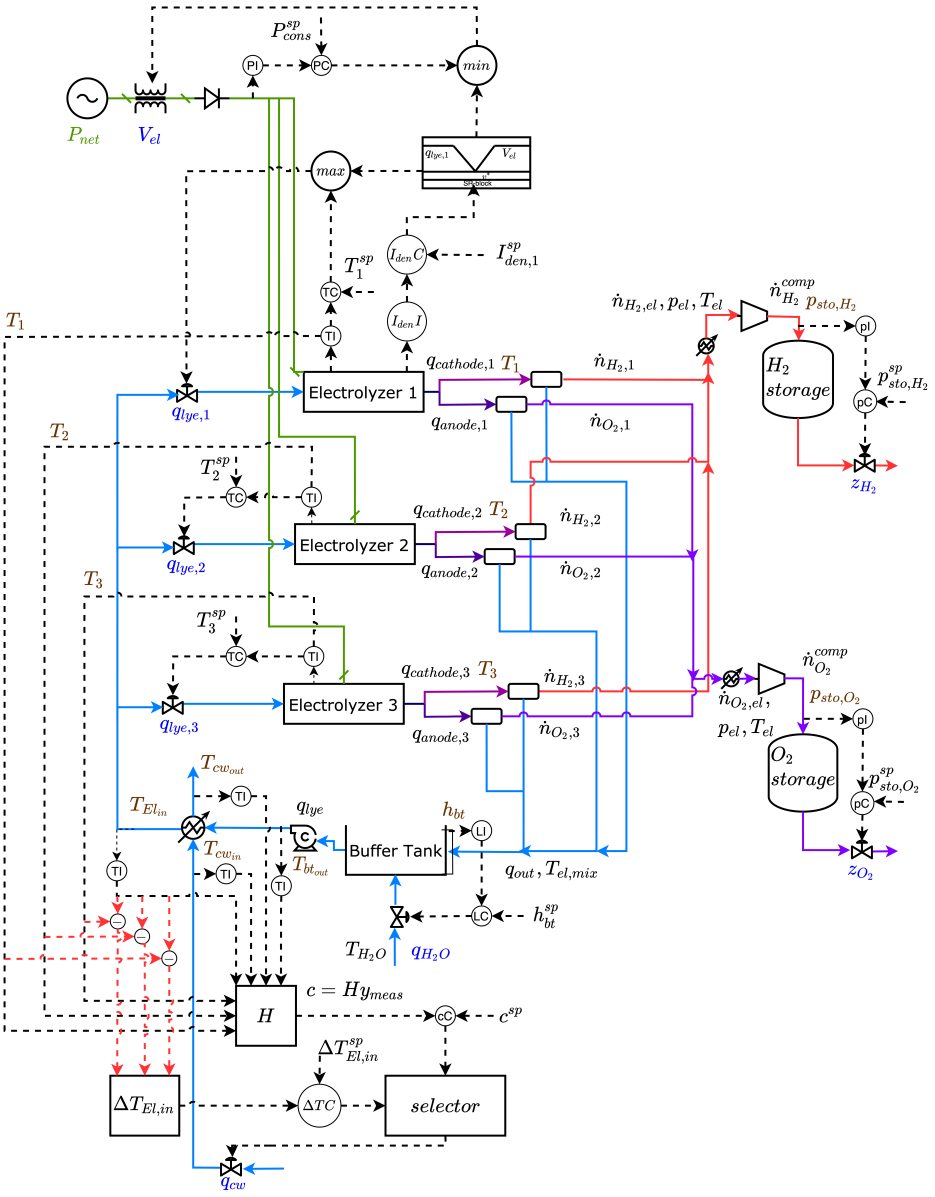

Figure 5.8: Supervisory layer control structure for the state of the art electrolyzer plant. This control structure handles the three operating regions.

5.4 Concluding remarks

Using the systematic procedure proposed by Reyes Lúa [20] and Krishnamoorthy [16] we have designed a control structure for the state of the electrolyzer plant. Here, we demonstrated that how a near-optimal steady-state operation can be achieved using simple PI(D) based control structures. The switching strategies proposed here perform CV-CV switching, MV-MV switching, and MV-CV switching using split range control and selectors. However, it is important to note that success during the final implementation of the proposed control structure would consider system dynamics. This is planned to be continued during the future work on this project.

Chapter 6

Conclusions and future work

6.1 Conclusions

This master project continues further the work on the dynamic model of the alkaline water electrolyzer plant performed during specialization project [33]. Firstly, the mathematical model from the previous work is scaled-up to the state of the art electrolyzer plant. This scaled-up plant has a nominal power consumption of 6.42 MW when all three electrolyzers are new. The design parameters like the size of the heat exchanger, lye circulation rate, size of the buffer tank, and volume of the gas storage tanks are estimated for the state of the art alkaline water electrolyzer plant.

Secondly, we have dealt with the challenges related to flowsheet design for the state of the art electrolyzer plant. The electrolyzer flowsheet design selection includes decisions on questions like:

- Should electrolyzers have shared BoP systems? or should we install separate BoP systems for each electrolyzer?
- What should be the design basis of the heat exchanger sizing? Should we design heat exchanger based on the cooling requirement of a newly commissioned plant when all the electrolyzers are new? or should we design it to match the cooling demand of a plant with electrolyzers nearing the end of their lifetime?
- What is the effect of the variability of the electrolyzer inlet lye flowrate? Should flowsheet design have fixed inlet lye flowrate? or a variable lye flowrate?

The questions above are answered systematically by considering all the possible flowsheet designs (12 in total). The comparison of flowsheets utilizes the total hydrogen production and initial investment cost as the performance criteria. The higher hydrogen production by a given flowsheet should not encourage expensive capital investments. This analysis concluded that the flowsheet design with shared BoP systems and heat exchanger design based on the cooling requirement of the electrolyzer plant at the end of lifetime, and also having

variable inlet lye flowrate is practically most attractive flowsheet design. This flowsheet is denoted as $F_1HX_{EoL}q_{lye,var}$ based on the nomenclature defined in Chapter 4. Comparison of the flowsheet performances also outlines several important insights on plant behaviour. Section 4.4 concludes all these insights in detail.

Lastly, the plantwide control structure is proposed for flowsheet $F_1HX_{EoL}q_{lye,var}$. For the control structure design; the electrolyzer plant is considered to be in *State 2* (i.e. with degraded electrolyzers). This work employs systematic procedure for control structure design of chemical plants given by Skogestad [41]. Because of the disturbances in the input power, the active constraint set is changed and therefore, to ensure the optimal operations we need to switch between the active constraint regions. In this work, these active constraint regions correspond to three ranges of the input power, i.e. high power range, medium power range and low power range. The classical advanced control structures like selectors and split range controller are used in supervisory control layer to perform switching between these active constraint regions. This design of supervisory control layer follows the systematic design framework proposed by Reyes Lúa [20]. The work concludes by proposing a control structure for the electrolyzer plant that is capable of handling the optimal operation across three active constraint regions. However, the success of the proposed control structure during implementation would consider system dynamics. But because of the time constrictions, dynamic simulations to investigate the performance of the proposed control structure was not possible.

It will be an injustice not to point the reader to the limitations of this work. As discussed earlier, this work proposes a control structure for the electrolyzer plant flowsheet when the electrolyzers are degraded and have non-identical performance (i.e. in *State 2*). However, for the same flowsheet (i.e. $F_1HX_{EoL}q_{lye,var}$) different active constraint regions were observed when the electrolyzers are new and have identical performances (i.e. in *State 1*). In simple terms, this means the behaviour of the electrolyzer plant is dependent on the degradation state of the electrolyzers. Therefore, the control structure designed using classical advanced control structures for *State 2* of the electrolyzer flowsheet might not give steady-state optimal performance when the electrolyzers are new, i.e. in *State 1*. This limitation is a very significant motivation to design the supervisory control layer using a multivariable controller like MPC.

6.2 Future work

Recommendations for future work on the control structure design for the state of the art electrolyzer plant are outlined below:

- First step should be to identify the self-optimizing control variable c using available temperature measurements. This self-optimizing variable (SOC) is paired to the cooling water flowrate, q_{cw}. q_{cw} is an unconstrained degree of freedom (DOF) in medium and low power ranges. Thus, pairing the unconstrained DOF to self-optimizing control variable will lead to a near-optimal performance with acceptable steady-state loss. Also, it is important to note that different active constraints regions

will have different SOC variable c, and additional switching logics are required to maintain optimal operations across these active constraint regions.

- Once, the self-optimizing variable is identified, and switching logics finalized, we suggest performing dynamic simulations to investigate the performance of the proposed control structure for *State 2* of the flowsheet $\mathrm{F_1HX_{EoL}q_{lye,var}}$.
- Design the supervisory control layer using a multivariable controller like model predictive control (MPC). Then a comparison of classical advanced control structures and MPC as candidates for the supervisory layer can be drawn. This comparison will surely be helpful to steer the choice for the control structure design for overall electrolyzer plant.
- Lastly, as highlighted in Chapter 4, at very low input power values, it would be optimal to turn off the cooling in the lye circulation loop. However, it is not possible as setting q_{cw} to zero has associated numerical difficulties. This limitation is an artefact of the heat exchanger model that we have developed for this study. Therefore, the heat exchanger model should be updated to eliminate this effect to make the plant model more realistic.

Bibliography

[1] Bruce J. Allison and Shiro Ogawa. Design and tuning of valve position controllers with industrial applications. *Transactions of the Institute of Measurement and Control*, 25(1):3–16, 2003.

[2] Alstad Vidar and Skogestad Sigurd. Null Space Method for Selecting Optimal Measurement Combinations as Controlled Variables. *Industrial & Engineering Chemistry Research*, 46(3):846–853, 2007.

[3] Joel A.E. Andersson, Joris Gillis, Greg Horn, James B. Rawlings, and Moritz Diehl. CasADi: a software framework for nonlinear optimization and optimal control. *Mathematical Programming Computation*, 11(1), 2019.

[4] Cyril Bourasseau and Benjamin Guinot. Chapter 8 Hydrogen: A Storage Means for Renewable Energies. *Hydrogen Production: by Electrolysis*, 2015.

[5] Boyun Guo, Xinghui Liu, and Xuehao Tan. Chapter 11 - Transportation Systems. *Petroleum Production Engineering*, pages 275–325, 2017.

[6] Bristol E. On a new measure of interaction for multivariable process control. *IEEE Transactions on Automatic Control*, 11(1):133–134, 1996.

[7] Alexander Buttler and Hartmut Spliethoff. Current status of water electrolysis for energy storage, grid balancing and sector coupling via power-to-gas and power-to-liquids: A review. *Renewable and Sustainable Energy Reviews*, 82:2440–2454, 2 2018.

[8] Jan Willem Erisman, Mark A. Sutton, James Galloway, Zbigniew Klimont, and Wilfried Winiwarter. How a century of ammonia synthesis changed the world. *Nature Geoscience*, 1:636–639, 2008.

[9] Bjarne Foss and N Aksel, Tor Heirung. *Merging Optimization and Control*. 2013.

[10] Alan C. Hindmarsh, Peter N. Brown, Keith E. Grant, Steven L. Lee, Radu Serban, Dan E. Shumaker, and Carol S. Woodward. SUNDIALS: Suite of nonlinear and dif-

ferential/algebraic equation solvers. *ACM Transactions on Mathematical Software*, 31(3):363–396, 2005.

[11] International Fertilizer Association. Estimating & Reporting Fertilizer-Related Greenhouse Gas Emissions: linking Fertilizer Best Management Practices with national climate change mitigation targets. pages 1–12, 2018.

[12] Magnus G. Jacobsen and Sigurd Skogestad. Active Constraint Regions for Optimal Operation of Distillation Columns. *Industrial & Engineering Chemistry Research*, 51(7):2963–2973, 2012.

[13] Jäschke Johannes, Cao Yi, and Kariwala Vinay. Self-optimizing control – A survey. *Annual Reviews in Control*, 43:199–223, 2017.

[14] Ali Keçebaş, Muhammet Kayfeci, and Mutlucan Bayat. Electrochemical hydrogen generation. *Solar Hydrogen Production*, pages 299–317, 2019.

[15] H. Kojima, T. Matsuda, H. Matsumoto, and T. Tsujimura. Development of dynamic simulator of alkaline water electrolyzer for optimizing renewable energy systems. *Journal of International Council on Electrical Engineering*, 8(1):19–24, 1 2018.

[16] Dinesh Krishnamoorthy. *Novel Approaches to Online Process Optimization under Uncertainty*. PhD thesis, Norwegian University of Science and Technology, 2019.

[17] Dinesh Krishnamoorthy and Sigurd Skogestad. Online Process Optimization with Active Constraint Set Changes using Simple Control Structures. *Industrial & Engineering Chemistry Research*, 58(30):13555–13567, 2019.

[18] Truls Larsson and Sigurd Skogestad. Plantwide control-A review and a new design procedure. *Modeling, Identification and Control*, 21:209–240, 2000.

[19] Rodney L. LeRoy. The Thermodynamics of Aqueous Water Electrolysis. *Journal of The Electrochemical Society*, 127(9):1954, 1980.

[20] Adriana Reyes Lúa. *Systematic design of advanced control structures*. PhD thesis, Norwegian University of Science and Technology, 2020.

[21] Adriana Reyes Lúa, Cristina Zotică, Tamal Das, Dinesh Krishnamoorthy, and Sigurd Skogestad. Changing between Active Constraint Regions for Optimal Operation: Classical Advanced Control versus Model Predictive Control. *Computer Aided Chemical Engineering*, 43:1015–1020, 2018.

[22] Manum Henrik and Skogestad Sigurd. Self-optimizing control with active set changes. *Journal of Process Control*, 22:873–883, 2012.

[23] D Q Mayne, J B Rawlings, C V Rao, and P O M Scokaert. Survey Paper Constrained model predictive control: Stability and optimality. *Automatica*, 36:789–814, 2000.

[24] David Q. Mayne. Model predictive control: Recent developments and future promise. *Automatica*, 50(12):2967–2986, 2014.

[25] Warren L. McCabe, Julian C. Smith, and Peter Harriott. *Unit operations of chemical engineering (5th ed.).* 1993.

[26] Vladimiros Minasidis, Sigurd Skogestad, and Nitin Kaistha. Simple Rules for Economic Plantwide Control. *Computer Aided Chemical Engineering*, 37:101–108, 2015.

[27] Nel ASA. Specification of A485 Atmospheric Alkaline Electrolyzer available on https://nelhydrogen.com/product/atmospheric-alkaline-electrolyser-a-series/, accessed on 6 May, 2020.

[28] Nobel Media AB 2020. The Nobel Prize in Chemistry 1918. https://www.nobelprize.org/prizes/chemistry/1918/summary/ accessed on 28 Jun 2020.

[29] Occidental Chemical Corporation (OxyChem). Caustic Potash Handbook. 2018.

[30] Joris Proost. State-of-the art CAPEX data for water electrolysers, and their impact on renewable hydrogen price settings. *International Journal of Hydrogen Energy*, pages 4406–4413, 2 2019.

[31] Adriana Reyes-Lúa, Cristina Zotică, and Sigurd Skogestad. Optimal Operation with Changing Active Constraint Regions using Classical Advanced Control∗. *IFAC-PapersOnLine*, 51(18):440–445, 1 2018.

[32] Daniel E Rivera, Manfred Morari, ', and Slgurd Skogestad. Internal Model Control. 4. PID Controller Design. Technical report, 1986.

[33] Md Rizwan. Dynamic modeling and control of a system of electrolyzers for hydrogen production. *Specialization project report*, NTNU, 2019.

[34] Tariq Samad. A survey on industry impact and challenges thereof, 2 2017.

[35] Seborg Dale E., Edgar Thomas F., Mellichamp Duncan A., and Doyle Francis J. *Process Dynamics and Control*. Wiley, 4 edition, 2016.

[36] F G Shinskey. The stability of interacting control loops with and without decoupling. In *IFAC Proceedings Volumes*, pages 21–30, 1977.

[37] Sigurd Skogestad. Plantwide control: the search for the self-optimizing control structure. *Journal of Process Control*, 2000.

[38] Sigurd Skogestad. Plantwide control: Towards a systematic procedure. In *Computer Aided Chemical Engineering*, volume 10, pages 57–69. Elsevier, 2002.

[39] Sigurd Skogestad. Control structure design : What should we control , measure and manipulate? *First African Control Conference, Cape Town*, 2003.

[40] Sigurd Skogestad. Simple analytic rules for model reduction and PID controller tuning. *Journal of Process Control*, 13(4):291–309, 2003.

[41] Sigurd Skogestad. Control structure design for complete chemical plants. In *Computers and Chemical Engineering*, volume 28, pages 219–234. Elsevier Ltd, 1 2004.

[42] Sigurd Skogestad. *Chemical and Energy Process Engineering*. Taylor & Francis Group, 2008.

[43] Sigurd Skogestad and Ian Postlethwaite. *Multivariable Feedback Control Analysis and Design*. Wiley, 2nd edition, 2005.

[44] Stephanopoulos George. *Chemical Process Control: An Introduction to Theory and Practice*. Prentice Hall PTR, 1st edition, 1984.

[45] Oystein Ulleberg. Modeling of advanced alkaline electrolyzers: a system simulation approach. *International Journal of Hydrogen Energy*, 28(1):21–33, 2003.

[46] Alfredo Ursúa, Luis M. Gandía, and Pablo Sanchis. Hydrogen production from water electrolysis: Current status and future trends. *Proceedings of the IEEE*, 100(2):410–426, 2 2012.

[47] Wikipedia. Wikipedia page on Ammonia, available on https://en.wikipedia.org/wiki/Ammonia accessed on 22 June, 2020.

[48] Tao Zhou and Bruno Francois. Modeling and control design of hydrogen production process for an active hydrogen/wind hybrid power system. *International Journal of Hydrogen Energy*, 34(1):21–30, 1 2009.

[49] J. G. Ziegler and N. B Nichols. Optimum settings for automatic controllers. *trans. ASME*, 64, 1942.

Appendices

A U-I curve parameters for the electrolyzers in *State 1* and *State 2*

In this section the parameter values for the electrolyzers performance equations (U-I curve) is given. In *State 1* all the electrolyzers have similar performances and thus they have identical parameter values. Whereas in *State 2*, electrolyzers have different performance curve and hence have different parameter values.

Parameter	Unit	Electrolyzer 1	Electrolyzer 2	Electrolyzer 3
r_1	Ωm^2	2.18×10^{-4}	2.18×10^{-4}	2.18×10^{-4}
r_2	$\Omega m^2/°C$	-4.25×10^{-7}	-4.25×10^{-7}	-4.25×10^{-7}
s	V	117.93×10^{-3}	117.93×10^{-3}	117.93×10^{-3}
t_1	m^2/A	-145.29×10^{-3}	-145.29×10^{-3}	-145.29×10^{-3}
t_2	$m^2\ °C/A$	11.794	11.794	11.794
t_3	$m^2\ °C^2/A$	395.68	395.68	395.68
f_1	mA^2/cm^4	120	120	120
f_2	$-$	0.98	0.98	0.98

Table 1: U-I curve parameter values for the electrolyzers in *State 1*

Parameter	Unit	Electrolyzer 1	Electrolyzer 2	Electrolyzer 3
r_1	Ωm^2	2.18×10^{-4}	2.62×10^{-4}	2.84×10^{-4}
r_2	$\Omega m^2/°C$	-4.25×10^{-7}	-4.25×10^{-7}	-4.25×10^{-7}
s	V	117.93×10^{-3}	141.52×10^{-3}	153.31×10^{-3}
t_1	m^2/A	-145.29×10^{-3}	-145.29×10^{-3}	-145.29×10^{-3}
t_2	$m^2\ °C/A$	11.794	11.794	11.794
t_3	$m^2\ °C^2/A$	395.68	395.68	395.68
f_1	mA^2/cm^4	120	144	156
f_2	$-$	0.98	0.97	0.96

Table 2: U-I curve parameter values for the electrolyzers in *State 2*

B Summary: Total hydrogen produced at a given input power for all possible electrolyzer plant flowsheet configurations

This section provides a comparison of the total hydrogen production at steady state for different flowsheet configuration at a given input power. Following table shows the hydrogen produced at steady state by different flowsheet designs when the electrolyzers are new i.e. in *State 1*.

Input Power	Flowsheet state	F_1 HX_{BoL} $q_{lye,var}$	F_1 HX_{OS} $q_{lye,var}$	F_1 HX_{EoL} $q_{lye,var}$	F_1 HX_{BoL} $q_{lye,fix}$	F_1 HX_{OS} $q_{lye,fix}$	F_1 HX_{EoL} $q_{lye,fix}$	F_2 HX_{BoL} $q_{lye,var}$	F_2 HX_{OS} $q_{lye,var}$	F_2 HX_{EoL} $q_{lye,var}$	F_2 HX_{BoL} $q_{lye,fix}$	F_2 HX_{OS} $q_{lye,fix}$	F_2 HX_{EoL} $q_{lye,fix}$
7	1	1454.83	1454.83	1454.83	1454.83	1454.83	1454.83	1454.83	1454.83	1454.83	1454.83	1454.83	1454.83
6.7	1	1454.83	1454.83	1454.83	1454.83	1454.83	1454.83	1454.83	1454.83	1454.83	1454.83	1454.83	1454.83
6.4	1	1454.60	1454.60	1454.60	1454.60	1454.60	1454.60	1454.60	1454.60	1454.60	1454.60	1454.60	1454.60
6.1	1	1398.51	1398.51	1398.51	1398.51	1398.51	1398.51	1398.51	1398.51	1398.51	1398.51	1398.51	1398.51
5.8	1	1341.63	1341.63	1341.63	1341.63	1341.63	1341.63	1341.63	1341.63	1341.63	1341.63	1341.63	1341.63
5.5	1	1283.91	1283.91	1283.91	1283.91	1283.91	1283.91	1283.91	1283.91	1283.91	1283.91	1283.91	1283.91
5.2	1	1225.31	1225.31	1225.31	1225.31	1225.31	1225.31	1225.31	1225.31	1225.31	1225.31	1225.31	1225.31
4.9	1	1165.79	1165.79	1165.79	1165.79	1165.79	1165.79	1165.79	1165.79	1165.79	1165.79	1165.79	1165.79
4.6	1	1105.29	1105.29	1105.29	1105.29	1105.29	1105.29	1105.29	1105.29	1105.29	1105.29	1105.29	1105.29
4.3	1	1043.76	1043.76	1043.76	1043.76	1043.76	1043.76	1043.76	1043.76	1043.76	1043.76	1043.76	1043.76
4	1	981.13	981.13	981.13	981.13	978.40	981.13	981.13	981.13	981.13	981.13	978.38	981.13
3.7	1	917.32	912.08	914.74	914.62	905.41	910.15	917.32	912.08	914.74	914.61	905.40	910.14
3.4	1	843.20	838.42	840.74	840.61	832.55	836.70	843.20	838.42	840.74	840.60	832.54	836.69
3.1	1	768.96	764.81	766.82	766.69	759.68	763.28	768.96	764.81	766.82	766.68	759.66	763.27
2.8	1	694.67	691.10	692.83	692.69	686.64	689.75	694.67	691.10	692.83	692.69	686.63	689.74
2.5	1	620.18	617.14	618.61	618.47	613.30	615.96	620.18	617.14	618.61	618.47	613.29	615.95
2.2	1	545.31	542.76	543.99	543.85	539.50	541.73	545.31	542.76	543.99	543.85	539.49	541.72
1.9	1	469.85	467.75	468.76	468.63	465.02	466.86	469.85	467.75	468.76	468.62	465.01	466.86
1.6	1	393.52	391.83	392.64	392.51	389.59	391.08	393.52	391.83	392.64	392.51	389.58	391.08
1.3	1	315.90	314.58	315.22	315.10	312.81	313.98	315.90	314.58	315.22	315.09	312.81	313.97
1.2	1	289.64	288.44	289.02	288.90	286.81	287.88	289.64	288.44	289.02	288.90	286.81	287.87
1.1	1	263.13	262.04	262.57	262.45	260.56	261.52	263.13	262.04	262.57	262.45	260.56	261.52

Table 3: Comparison of total hydrogen produced $[Nm^3/hr]$ by different flowsheet configurations in *State 1* for a given input power $[MW]$

Following table shows the hydrogen produced at steady state by different flowsheet designs when the electrolyzers are degraded i.e. in *State 2*.

Input Power	Flowsheet state	F_1 HX_{BoL} $q_{lye,var}$	F_1 HX_{OS} $q_{lye,var}$	F_1 HX_{EoL} $q_{lye,var}$	F_1 HX_{BoL} $q_{lye,fix}$	F_1 HX_{OS} $q_{lye,fix}$	F_1 HX_{EoL} $q_{lye,fix}$	F_2 HX_{BoL} $q_{lye,var}$	F_2 HX_{OS} $q_{lye,var}$	F_2 HX_{EoL} $q_{lye,var}$	F_2 HX_{BoL} $q_{lye,fix}$	F_2 HX_{OS} $q_{lye,fix}$	F_2 HX_{EoL} $q_{lye,fix}$
7	2	1219.34	1264.23	1264.23	1099.15	1096.12	1095.52	1300.81	1438.61	1386.52	1291.25	1425.98	1367.74
6.7	2	1219.34	1264.23	1264.23	1099.15	1096.12	1095.52	1300.81	1422.51	1386.52	1291.25	1422.51	1367.74
6.4	2	1219.34	1264.23	1264.23	1099.15	1096.12	1095.52	1300.81	1373.57	1373.50	1291.25	1373.57	1367.74
6.1	2	1219.34	1264.23	1264.23	1099.15	1096.12	1095.52	1300.81	1323.02	1323.02	1291.25	1323.02	1323.02
5.8	2	1219.34	1257.55	1257.55	1099.15	1096.12	1095.52	1271.28	1271.28	1271.28	1271.27	1271.28	1271.28
5.5	2	1209.99	1209.99	1209.99	1099.15	1096.12	1095.52	1218.25	1218.25	1218.25	1218.25	1218.25	1218.25
5.2	2	1161.48	1161.48	1161.48	1099.15	1096.12	1095.52	1163.81	1163.81	1163.81	1163.81	1163.81	1163.81
4.9	2	1107.98	1107.98	1107.98	1099.15	1096.12	1095.52	1107.98	1107.98	1107.98	1107.98	1107.98	1107.98
4.6	2	1051.14	1051.14	1051.14	1044.59	1044.10	1044.01	1051.14	1051.14	1051.14	1051.14	1051.14	1051.14
4.3	2	993.26	993.26	993.26	987.77	987.36	987.29	993.26	993.26	993.26	993.26	993.26	993.26
4	2	934.28	934.28	934.28	929.74	929.41	929.35	934.28	934.28	934.28	934.28	934.28	934.28
3.7	2	874.11	874.11	874.11	870.43	870.16	870.11	874.11	874.11	874.11	874.11	873.88	874.08
3.4	2	812.66	810.58	812.66	809.74	806.87	809.50	812.60	812.19	812.47	812.46	807.16	811.22
3.1	2	745.27	740.34	742.72	743.52	735.40	739.57	746.23	742.11	744.11	744.01	736.76	740.60
2.8	2	673.22	668.96	671.11	670.90	663.94	667.51	674.22	670.39	672.24	672.12	665.70	669.00
2.5	2	600.62	596.62	598.64	598.19	592.26	595.30	601.51	598.16	599.79	599.67	593.86	596.88
2.2	2	526.86	523.80	525.33	525.15	520.16	522.72	527.71	524.71	526.16	526.03	520.95	523.55
1.9	2	452.62	450.12	451.33	451.50	447.37	449.49	453.41	450.99	452.16	452.03	447.90	450.02
1.6	2	377.58	375.47	376.48	376.93	373.56	375.28	378.55	376.61	377.54	377.41	374.09	375.79
1.3	2	301.16	299.23	300.18	0.00*	0.00*	0.00*	302.51	300.99	301.72	301.60	298.99	300.32
1.2	2	272.06	272.06	272.06	0.00*	0.00*	0.00*	276.79	275.40	276.07	275.95	273.56	274.78
1.1	2	0.00*	0.00*	0.00*	0.00*	0.00*	0.00*	250.82	249.56	250.17	250.05	0.00	248.99

Table 4: Comparison of total hydrogen produced [Nm^3/hr] by different flowsheet configurations in *State 2* for a given input power [MW]

*Total hydrogen production of 0.00 Nm^3/hr represents it is infeasible to operate the flowsheet configuration for given input power in $State2$

C MATLAB Code

This section contains some important pieces of the source code developed during this work.

C.1 Parameter values for the simulation

The function **parElectrolyzer** consists of the all the parameter values that are used for the simulation of the state of the art electrolyzer plant

```
function par = parElectrolyzer(N)

%This script defines values of the input parameters for all ...
    electrolyzers.

par.Const = ...
    struct('ze',2,'FC',96485,'R',8.314,'Cp',4.186,'CpLye',3.1006,...
    'Mwt',18,'MwtH2',2.01588,'Tref',25,'rho',1000,'rhoLye',1258.2,'Vc',...
    2.0681,'Vh',1.9944);
%Cp=specific heat of water, [J/gK];Mwt=mol. wt of H2O, rho=density of
%water/lye[kg/m3],Vc=volume of cold side of heat ...
    exchanger[m3],Vh=volume of
%hot side of heat exchanger[m3]

par.Comp = struct('alpha',0.63,'k',1.62,'Tel',25+273,'Pel',3);
par.Storage = struct('VstoH2',965000,'VstoO2',482500,'PoutH2',19,...
    'PoutO2',19,...
    'TstoH2',25+273.15,'TstoO2',25+273.15,'Rg',8.314e-2,'VdispH2',...
    0.5,'VdispO2',0.5);
%VstoH2 and VstoO2 are in litres

par.Tw_in = 10;              %inlet temperature of the cooling water ...
    in lye circulation heat exchanger
par.Hex.UA = 20.48e3;       %UA of heat exchanger [W/K], based on ...
    EoL design
par.kvalveH2 = 14.723;       %valve constant for the outlet valve of ...
    hydrogen storage tank, calculated for 25 bar storage pressure ...
    at SS
par.kvalveO2 = 7.362;        %valve constant for the outlet valve of ...
    oxygen storage tank, calculated for 25 bar storage pressure at SS
par.sigma = 5.672*10^-8;     %stefan-boltzmann constant [W/m^2 K^4]
par.em = 0.8;                %emissivity [-]

%% Parameters for U-I relationship in Ulleberg's model
par.U = struct([]);
par.TherMo = struct([]);
par.EL = struct([]);
for i =1:N
    %U-I curve Parameters
    par.U(i).r1 = 0.000218155;          %ohm m^2
    par.U(i).r2 = -0.000000425;          %ohm m^2 C^-1
    par.U(i).s = 0.1179375;              %Vs
    par.U(i).t1 = -0.14529;              %A^-1 m^2
    par.U(i).t2 = 11.794;                %A^-1 m^2 C^-1
```

```
37      par.U(i).t3 = 395.68;                %A^-1 m^2 C^-2
38      par.U(i).f1 = 120;                   %mA^2 cm^-4
39      par.U(i).f2 = 0.98;                  %dimensionless
40
41      %% Parameters for the thermal model
42      par.TherMo(i).CtS = 625/27;          %Specific thermal capacity ...
            of electrolyzer i.e. Ct/P, [kJ/kWatts*C]
43      par.TherMo(i).Ct = 625/27*2135;      %Cts*Pnom [kJ/C]or[kJ/K], ...
            Assuming Pnom = 2135 kWatts
44      par.TherMo(i).hc = 5.5;              %convective heat transfer ...
            coefficient W/m^2 C
45      par.TherMo(i).A_surf = 0.1;          %specific radition area per ...
            kA current per cell, [m^2/kA*Ncell]
46      par.TherMo(i).A_El = 0.1*5.72*230;   %surface area of the ...
            electrolyzer, A_surf*Inom*Ncell [m^2]
47
48      %% Parameters for Faraday effeciency calculations
49      par.EL(i).Utn = 1.482;               %thermoneutral voltage, [V]
50      par.EL(i).nc = 230;                  %no. of cells
51      par.EL(i).A = 2.6;                   %electrode area of each ...
            cell, [m^2]
52      par.EL(i).Ta = 20;                   %ambient temp, [C]
53      par.EL(i).Tstd = 25;                 %standard temperature, [C]
54
55  end
56  % El #2, performing at 85% of electrolyzer 1
57  par.U(2).r1 = par.U(2).r1*1.2;              %ohm m^2
58  par.U(2).s = par.U(2).s*1.2;                %V
59  par.U(2).f1 = par.U(2).f1*1.2;              %mA^2 cm^-4
60  par.U(2).f2 = 0.97;
61
62  %El #3, performing at 70% of electrolyzer 1
63  par.U(3).r1 = par.U(3).r1*1.3;               %ohm m^2
64  par.U(3).s = par.U(3).s*1.3;                 %V
65  par.U(3).f1 = par.U(3).f1*1.3;               %mA^2 cm^-4
66  par.U(3).f2 = 0.96;
67
68  par.N=N;
69  end
```

C.2 Main code file

Following code is the source code for electrolyzer plant. Solution of the steady state problem is used to initialize the dynamic problem.

```
1  clc
2  clear
3  close all
4
5  %% Load CasADi
6  addpath('/Users/mdrizwan/Documents/MATLAB/casadi-osx-matlabR2015a-v3.5.1')
7  import casadi.*
8
9  %% Loading parameters
```

```
N = 3;                                  %no. of electrolyzers
par = parElectrolyzer(N);

%% Inputs for the simulation
num_hr = .25;                           %no. of hours
t0 = 1;                                 %start, [s)]
ts = 1;                                 %time step, [s]
tf = num_hr*60*60;                      %final, [s]
tsamp = t0:ts:tf;
len = length(tsamp);                    %number of simulation time ...
    steps
tstep = 200;

%% Initial guess for steady state solution using IPOPT

%disturbance is total power
Pnet = 9e6;% total input power

%algebriac state variables('z')
u_k0 = 1.8*ones(1,par.N);               %initial guess for cell voltage
P_k0 = Pnet/par.N*ones(1,par.N);        %intial guess is power ...
    divided equally among electrolyzers
i_k0 = P_k0./(u_k0.*par.EL(1).nc);      %initial guess for current
Feff_k0 = 0.97*ones(1,par.N);
nH2_k0 = 6*ones(1,par.N);               %[mol/s]
qH2Oloss_k0 = nH2_k0*par.Const.Mwt.*ones(1,par.N);%[g/s]
nH2El_net0 = sum(nH2_k0);               %[mol/s]
nH2out_net0 = sum(nH2_k0);
nO2El_net0 = 0.5*nH2El_net0;
nO2out_net0 = 0.5*nH2out_net0;
T_El_out0 = 80;                         %initial guess for the ...
    temperature of lye entering in the heat exchanger

%differential state variables('x')
T_k0 = 75*ones(1,par.N);
Psto_H20 = 25;        %initial H2 storage pressure (calculated from ...
    steady state solution) [bar]
Psto_O20 = 25;        %initial O2 storage pressure (calculated from ...
    steady state solution) [bar]
Mass_Bt0 = 6000000;   %mass of the liquid in the buffer tank,[g] 6000kg
T_bt_out0 = 70;       %Initial guess for the temperature of lye ...
    mixture at the exit of the buffer tank,[degC]
T_El_in0 = 65;        %initial guess for the temperature of inlet ...
    lye into the electrolyzer, [deg C]
T_cw_out0 = 20;       %initial guess for the exit temperature of ...
    the cooling water leaving heat exchanger,[deg C]

z_guess = [u_k0 i_k0 P_k0 Feff_k0 nH2_k0 qH2Oloss_k0 nH2El_net0 ...
    nH2out_net0 nO2El_net0 nO2out_net0 T_El_out0];
x_guess = [T_k0 Psto_H20 Psto_O20 Mass_Bt0 T_bt_out0 T_El_in0 ...
    T_cw_out0];

%initial guess for input variables('u')
U_El_k_0 = 414.0301*ones(1,par.N);      %voltage across ...
    electrolyzers, [Volts]
q_lye_k_0 = 6648*ones(1,par.N);         %lye flowrate, [g/s]
q_cw_0 = 2.0698e4;                      %cooling water flow rate, [g/s]
```

```
zH2_0 = 0.4;
zO2_0 = 0.4;
q_H2O_0 = 324.2657;                         %total water lost during ...
    electrolysis, [grams/sec]

u_guess = [U_El_k_0 q_lye_k_0 q_cw_0 zH2_0 zO2_0 q_H2O_0];

counter = 1;
flag = {};

for Pnet = 7e6:-0.1e6:1.1e6

X_guess = [z_guess x_guess u_guess];

%% Solve the steady state problem
[z0, x0, u0, EXIT] = El_SteadyStateOptimization(N,X_guess,Pnet);

z_guess = z0;
x_guess = x0;
u_guess = u0;

T_El_in_set = x0(par.N+5);%setpoint for the temperature of lye ...
    entering the electrolyzer
T_cw_out = x0(par.N+6);
T_bt_out = x0(par.N+4);

%Initial value of the MVs
Vss = u0(1:par.N);
q_lyek = u0(par.N+1:2*par.N);
qlye_kgs = q_lyek/1000;
qf_cw = u0(2*par.N+1);
qcw_kgs = qf_cw/1000;
zH2 = u0(2*par.N+2);
zO2 = u0(2*par.N+3);
Qwater = u0(2*par.N+4);
nH2 = sum(z0(4*par.N+1:5*par.N));

Pcons = sum(z0(2*par.N+1:3*par.N));
Iden = 0.1*z0(par.N+1:2*par.N)./par.EL(1).A;
Tk = x0(1:par.N);
V_H2_ini = z0(4*par.N+1:5*par.N)*0.0224136*3600;

for nEl = 1:par.N
    Qlyeloss(nEl) = ...
        (q_lyek(nEl)*par.Const.CpLye*(T_El_in_set-Tk(nEl)));
    Qgenk(nEl) = ...
        par.EL(nEl).nc*(z0(nEl)-par.EL(nEl).Utn)*z0(par.N+nEl);
    Qlossk(nEl) = par.TherMo(nEl).A_El*(par.TherMo(nEl).hc*(Tk(nEl)-...
        par.EL(nEl).Ta) + par.sigma*par.em*((Tk(nEl)+273.15)^4-...
        (par.EL(nEl).Ta+273.15)^4));
    Qnet(nEl) = Qlyeloss(nEl)+Qgenk(nEl)-Qlossk(nEl);
end

row_C_S2(counter,:) = [Pnet/1e6,Pcons/1e6,qlye_kgs,qcw_kgs,Iden,Tk,...
    T_El_in_set,T_cw_out,T_bt_out,V_H2_ini, sum(V_H2_ini)];

if strcmp(EXIT,'Solve_Succeeded')
```

```
110      ac_C_S2(counter,:) = [Iden/198.5, 32./Iden, Tk/80, 25./Tk,...
111          (max(Tk)-T_El_in_set)/30, Pcons/Pnet,...
112          qlye_kgs/10, 0.5./qlye_kgs, qcw_kgs/80 1e-5/qcw_kgs];
113      plot_C_S2_DegHex(counter,:) = [Pnet/1e6,Pcons/1e6,qlye_kgs,...
114          qcw_kgs,Iden,Tk,T_El_in_set,T_cw_out,T_bt_out,V_H2_ini, ...
115          sum(V_H2_ini)];
116  else
117      ac_C_S2(counter,:) = NaN*ones(1,6*par.N+4);
118      plot_C_S2_DegHex(counter,:) = 0*ones(1,4*par.N+7);
119  end
120
121  flag = {flag{:},EXIT}';
122  counter = counter+1;
123
124  end
125
126  %% Build the plant model
127  [xDiff, xAlg, input, eqnAlg, eqnDiff, F] = model(par.N);
128
129  %% Manipulated variables
130  %these are the degree of freedoms that we will utilise to control ...
         the system
131
132  V_El = zeros(len,N);                              %voltage across the ...
         electrolyzer, [Watt], len is the length of time vector
133  for j = 1:N
134      V_El(1:end,j) = Vss(j)*1;                     %incremental step ...
           change in common voltage across all electrolysers
135  % V_El(tstep:end,j)=Vss(j)*1;
136  end
137
138  qlye = zeros(len,N);                              %lye flowrate, [g/s]
139  for j = 1:N
140      qlye(1:end,j) = q_lyek(j)*1;                  %assumed same lye ...
           flowarate to all the electrolyzers
141  end
142  % qlye(tstep:end,2) = q_lyek(2)*1.2;
143
144  q_cw = qf_cw*ones(len,1);                         %cooling water flow ...
         rate as a manipulated variable, [g/s]
145  % q_cw(tstep:end) = qf_cw*1.1;                    %incremental step ...
         change in cooling water flowrate
146
147  ZH2 = zH2*ones(len,1);                            %H2 valve ...
         displacement as a manipulated variable
148  % ZH2(tstep:end) = .2;                            %change in H2 valve ...
         displacement
149
150  ZO2 = zO2*ones(len,1);                            %O2 valve ...
         displacement as a manipulated variable
151  % ZO2(tstep:end) = .7;                            %change in O2 valve ...
         displacement
152
153  qH2O = Qwater*ones(len,1);                        %flow rate of water ...
         added to buffer tank as a manipulated variable, [g/s]
154  % qH2O(tstep:end)=Qwater*1.2;                     %incremental step ...
         change in the water flow rate
```

```
155
156 %% Initialize plotting variables
157 Temp = zeros(len,N);                    %temp of the electrolyzer, [C]
158 PstoH2 = zeros(len,1);                  %H2 storage pressure, [bar]
159 PstoO2 = zeros(len,1);                  %O2 storage pressure, [bar]
160 U = zeros(len,1);                       %voltage/cell in each of ...
        the electrolyzer, [V]
161 I = zeros(len,1);                       %current in each ...
        electrolyzer, [A]
162 P = zeros(len,1);
163 I_den = zeros(len,1);                   %current density in the ...
        electrolyzer, [A/m^2]
164 nH2in = zeros(len,1);                   %net hydrogen flow rate in ...
        to the storage, [mol/s]
165 nH2out = zeros(len,1);                  %net hydrogen flowrate out ...
        from the storage, [mol/s]
166 nH2elout = zeros(len,1);                %hydrogen flowrate from ...
        each of the individual electrolyzer, [mol/s]
167 nO2in = zeros(len,1);                   %net oxygen flow rate in to ...
        the storage, [mol/s]
168 nO2out = zeros(len,1);                  %net oxygen flowrate out ...
        from the storage, [mol/s]
169 Telout = zeros(len,1);
170 Tbtout = zeros(len,1);                  %temperature of lye mixture ...
        at the exit of the buffer tank, [degC]
171 Telin = zeros(len,1);
172 mBufferT = zeros(len,1);
173 Tw_out = zeros(len,1);
174 SpecEl = zeros(len,1);
175 PcompH2 = zeros(len,1);                 %compressor power for ...
        hydrogen, [watts]
176 PcompO2 = zeros(len,1);                 %compressor power for ...
        oxygen, [watts]
177 Qloss = zeros(len,1);                   %heat loss to surrounding ...
        in the electrolyzer, [watts]
178 Qgen = zeros(len,1);                    %heat generated in the ...
        electrolyzer, [watts]
179 Qlosslye = zeros(len,1);                %heat taken out by the lye ...
        from the electrolyzer, [watts]
180 P_net = zeros(len,1);                   %net power to the ...
        electrolyzer assembly, [watts]
181
182 %% Integrate plant over the time horizon
183
184 for i=1:len
185     %i = timestamp
186     %j = electrolyzer sequence
187
188     r =  F('x0',x0,'z0',z0,'p',[V_El(i,:), qlye(i,:), q_cw(i), ...
            ZH2(i),...
189          ZO2(i), qH2O(i)]);
190     x0 = full(r.xf);            %updating solution as new initial ...
            conditions
191     z0 = full(r.zf);
192
193
194     %% Storing values in plotting variables
```

```
195
196     %calculation of compressor power
197     PcompH2(i) = ...
            full(((r.zf(6*N+1)*par.Comp.k*par.Const.R*par.Comp.Tel)...
198         /(par.Comp.alpha*(par.Comp.k-1)))*(((r.xf(N+1)/par.Comp.Pel)^...
199         ((par.Comp.k-1)/par.Comp.k))-1));
200     PcompO2(i) = ...
            full(((r.zf(6*N+3)*par.Comp.k*par.Const.R*par.Comp.Tel)...
201         /(par.Comp.alpha*(par.Comp.k-1)))*(((r.xf(N+2)/par.Comp.Pel)^...
202         ((par.Comp.k-1)/par.Comp.k))-1));
203     %assuming same k and Tel for O2
204
205
206     nH2in(i) = full(r.zf(6*N+1));      %net hydrogen flow rate in to ...
            the storage at all timestamps, [mol/s]
207     nH2out(i) = full(r.zf(6*N+2));     %net hydrogen flowrate out ...
            from the storage at all timestamps, [mol/s]
208     nO2in(i) = full(r.zf(6*N+3));      %net oxygen flow rate in to ...
            the storage at all timestamps, [mol/s]
209     nO2out(i) = full(r.zf(6*N+4));     %net oxygen flowrate out from ...
            the storage at all timestamps, [mol/s]
210     Telout(i) = full(r.zf(6*N+5));     %temperature of lye after ...
            mixing before going to the buffer tank, [celsius]
211
212     PstoH2(i) = full(r.xf(N+1));       %hydrogen storage pressure at ...
            all timestamps, [bar]
213     PstoO2(i) = full(r.xf(N+2));       %oxygen storage pressure at ...
            all timestamps, [bar]
214     mBufferT(i) = full(r.xf(N+3));     %
215     Tbtout(i) = full(r.xf(N+4));       %temperature of lye mixture ...
            at the exit of the buffer tank, [degC]
216     Telin(i) = full(r.xf(N+5));        %temperature of lye going ...
            into the electrolyzer, [celsius]
217     Tw_out(i) = full(r.xf(N+6));       %exit temperature of the ...
            cooling water, [celsius]
218
219
220     for j=1:N
221         U(i,j) = full(r.zf(j));                  %voltage/cell, [V]
222         I(i,j) = full(r.zf(N+j));                %current, [A]
223         P(i,j) = full(r.zf(2*N+j));              %power, [Watts]
224         nH2elout(i,j) = full(r.zf(4*N+j));       %hydrogen ...
                production rate from individual electrolyzer, [mol/s]
225
226         Temp(i,j)= full(r.xf(j));                %temperature of ...
                electrolyzers at all timestamps, [celsius]
227
228         I_den(i,j) = 0.1*I(i,j)/par.EL(j).A;     %current density, ...
                [mA/cm^2]
229
230         Qloss(i,j) = ...
                par.TherMo(j).A_El*(par.TherMo(j).hc*(Temp(i,j)-...
231             par.EL(j).Ta) + par.sigma*par.em*((Temp(i,j)+273.15)^4-...
232             (par.EL(j).Ta+273.15)^4));
233         %heat loss to surrounding in the electrolyzer, [watts]
234
235         Qgen(i,j) = par.EL(j).nc*(U(i,j)-par.EL(j).Utn)*I(i,j);
```

```
236         %heat generated in the electrolyzer, [watts]
237
238         Qlosslye(i,j) = qlye(i,j)*par.Const.CpLye*(Telin(i)-Temp(i,j));
239         %heat taken out by the lye from the electrolyzer, [watts]
240
241         V_H2(i,j) = nH2elout(i,j)*0.0224136*3600;    %hydrogen ...
                production rate from individual electrolyzer, [Nm3/h]
242         Ps(i,j) = P(i,j)/(1000*V_H2(i,j));           %Specific ...
                electricity consumption, [kWh/Nm3]
243     end
244
245     P_net(i)=sum(P(i,:));
246
247     if rem(i,100)==0
248         disp(i)
249     end
250
251 end
252
253 %% Plotting the results
254
255 figure()
256 subplot(2,1,1)
257 plot(V_H2)
258 xlabel('Time, s')
259 ylabel('H_2 production rate, [Nm^3/hr]')
260 legend('El 1','El 2', 'El 3')
261 grid on
262
263 subplot(2,1,2)
264 plot(Ps)
265 xlabel('Time, s')
266 ylabel('Specific electricity consumption, [kWh/Nm^3]')
267 ylim([4.3, 4.7])
268 legend('El 1','El 2', 'El 3')
269 grid on
270
271 figure()
272 plot(PstoH2)
273 xlabel('Time, s')
274 ylabel('H_2 Storage pressure, [bar]')
275 grid on
276
277 figure()
278 subplot(2,1,1)
279 plot(Temp(:,1))
280 hold on
281 plot(Temp(:,2))
282 hold on
283 plot(Temp(:,3))
284 xlabel('Time, s')
285 ylabel('T_k, [ ^0C]')
286 ylim([69, 82])
287 grid on
288 subplot(2,1,2)
289 plot(Telout)
290 xlabel('Time, s')
```

```
ylabel('T_o_u_t,[ ^0 C]')
grid on

figure()
subplot(3,1,1)
plot(qlye(:,1))
xlabel('Time, s')
ylabel('Lye flowrate to El 1, g/s')
grid on
subplot(3,1,2)
plot(q_cw)
xlabel('Time, s')
ylabel('Cooling water flowrate, g/s')
grid on
subplot(3,1,3)
plot(Telin,'k')
hold on
plot(T_El_in_set,'r--')
xlabel('Time, s')
ylabel('T_E_l_ _i_n, [ ^0C]')
grid on

figure()
plot(mBufferT./1000)
ylabel('Mass of liquid in the buffer tank, [kg]')
xlabel('Time, s')
grid on
```

C.3 Solving steady state optimization problem

The following function file solves a nonlinear steady state optimization problem for the electrolyzer plant. This function gives out the steady state optimal solution for a given input power.

```
function [z0, x0, u0,EXIT] = El_SteadyStateOptimization(N,X0,P0)
%This script solves the steady state optimization problem
import casadi.*
par = parElectrolyzer(N);

%% Build the plant model and solve steady state optimization problem
[xDiff, xAlg, input, eqnAlg, eqnDiff] = model(par.N);
x = [xAlg;xDiff];

%% Defining the disturbance
Pnet = SX.sym('Pnet');
Ptot = SX.zeros(1,1);

for nEl = 1:par.N
    Ptot = Ptot + xAlg(2*par.N+nEl);
end
eqnPnet = Pnet - Ptot;%Total power = sum of power of the individual ...
    electrolyzer

%% preparing symbolic variables
```

```
w = {};
% preparing numeric variables and bounds
w0 = [];
lbw = [];
ubw = [];

% declaring them symbolic
w = {w{:},x,input};
% declaring them numerically
w0 = [w0;X0']; %initial guess

%defining constraints on the decision variables (states and inputs ...
    i.e. MVs)

%constraints on states
lbu_k = 0*ones(par.N,1);     %lower bound on cell voltage
ubu_k = inf*ones(par.N,1);

lbi_k = zeros(par.N,1);      %lower bound on current
ubi_k = inf*ones(par.N,1);

lbP_k = 0*ones(par.N,1);     %lower bound on power
ubP_k = inf*ones(par.N,1);

lbFeff_k = 0*ones(par.N,1); %lower bound on faraday efficiency
ubFeff_k = 1*ones(par.N,1);

lbnH2_k = zeros(par.N,1);    %lower bound on hydrogen production
ubnH2_k = inf*ones(par.N,1);

lbqH2Oloss_k = zeros(par.N,1);  %lower bound on water loss
ubqH2Oloss_k = inf*ones(par.N,1);

lbnH2el_net = 0;                %lower bound on net hydrogen ...
    production from the electrolyzer
ubnH2el_net = inf;

lbnH2out_net = 0;               %lower bound on hydrogen from the ...
    storage tank outlet
ubnH2out_net = inf;

lbnO2el_net = 0;                %lower bound on net oxygen ...
    production from the electrolyzer
ubnO2el_net = inf;

lbnO2out_net = 0;               %lower bound on oxygen from the ...
    storage tank outlet
ubnO2out_net = inf;

lbT_el_out = 0;                 %lower bound on the temperature at ...
    electrolyzer outlet
ubT_el_out = inf;

lbT_k = 25*ones(par.N,1);       %lower bound on the electrolyzer ...
    temperature
ubT_k = 80*ones(par.N,1);

```

```
lbPstoH2 = 20;                  %lower bound on the hydrogen ...
    storage pressure
ubPstoH2 = 30;

lbPstoO2 = 20;                  %lower bound on the oxygen storage ...
    pressure
ubPstoO2 = 30;

lbMbt = 0;                      %lower bound on the mass in the ...
    buffer tank
ubMbt = 6000000;

lbT_bt_out = 0;                 %lower bound on the temperature of ...
    lye leaving the buffer tank
ubT_bt_out = inf;

lbT_el_in = 0;                  %lower bound on the temperature at ...
    electrolyzer inlet
ubT_el_in = inf;

lbT_cw_out = 0;                 %lower bound on the coolant outlet ...
    temperature
ubT_cw_out = inf;

%constraints on the inputs
lbU_el_k = zeros(par.N,1);      %lower bound on the electrolyzer ...
    voltage
ubU_el_k = inf*ones(par.N,1);
lbq_lye_k = 500*ones(par.N,1);  %lower bound on the lye flowrate
ubq_lye_k = 10000*ones(par.N,1);
lbq_cw = 0.01;                  %lower bound on the coolant flow rate
ubq_cw = 80000;
lbzH2 = 0;                      %lower bound on hydrogen outlet ...
    valve opening
ubzH2 = 1;
lbzO2 = 0;                      %lower bound on oxygen outlet valve ...
    opening
ubzO2 = 1;
lbqH2O = 0;                     %lower bound on total water lost ...
    during electrolysis
ubqH2O = inf;

lbw = ...
    [lbw;lbu_k;lbi_k;lbP_k;lbFeff_k;lbnH2_k;lbqH2Oloss_k;lbnH2el_net;...
    lbnH2out_net;lbnO2el_net;lbnO2out_net;lbT_el_out;lbT_k;lbPstoH2;...
    lbPstoO2;lbMbt;lbT_bt_out;lbT_el_in;lbT_cw_out;lbU_el_k;lbq_lye_k;...
    lbq_cw;lbzH2;lbzO2;lbqH2O];%bounds on all the variables
ubw = ...
    [ubw;ubu_k;ubi_k;ubP_k;ubFeff_k;ubnH2_k;ubqH2Oloss_k;ubnH2el_net;...
    ubnH2out_net;ubnO2el_net;ubnO2out_net;ubT_el_out;ubT_k;ubPstoH2;...
    ubPstoO2;ubMbt;ubT_bt_out;ubT_el_in;ubT_cw_out;ubU_el_k;ubq_lye_k;...
    ubq_cw;ubzH2;ubzO2;ubqH2O];


%% preparing symbolic constraints
g = {};
% preparing numeric bounds
```

```
115 lbg = [];
116 ubg = [];
117
118 % declaring constraints
119 uElconst = [];
120 for nEl=1:par.N-1
121     uElconst = [uElconst;xAlg(nEl)-xAlg(nEl+1)];
122 end
123
124 deltaT1 = xDiff(par.N+5)-par.Tw_in;
125 deltaT2 = xDiff(par.N+4)-xDiff(par.N+6);
126
127 % impose the connstraint on the maximum temperature difference ...
        between the inlet lye temp. and the electrolyzer temp.
128 deltaT_El1 = xDiff(1) - xDiff(par.N+5);
129 deltaT_El2 = xDiff(2) - xDiff(par.N+5);
130 deltaT_El3 = xDiff(3) - xDiff(par.N+5);
131
132 Iden = SX.zeros(par.N,1);
133 for nEl = 1:par.N
134     Iden(nEl) = (0.1*xAlg(par.N+nEl))/par.EL(nEl).A; %current ...
            density in mA/cm2
135 end
136 IdenMin = 32;   %minimum current density, 32 mA/cm2
137 IdenMax = 198.5;%maximum current density, 198.5 mA/cm2
138
139 g = {g{:},eqnAlg, eqnDiff,uElconst, ...
        Iden,eqnPnet,deltaT_El1,deltaT_El2,...
140     deltaT_El3,deltaT1,deltaT2};
141 lbg = ...
        [lbg;zeros(7*par.N+11,1);zeros(par.N-1,1);IdenMin*ones(par.N,1);...
142     0;0;0;0;2e-3;2e-3];
143 ubg = ...
        [ubg;zeros(7*par.N+11,1);zeros(par.N-1,1);IdenMax*ones(par.N,1);...
144     P0;30;30;30;inf;inf];
145
146 Objvol_H2 = SX.zeros(par.N,1);
147 PconsEl = SX.zeros(par.N,1);
148 qlyeEl = SX.zeros(par.N,1);
149 for nEl = 1:par.N
150     Objvol_H2(nEl) = (xAlg(4*par.N+nEl)*0.0224136*3600);%[Nm3/h]
151     PconsEl(nEl) = xAlg(2*par.N+nEl);
152     qlyeEl(nEl) = input(par.N+nEl);
153 end
154 Pcons = sum(PconsEl);
155 qlyeTot = sum(qlyeEl);
156 J = -(Objvol_H2(1)+Objvol_H2(2)+Objvol_H2(3));
157
158 % J = 10;
159
160 %% formalize into an NLP problem
161 nlp = struct('x',vertcat(w{:}),'g',vertcat(g{:}),'f',J,'p',Pnet);
162
163 options = struct;
164 options.ipopt.print_level = 0;
165
166 % assign solver - IPOPT in this case
```

```
solver = nlpsol('solver','ipopt',nlp,options);

% solve - using the defined initial guess and bounds
sol = solver('x0',w0,'lbx',lbw,'ubx',ubw,'lbg',lbg,'ubg',ubg,'p',P0);
res = full(sol.x);

EXIT = solver.stats.return_status;

%% Extracting results
Uk = [];
Ik = [];
Pk = [];
Feffk = [];
nH2k = [];
qH2Olossk = [];
Tk = [];
Vss = [];
q_lyek = [];

for nEl = 1:par.N
    %optimal value of the algebriac state
    Uk = [Uk res(nEl)];                          %cell voltage of ...
        the electrolyzer
    Ik = [Ik res(par.N+nEl)];                    %current in the ...
        electrolyzer
    Pk = [Pk res(2*par.N+nEl)];                  %power of the ...
        individual electrolyzer
    Feffk = [Feffk res(3*par.N+nEl)];            %faraday efficiency ...
        of each electrolyzer
    nH2k = [nH2k res(4*par.N+nEl)];              %hydrogen produced ...
        form each individual electrolyzer
    qH2Olossk = [qH2Olossk res(5*par.N+nEl)];    %water loss during ...
        electrolysis in kth electrolyzer
    %optimal value of the differential state
    Tk = [Tk res(6*par.N+5+nEl)];                %temperature of the ...
        individual electrolyzer
    %optimal value of the inputs
    Vss = [Vss res(7*par.N+11+nEl)];             %electrolyzer voltage
    q_lyek = [q_lyek res(8*par.N+11+nEl)];       %lye flowrate
end

%optimal value of the algebriac state
nH2El_tot=res(6*par.N+1);
nH2out_tot=res(6*par.N+2);
nO2El_tot=res(6*par.N+3);
nO2out_tot=res(6*par.N+4);
T_el_out=res(6*par.N+5);        %temp after mixing of the exiting ...
    liquid streams from all electrolyzers
%optimal value of the differential state
PstoH2=res(7*par.N+6);
PstoO2=res(7*par.N+7);
massBt=res(7*par.N+8);
T_bt_out=res(7*par.N+9);
T_el_in=res(7*par.N+10);         %temp of inlet lye stream coming ...
    into the electrolyzer
T_CW_out=res(7*par.N+11);
%optimal value of the inputs
```

```
215 qf_cw=res(9*par.N+12);
216 zH2=res(9*par.N+13);
217 zO2=res(9*par.N+14);
218 Qwater=res(9*par.N+15);
219
220
221 %% Calculation of initial state vector
222
223 %Nominal load H2 production and specific electricity consumption
224 V_H2_ini = nH2k*0.0224136*3600;%[Nm3/h]
225 for nEl = 1:par.N
226     Ps_ini(nEl) = ...
          (Uk(nEl)*Ik(nEl)*par.EL(nEl).nc)/(1000*V_H2_ini(nEl));%[kWh/Nm3]
227     Iden(nEl) = 0.1*Ik(nEl)/par.EL(nEl).A;
228 end
229
230 Pnet = sum(Pk);
231 Ps_ini;
232 Eff_El = 3.55./Ps_ini;
233
234 z0 = [Uk Ik Pk Feffk nH2k qH2Olossk nH2El_tot nH2out_tot nO2El_tot ...
235     nO2out_tot T_el_out];
236 x0 = [Tk PstoH2 PstoO2 massBt T_bt_out T_el_in T_CW_out];
237 u0 = [Vss q_lyek qf_cw zH2 zO2 Qwater];
238
239 end
```